Mechanical Behavior of Carbon and Glass Fiber Reinforced Composite Materials Under Varying Loading Rates

by

Venkata Naga Prakash Mallik Pariti

A thesis submitted in partial fulfillment
of the requirements for the degree of
Master of Science in Engineering
(Mechanical Engineering)
in the University of Michigan–Dearborn
2017

Master's Thesis Committee:

Associate Professor German Reyes-Villanueva, Chair
Professor HongTae Kang
Assistant Professor Tanjore V Jayaraman

To My Parents, Mr. Soma Sekhar Pariti and Mrs. Ramalakshmi Pariti

And

To My Siblings, Bhaskar Pariti and Nara Pariti

For their endless love, support and encouragement

ACKNOWLEDGEMENTS

I would like to express my sincere thanks and deepest gratitude to my advisor Dr. German Reyes-Villanueva for his vast knowledge, expertise, understanding and patience. Without his technical, financial and moral support this work could never be possible. I will forever be indebted to him for giving me a rewarding graduate school experience.

I would like to thank Dr. HongTae Kang for taking time to evaluate my thesis and helping me choose my career interests as a research student when I first joined the University of Michigan-Dearborn. I also would like to thank Dr. Tanjore V Jayaraman for taking time to evaluate my thesis.

I would like to thank Roush Industries for providing the test panels that are used in this study.

I would like to express my profound gratitude to my parents and siblings for their unfailing support and encouragement throughout my thesis. I also would like to thank the office staff of the mechanical engineering department whose assistance helped me along the way. I would like to thank my friends: Sai Kalyan, Sandeep, Vinay Satya, Sai Vinay, Sidharth, Sri, Vijay, Sai Kiran, Nikhilesh and Shravan for all the good times we had and being tolerant enough during my two years at the graduate school. I would like to thank Ali and Sravani for helping me edit this thesis. Finally, I would like to thank my colleagues at the crash mechanics lab: Krunal and Aqheel for all the support and learnings we had during the past few months.

TABLE OF CONTENTS

LIST OF FIGURES

LIST OF TABLES

ABSTRACT

Composite materials reinforced by carbon and/or glass fibers offer a set of attractive properties such as high strength and stiffness, excellent corrosion resistance and improved fatigue properties, making them suitable for a variety of structural applications. The use of these composites is becoming critical for applications where the structures may be subjected to dynamic loading conditions. Therefore, it is important to investigate the effect of strain rate on the mechanical response of these lightweight composite materials when subjected to dynamic loading conditions. In this thesis, woven carbon and glass fiber reinforced composites based on an epoxy matrix were tested under tensile loading using a screw-driven Instron universal testing machine, a high-speed servo-hydraulic MTS test system and an in-house pneumatic system in order to achieve strain rates of 0.0025 s^{-1}, 0.25 s^{-1}, 10 s^{-1},100 s^{-1}, 500s^{-1} and 1000s^{-1}.Furthermore, to investigate the mechanical behavior of these materials under such loading conditions a high-speed DIC (Digital Image Correlation) system was also used consisting of two high-speed cameras capable of recording over 200,000 frames per second. Experimental results revealed that these materials maintained their high strength properties even under high strain rates and could be the material of choice for lightweight structures that may be subjected to dynamic loading conditions. Furthermore, the high speed DIC system revealed local and global strain distributions within the woven composites highlighting their failure mechanisms.

CHAPTER 1. INTRODUCTION

1.1 Composite Materials

With the increasing demand for improved performance, which may be specified by less weight, increased strength, and stiffness, there is a need to use light weight composite materials replacing conventional metallic materials. A composite material is produced using at least two constituents with altogether different physical or chemical properties that when combined create a material with properties that are unique in relation to the individual constituents [1].

1.2 History of Composite Materials

The idea of a composite material is not a new one. In 1500 B.C., early Egyptians and Israelites used a combination of mud and straw to create strong buildings. Nature is another example where the idea of a composite material can be found. Wood is a naturally occurring composite material which falls under the category of fibrous composites, with cellulose fibers embedded in a lignin matrix. Another example is gluing wood strips along different orientations to produce plywood. Concrete can also be considered a composite since it consists of a mixture of stones held together by cement. Ancient Mongolians used composite bows made from wood, bone, and bamboo bonded with a naturally occurring pine resin. These bows are said to be very powerful and accurate [2]. The evolution of modern composites started when researchers developed synthetic resins in the early 1900's. The application of composite materials in the Aerospace industry started with the development of the Phenolic resin. This development led to the fabrication of transport aircraft. Owens Corning had produced the first commercial composite material called Fiberglass®: Glass fibers combined with a synthetic polymer which created incredibly light weight and strong structures. This invention led to the development of fiber reinforced polymers which resulted in the use of new composite materials to replace traditional metallic materials. The US Military and Navy heavily rely upon Fiberglass® because of its superior strength to weight ratio and intrinsic resistance to environmental and corrosive conditions. Boats that are made of Fiberglass® offer

competitive strength and are not subjected to rusting. Fiberglass® has also been used to produce printed circuit boards, helicopter blades, the body of the corvette, sports cars etc. [1]

The US Navy incorporated the use of glass fiber-melamine composite boards in electrical terminal boards since they provide better insulation [3]. In addition, the advancements in science and technology prompted the need for the development of new materials with higher modulus fibers. In the 1960's, new and stronger reinforcing fibers like Carbon and Graphite, were produced using Rayon as the precursor. Boron fibers, which were developed around this period also found potential applications in the Military and Aerospace industries where strength and stiffness are of major concern. Meanwhile, in Japan, high strength Graphite fibers were developed using Polyacrylonitrile (PAN) as the precursor replacing Rayon. In the early 1970's, Kevlar®, fibers based on Aramid (Aromatic Polyamide), were produced and were found to be much stiffer and stronger than the existing fibers. The development of these fibers led to replacing of steel belts with polymer based cords in radial tires used in Automobiles, thus reducing their overall weight and overall fuel consumption. A small alteration in the chemical structure of the Aramid fibers gave rise to another fire-resistant fiber called Nomex®, which is generally used to develop bullet proof vests and protective gear for fire fighters. The use of these strong fibers as skins with some integral honeycomb stiffeners also led to the development of sandwich structures which have been used in the Aerospace industry. In recent years, the use of composite materials has widely spread to different industries like Aerospace, Military, Automotive, Sporting goods etc. [6]

1.3 Advantages of Composites

Composites can be considered as a superior type of material which has a wide range of applications in several industries like Aircraft, Marine, Military, Automotive, and Medical. One primary characteristic of these composites is the possibility to change the stacking sequence of the plies or lamina to obtain structures with the desired mechanical properties. The following are some of the advantages of the high-performance fiber reinforced polymer matrix composites [1-2, 6]:

- Lightweight: Composite structures are generally lighter than the metallic counterparts which make them suitable for applications in Aircraft and Automotive industry. The lower weight of the composite materials results in lower fuel consumption and lower emissions.

- High Strength: Composites possess high strength compared to many of the conventional metallic materials and have the flexibility to be engineered and be stronger in a specific direction.
- High Strength-to-Weight ratio: This property is taken in to consideration when building Aircrafts and other structures where high strength and less weight are desirable. The specific strength of composites is superior to that offered by Aluminum and Steel.
- Corrosion Resistance: Composites can withstand harsh environmental conditions and contact with several reactive chemicals. Tubes made from Fiberglass® can be used for transporting fuel from refineries.
- High Impact Strength: Composites are engineered in a suitable way to resist the impact from a blast or an explosion. Because of this property composites are used in building military vehicles and bullet proof vests.
- Design Flexibility and Dimensional Stability: Composite materials can be designed for complex shapes and can be molded easily. They have better dimensional stability as they retain their size when hot or cold, thus not allowing any expansions or shrinkage in dimensions which makes them a better fit in applications like Airplane wings etc.
- Part Consolidation: A single composite structure can replace the existing assemblies made using the conventional metallic materials thus reducing the overall cost.
- Low Thermal Conductivity: Composite materials do not conduct heat or cold and thus can be used in applications pertaining to harsh weather conditions.
- Nonmagnetic and Nonconductive: Composite materials do not conduct electricity through them thus making them suitable for applications to develop insulated switch boards, electric poles etc.
- Radar Transparent: Structures made from composite materials cannot be detected by the radar signals and thus can be used in several military applications generally as fighter jets.
- Durability: Composite materials, in general, have a long life and requires less maintenance.

1.4 Types of Materials

1.4.1 Reinforcements

Reinforcements in composites provide the necessary strength and stiffness. In many cases, reinforcements can be fibers or particulates. Particulate reinforcements are weaker, and brittle compared to the fiber reinforcements. Fibers alone cannot be used in structures even though they

possess high tensile strength because they cannot alone support the compressive loads. Fibers form the main constituent in the fiber reinforced composites, as they satisfy the required conditions and transfer the strength to the constituent matrix and they take the majority space in a composite structure. The performance of a composite is dependent upon several factors like material of the fiber, length of the fiber, the shape of the fiber, the orientation of the fiber, and composition of the fiber. The orientation of the fiber plays a significant role in indication of the strength of the composite structure. The four types of fibers that are currently in use across different industries are Glass, Carbon, Aramid, and Boron. There are other types of fibers like extended chain Polyethylene fibers, Ceramic fibers apart from the naturally occurring fibers like Jute, Coir etc. [6].

Glass fibers

Glass fibers are the most common type of fibers in the fiber reinforced polymers. Glass fiber primarily consists of Silica (SiO_2-Silicon dioxide) apart from the other metallic oxides in minor portions. The raw ingredients are initially fed into a hopper where they are melted and this molten liquid is then fed through electrically heated platinum bushings consisting of 200 small orifices at its base. The molten liquid flows through these orifices because of the gravity thus forming fine continuous filaments. Glass fibers are easily damaged due to the presence of the surface flaws [1]. This can be minimized by providing a proper sizing treatment to the extruded fibers. These protective treatments bind the filaments together into a strand. The Glass fibers are generally available as a strand. These fibers are available in other forms like continuous strand roving, woven roving, chopped strands etc. These fibers can be pre-impregnated with a layer of resin to form a prepreg. Prepregs are easy to stack, cut into required dimensions and easy to shape. There are two types of Glass fibers that are widely used as the reinforcements in the fiber reinforced composites. E-glass (named because the chemical composition makes it a better electrical insulator) and S-glass. Another among these is C-glass which is generally known for its superior corrosion resistant properties. Among these fibers, E-glass has the lowest cost and hence it is the main reason for the widespread applications of E-glass. S-glass has the highest tensile strength and higher modulus which makes it suitable for manufacturing Aircraft components and Missile casings. The density of the glass fibers is low and the strength is high. The modulus is moderate, thus making an average overall modulus to weight ratio. This led to the development of high modulus fibers like Carbon fiber, Boron fiber etc., The Glass fibers are susceptible to moisture thus decreasing the overall

strength of the fibers. These fibers are widely used in building and construction as support for other structural materials, window frames, bathroom units etc. Boat hulls are also made initially with the Glass fibers. The Transportation industry, Aerospace industry, and Chemical industry have huge applications of Glass fiber reinforced composites [6].

Carbon Fibers

Carbon fibers and Graphite fibers are commonly used reinforcements that are generally used in applications which require higher strength and stiffness and higher modulus. The basic difference between the Carbon and Graphite fibers is the Carbon content within the fiber and the process of fabricating the fibers. There are quiet few disadvantages with the Carbon fiber like a low strain to failure, poor impact resistance, and very high electrical conductivity. They are generally used in the Aerospace applications where weight saving is the key. The Carbon fibers have amorphous Carbon and a Graphitic blend of carbon in almost equal compositions because of which the carbon fibers are usually stronger. The crystal structure of Carbon generally has the carbon atoms arranged in parallel planes and these planes are held together by the Van der Waals forces, and adjacent Carbon atoms in the same plane are held together by a strong covalent bond, thus strengthening the entire Carbon crystal. Figure 1 shows the arrangement of Carbon atoms in a Graphite crystal.

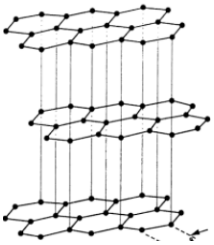

Figure 1 Arrangement of Carbon atoms in Graphite crystal. [4]

Carbon fibers are basically manufactured from two types of precursors namely Polyacrylonitrile (PAN) and pitch. The crystal structure of PAN basically comprises of highly polar CN groups. The crystal structure of Polyacrylonitrile consists of the repeating units shown in Figure 2.

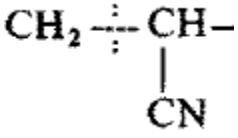

Figure 2 monomer unit of PAN. [5]

Filaments of PAN are wet spun from a solution of PAN and are stretched at elevated temperatures. These stretched filaments are oxidized at a temperature of 200-300^{o}C for two hours and the

filaments are again pyrolyzed for half an hour thus producing filaments of carbon. The key difference between the fabrication of Carbon and Graphite fibers is the temperature of the pyrolysis process. The result of different pyrolysis temperatures is fibers with different carbon content. Pyrolysis at elevated temperature yields Graphite fibers with a Carbon content of 99% whereas at a lower temperature, yields Carbon fibers with a Carbon content of 95%. On the other hand, pitch, generally a byproduct of petroleum refinement, can also be used instead of PAN as a precursor. The Carbon fibers produced with the pitch as the precursor usually have the highest modulus compared to PAN carbon fibers. However, tensile strength is lower compared to PAN carbon fibers. Pitch Carbon fibers possess better electrical and thermal conductivities over the PAN Carbon fibers [6]. Carbon fibers commercially exist as a long and continuous tow, chopped fibers and milled fibers. The long continuous tow usually has an arrangement of parallel strands and is generally used for high performance applications. Carbon fibers are used in numerous applications because of its high modulus and high tensile strength-to-weight ratio. The applications of Carbon fibers range from Sporting goods to Rocket casings in the Aerospace industry. Commercial Aircrafts also use Carbon fiber Epoxy composites in few of its structural applications. With increased production of the Carbon fiber, the overall price is decreased and the carbon fiber has found a potential use in the Medical industry, where Carbon fiber may be used to produce certain equipment and as implant materials (Joint replacements). Carbon fibers are also used in the production of heavy machinery such as turbines, compressors, windmill blades etc. [6].

Aramid Fibers

Aramid fibers are generally produced under the tradename of Kevlar®. There are two distinct types of fibers in Kevlar®: Kevlar® 29 which is used in tires, and the other is Kevlar® 49 which is used in structural applications that demand high strength and stiffness. Kevlar® has a low density but has a better specific strength compared to other reinforcement fibers [7]. Kevlar® also possesses superior toughness, good damping characteristics, and impact resistant properties compared to other structural composites. The structure of an Aramid fiber comprises of an Amide group linked to an aromatic Benzene ring. Extruding an acidic solution of a custom precursor through a spinneret results in highly anisotropic Kevlar® fibers, which possess better physical and mechanical properties. Aramid fibers when exposed to ultraviolet radiations, discolors and loses

its mechanical properties. Aramid fibers possess poor compressive properties, which is a major drawback [6].

Boron Fibers

Boron fibers are usually a coating of Boron on a substrate. Boron is usually brittle in nature. Boron is deposited on to the substrate usually by chemical vapor deposition. Since this process involves higher temperatures, a suitable substrate material like a Tungsten wire or Carbon may be used because of the superior thermal characteristics of the substrate materials. Because of the higher density, higher strength and stiffness than the Graphite fibers, Boron fibers are preferred for building Aerospace structures. However, the cost of the boron fibers is a major setback that prevents the use of them in a variety of structural applications [6].

1.4.2 Matrix Materials

Depending on the strength requirements, polymers, metals, and ceramics are used as a matrix material. Of the three, polymer matrix is preferred widely in making composite structures. The matrix has the following role in fiber reinforced composite materials.

- Holds the fibers together.
- Transfers load and stresses between the fibers.
- Prevents the fibers from environmental attacks such as chemicals and mechanical degradation of the surface of the fibers.
- Offers certain properties like ductility, toughness, and insulation which cannot be possible with fibers alone.

The fiber and matrix material should be chemically non-reactive at any given operating temperature. It is also important to consider the maximum operating temperature of a matrix material. Polymers exist either as a thermoset or a thermoplastic. Epoxy, Polyester, Phenolics etc., belongs to the thermoset category of polymers. Nylon, Polycarbonate, Polysulfone, Polyether Ether Ketone (PEEK) belong to thermoplastics [6].

Thermoplastic polymers

Thermoplastic polymers are linear polymers in which the molecules are held together by a weak bond and they are not cross-linked to form a rigid structure. The weak bonds break upon the application of heat and the molecules can move to a relatively new position upon the application

of heat and or force. Upon cooling, the molecules occupy a new position and the weak bonds are restored thus resulting in a new shape. Therefore, a thermoplastic polymer may be repeatedly melted and processed. However, the thermoplastic polymer may be mechanically degraded because of continuous exposure to elevated temperatures. Because of the linear arrangement of molecules in some thermoplastics, a higher strain to failure can be expected compared to that of cross-linked thermosets making thermoplastics tougher [1]. Common thermoplastic resins that are used as matrix materials are Nylon (PA), Polypropylene (PP), Polycarbonate (PC), and Polysulfone (PS). Polyether Ether Ketone (PEEK), Poly Phenylene Sulfide (PPS) are the new thermoplastics that are used currently as matrix materials. PEEK is preferred widely in a variety of applications because of its superior toughness and impact properties [6]. Figure 3 shows the monomer unit of widely used Polypropylene.

Figure 3 Monomer unit of Polypropylene. [8]

Thermoset Polymers

In a thermoset polymer, molecules are chemically joined together by crosslinking to form a rigid structure. Adjacent molecules are held together by strong covalent bonds. These polymers cannot be softened upon heating because of the crosslinking. Thermosets have higher modulus, high rigidity, and good dimensional stability when compared to thermoplastics. Epoxy is a thermoset resin which is widely used as a matrix material in many of the fiber reinforced composites. Epoxy resins are widely used because of a wide variety of properties like superior resistance to chemical and environmental attacks, good adhesion with the reinforcements and less shrinkage during curing. The major drawback of using Epoxy as the matrix is its high cost and long curing time [6].

The ideal matrix materials for high performance polymer matrix composites should have the following desirable mechanical properties.

- High Tensile Strength
- High Modulus
- High Fracture Toughness
- Resistance to Moisture and other Solvents
- Good Dimensional Stability

- Higher Glass Transition Temperature

Conventionally, thermoset polymers are preferred for fiber reinforced composites. Low molecular weight chemicals with lower viscosities are preferred as starting materials for the polymerization of the thermoset polymer. Fibers are then pulled through the chemical solution or immersed in them. Because of extremely low viscosity, it is possible to achieve a good wetting between fiber and matrix and this plays a crucial role in the enhanced mechanical performance of the composite. The benefit of using thermoset polymer matrix is enhanced thermal resistance and chemical resistance.

1.5 Applications of composites

1.5.1 Transportation

Composites are widely used materials because of their flexibility and adaptability to severe conditions. They can be easily blended with other materials to fill the desired needs and achieve attractive mechanical properties. Fiber reinforced composites are used in surface transportation because of their superior strength-to-weight ratio compared to the other conventional materials. The stiffness offered by the fiber reinforced composites and the cost makes them a better choice over traditional metallic materials. Carbon fiber reinforced Epoxies are used in making Racing cars. A Polyester resin reinforced with a variety of fibers was the first application of composites in transportation because of the low cost, the simplicity of design and ease of production [6].

1.5.2 Aircraft and military applications

The major structural applications of fiber reinforced composites are in the field of Military and Commercial Aircrafts. Weight reduction is critical in these applications to achieve high speeds and higher payloads. A Boron fiber reinforced Epoxy was the first composite ever used in the horizontal tail stabilizer of the F14. Since the origination of Carbon fibers in the early 1970's, Carbon fiber reinforced Epoxy composites are continuously being used in Aircraft components. Many of the Aircraft components like wings, fuselage, and stabilizers are produced using fiber reinforced composites. The structural strength and durability of these composites prompted the development of other Aircraft components. The Stealth Aircrafts today are made of Carbon fiber reinforced polymers because of the superior properties of Carbon fibers that help reducing heat radiation and radar reflections [6].

Figure 4 Stealth aircraft. [9]

Airbus was the first commercial Aircraft manufacturer to use composite materials in their aircraft. Airbus incorporated the use of composite materials in their A310 Aircraft, where 10% of total weight of the Aircraft was made using composite materials [6]. In 1988, Airbus used all composite tail for its A320 Aircraft, which include the tail cone, horizontal and vertical stabilizers. In 2006, Airbus introduced A380 Aircraft in which 25% of the total weight of the Aircraft is made of composites [10]. Major components that were made from the composites include the empennage, tail cone, wings, landing gear doors, radome, spoiler, flaps, central torsion box and other flight control surfaces. The principal reason fiber reinforced polymers are used in the Aircraft and Helicopter applications is because of weight reduction which reduces the fuel consumption and increases pay load. The principal advantages of using fiber reinforced polymers include higher strength and stiffness, higher fatigue and corrosion resistance, reduction in a number of components and fasteners. Figure 5 shows the Aircraft parts made from composite materials in the A380 Aircraft [10].

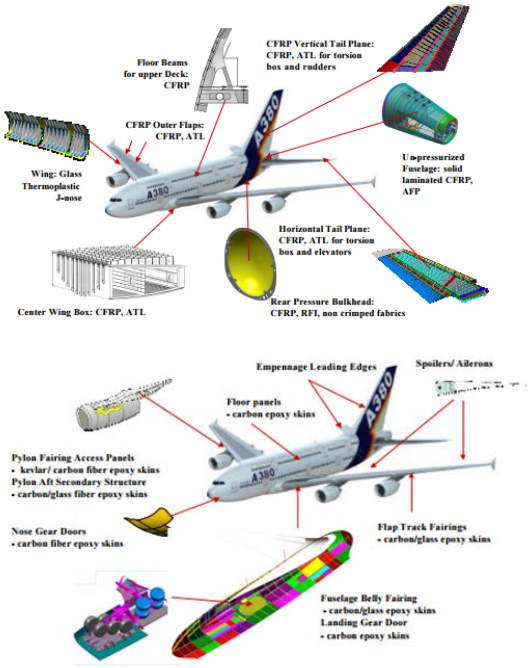

Figure 5 Use of fiber reinforced composites in Airbus A380. [10]

Boeing also started the use of composite materials in Boeing 777, where 10% of structural weight is made from Carbon Fiber Epoxy composites. The Rutan Voyager was the first all composite Aircraft to demonstrate the strength and efficiency by flying nonstop all over the world without refueling [11]. Carbon fiber or Glass Fiber Epoxy composites are used in the Helicopter rotor blades. Boeing used most of Carbon fiber reinforced composites rather than Aluminum alloys in their commercial Aircraft, Dreamliner.

1.5.3 Space applications

Reduction of mass is most critical in Space applications. The Satellite structure may use the sandwich plates with light alloy honeycomb cores. In few cases, pressure vessels are as well made of the composite tubes. Unidirectional Carbon fibers are wound around a mandrel to produce these tubes. Composites are also used as a material for insulation in Space vehicles. Space shuttles and Space vehicles use flywheels made from composite materials for the supply of electric power and for controlling the altitude. These flywheels deliver higher levels of power compared to the conventional flywheels because of the reduction in total mass of the flywheel. Composites such as Carbon-Carbon involves applications at higher temperatures. They are used in producing the structures like nose cap, nose landing gear door and outer edges of the wings. Space shuttles usually experience high temperatures around the nose and the leading edge of the wing. Hence

materials like Carbon-Carbon reinforcements are preferred as they can tolerate high varying environments from launch to reentry. Graphite Epoxy composite materials are also used in numerous Space applications because of their high strength and stiffness and non-zero coefficient of thermal expansion. SpaceX uses Carbon fiber in payload firing and interstage on its Falcon Spacecraft. The interstage is a composite structure consisting of an Aluminum honeycomb core surrounded by a Carbon fiber skin. Figure 6 shows the interstage used in the Falcon 9 of SpaceX [15].

Figure 6 Composite interstage in SpaceX's Falcon 9. [15]

1.5.4 Automotive applications

Fiber reinforced composites application in an Automobile may be classified in to three categories like body components, chassis, and engine components. These components must sustain the road loads and crash loads. During the early ages of application of fiber reinforced composites in the Automotive industry, some specialty cars were produced by the Lotus Company which used Glass fiber with a Polyester resin. In 1938, Ford first produced its fiber reinforced prototype of an Automobile. In this, the structure of the Automobile was made of Graphite fiber Epoxy composite. The vehicle was built completely by hand layup of Graphite Epoxy prepreg. This prototype was compared to the in-production vehicle made of Steel. This comparison demonstrated no or a little difference between the two [40]. Body components like a hood, door panel may require high stiffness and should be dent resistant. Also, the exterior body should have a smooth surface finish for appearance. In the engine compartment, Glass fiber reinforced polymers may replace certain metallic parts like cylinder head cover and oil pump cover, bearing cages etc. One of the main characteristics of the unidirectional composite is the ability to absorb elastic energy. Therefore, the

existing metallic suspension spring maybe replaced with a glass/resin composite spring because they are almost unbreakable [12]. Figure 7 shows the application of Carbon fiber reinforced Epoxy roof panel in a BMW M6 vehicle.

Figure 7 Carbon fiber reinforced Epoxy roof panel in BMW M6. [6]

Fiber reinforced composites have become widely used material in motor sports where light weight structures are used for attaining higher speeds. In 1950's, Glass fiber reinforced polymers were used as body panels replacing Aluminum body panels. The controlled crush behavior offered by the Carbon fiber Epoxy composite has found an important application in survival cells and nose cones which protect the driver in the event of the crash. McLaren produced the first composite motor sports car made from Carbon fiber monocoque [13]. Figure 8 shows a racing car that uses a Carbon fiber monocoque chassis.

Figure 8 Racing car with a Carbon fiber monocoque chassis. [13]

1.5.5 Sporting goods

Sporting goods like Tennis rackets, Athletic shoes, Ski boards etc., use composite materials because of their higher strength and stiffness, and lower weight. Additionally, fiber reinforced composites offer good damping and design flexibility. Bicycles and Canoes made of Carbon fiber reinforced composites helps in quick maneuvering because of their reduced weights in races. Fiber

reinforced composites provide faster damping of vibrations which makes them suitable to produce Tennis rackets to eliminate the shock transmission to the player's arm. The capability to store high elastic energy per unit weight of the fiber reinforced composite materials widens the use of the composite materials in Archery to produce bows which aid in propelling the arrow through longer distances [6]. Fiber reinforced composites are also found vastly in the production of golf shafts, fishing rods, auxiliary parts of bicycle etc. Figure 9 shows the bicycle made of Carbon Epoxy composite.

Figure 9 Carbon Fiber Epoxy bicycle frame. [6]

1.5.6 Marine Applications

The first composite boat was made in the early 1940's with the invention of the Fiberglass® reinforcement. Post the invention of the fiberglass, many of the war boats and ships use Fiberglass® reinforcements. The key advantage of using fiber reinforced composite materials in place of conventional materials is higher cruising speed because of the reduction in weight, easy maneuvering, and higher fuel efficiency. In recent years, the Fiberglass® has been replaced with Kevlar® 49 fibers because of their higher strength-to-weight ratio. Carbon fiber reinforced composites are sometimes used in racing boats because of their high strength-to-weight and high modulus-to-weight ratios. The complete hull, deck and other structural components are made of Carbon fiber. Sometimes, Carbon fibers are blended with other low density polymeric materials to improve the impact resistance of the boats. The hulls of large composite ships are generally made of Carbon fiber sandwich structure with PVC as the core. This results in a significant increase in strength and stiffness, and decrease in overall weight. Composite materials cannot be corroded or decayed easily when compared to conventional materials like steel and wood. Few subsea Submarines use composite materials for improved stealth capability. Fiber reinforced composites

are extensively used in Royal Swedish Navy's Visby-class Corvette which is the largest ship made of composites [6]. Figure 10 shows the Visby Corvette ship made of composite materials.

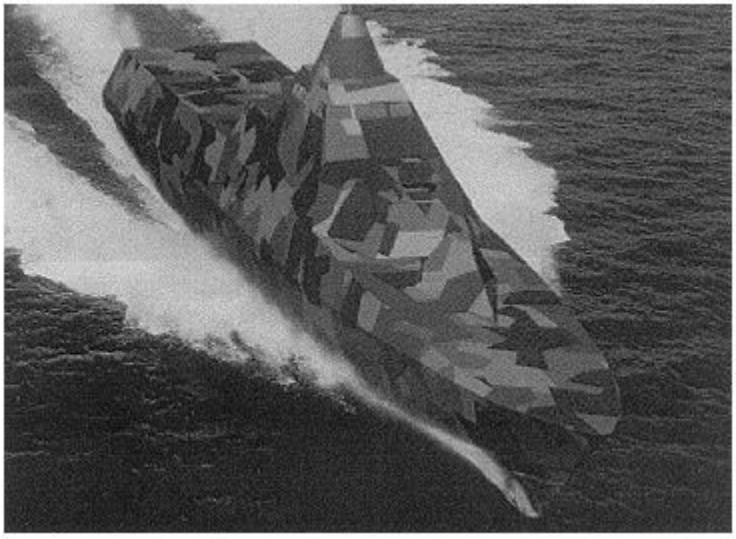

Figure 10 Visby Corvette ship. [14]

1.5.7 Miscellaneous Applications

Fiber reinforced composites are gradually replacing conventional materials like concrete, steel etc., used in civil applications. The main advantage of using fiber reinforced composites is the weight reduction of the total structure and resistance to corrosion. Apart from these advantages, fiber reinforced composites would reduce the overall cost for installations, consolidation of fabrication processes, reduced transportation costs, reduced maintenance cost due to improved corrosion resistance [1]. Application of fiber reinforced composites for the construction of Bridges is a large-scale application of the composite materials. The conventional bridges must support their own dead weight and therefore use light weight fiber reinforced composites would allow the bridge to accommodate a number of vehicles and heavier trucks as well [6].

Fiber reinforced composites are also used in producing small components like windows, doors, canopies etc., Composites are also used to produce large self-supporting structures like curved domes. Glass fiber reinforced composite has been used as a structural shell member in constructing the dome of Sharjah international airport. Composite materials today are also used as pultruded frames which form the skeleton of buildings. Load bearing members in civil engineering structures like pedestrian and vehicle bridges, bridge decks, energy absorbing guard rails, building systems, modular roof tops, electric poles, light towers etc., are made predominantly from fiber reinforced

composites. Fiber reinforced composites are also used as reinforcement bars, columns, panels, beams etc. [16]. Figure 11 shows the composite sandwich construction of a bridge.

Figure 11 Composite bridge. [16]

Composite materials are also used in the Medical field to build new Medical Devices and Artificial Human Bones. Composite materials are used as cladding materials, moderators and control rods in nuclear reactors. They are used widely in Electronics as printed circuit boards and because of the better insulation properties of composite materials, they are also used in making electrical panel boards [1].

1.6 Strain Rate Properties of Composites

Composites, now-a-days are used as primary load bearing components in many of the advanced engineering structures. High strain rate loading is possible in many engineering components where fiber reinforced composites are the main load bearing material [17-19]. Investigating the mechanical properties of these fiber reinforced composites and their variation with strain rate is crucial in designing structures made of such composites. Earlier, fiber reinforced composites have been tested at higher strain rates using numerous methods [20]. Testing of fiber reinforced composites at high rates of strain rates involve many complexities like the inability to measure deformation in the test coupon directly. Earlier, high strain rate testing was usually done on a split Hopkinson pressure bar, but the data that was obtained through these tests were not reliable and the test procedure was also complicated because of the presence of inertia [21]. High strain rate properties have also been tested using drop tower technique, but it has a limitation. High rates of strain cannot be achieved using the drop tower as the velocity of the impact is directly proportional to the height from which the impact occurs. Strain rates up to $10s^{-1}$ are usually tested on a hydraulic load frame or a screw-driven universal testing machine. The high strain rate properties of fiber reinforced composites have also been investigated using an expanding ring technique [22].

However, it was found that the data obtained through this technique was not reliable because of the presence of inertia. To achieve an accurate rate of strain using a hydraulic frame, it is equipped with a special device called as a slack adapter, which helps to attain the desired rate of strain [23]. Also, this minimizes the inertia caused due to the moving parts. Melin and Asp [24] experimentally investigated the strain rate dependency on Carbon fiber/Epoxy composite laminates. It was found that the transverse modulus is not dependent on the strain rate. However, the stress and strain-to-failure slightly increased with strain rate when the composite test coupons were subjected to transverse tensile loading. In this investigation, dog bone specimens were tested using a split hopkinson pressure bar with tensile testing fixtures. Harding and Welsh [25] conducted high strain rate tensile testing on Carbon/Epoxy, Glass/Epoxy, and Kevlar/Epoxy. It was determined that the stress at failure and strain are rate independent. High strain rate tensile test on unidirectional Carbon/Epoxy composites was experimentally investigated by Daniel and Hsiao [26] and it was found that the tensile modulus increased with the rate of loading, however, the stress and strain to failure did not vary significantly. The high strain rate tensile behavior of woven Carbon/Epoxy laminate under shear and tensile loading was studied by Chiem and Liu [27]. Here, an increase in strength and strain to failure with the increasing loading rate was reported. Norihiko et al. [28] experimentally investigated the high strain rate loading of unidirectional Carbon fiber reinforced composites and found that the tensile properties are independent of the strain rate. They reported that there are many factors that influence the high strain rate mechanical behavior of fiber reinforced composites. Staab and Gilat [29] experimentally investigated the tensile mechanical behavior of Glass/Epoxy laminates and found that these materials experience a higher tensile modulus at higher strain rates when compared to quasi static loading conditions. Mahmood and Majid [30] experimentally investigated the behavior of unidirectional Glass/Epoxy composite structures under high strain rate loading. Here, it was found that the failure mode of the composite laminate is entirely dependent on the strain rate. Laminates subjected to a low strain rate experienced failure in a smaller portion of the gage section whereas the laminate at higher strain rates covered the entire gage area. Also, the overall rate dependence in fibrous composite materials was found to depend on the rate dependence of the constituents of the composite material. It was also determined that several factors like the fiber configuration (i.e., unidirectional, woven or cross-ply), type of loading (tensile, compressive and shear), and orientation of the plies in the laminate played a crucial role in determining the mechanical properties of the coupons under test

[31]. It has also been reported that woven Glass/Epoxy laminates yield higher ultimate tensile strength and higher strain to failure at higher strain rates and that the fibers influence more the mechanical properties of the composite compared to the matrix [29]. Rotem and lifshitz [32] studied the dynamic behavior of unidirectional Glass/Epoxy composite and reported an increase in mechanical properties with increasing rate of strain. Vanessa Pickerd [33] used a non-contact strain measurement system in the event of high strain rate testing and it was found that the strain obtained through the digital image correlation technique is approximately equal to the strain obtained through strain gages. Powel et al. [34] experimentally investigated the dynamic behavior of woven Carbon fiber reinforced polymer and it was found that the ultimate strength increased by 8% when fibers are oriented longitudinally and 37% when fibers are oriented in the transverse direction. Reyes and Sharma [35] studied the effect of strain rate on thermoplastic composites and found that there was an increase in strength and stiffness and a decrease in strain-to-failure with increasing strain rates. Tarfaoui et al. [36] studied the influence of fiber orientation on the mechanical properties of Glass/Epoxy composite laminates subjected to high rates of strain. In this investigation, fibers with different orientations of 0°, 20°, 30°, 45°, 60°, 70° and 90° were experimentally tested and it was found that the modulus, maximum stress and strain to failure are strongly dependent on the fiber orientation. Eskandari and Nemes [37] investigated the rate dependency of Graphite/Epoxy composites and it was found that the tensile strength and strain to failure are higher for dynamic testing. Okoli and Smith [38] experimented on Glass/Epoxy composites at increasing rates of strain and it was found that a linear relationship exists between the mechanical properties and log of the strain rate. It was also reported that this relation could be extrapolated to deduce the material properties at higher rates of strain thus eliminating the effects of inertia during high rates of strain. Makarov et al. [39] experimentally studied the dynamic properties of Glass/Epoxy composites at higher rates of strain and found that the dynamic properties are mainly dominated by the Glass fiber properties. It was also found that the young's modulus was independent of the strain rate, however, the strength and strain to failure increased with the strain rate.

1.7 Summary

Fiber reinforced composites have a set of attractive material properties such as higher tensile strength, high Stiffness, corrosion resistance, and light weight which make them suitable for a variety of structural applications. The use of the fiber reinforced composites is turning out to be

progressively critical in applications where they encounter complex non-static loading and deform rapidly.

In addition, Automotive and Aerospace industries are mainly dependent upon the use of conventional materials like Steel and Aluminum in many of its structural applications. However, to improve the Automobile/Aircraft efficiency and to reduce the fuel consumption and to reduce the overall structural weight, traditional materials are replaced by lightweight composite materials [6]. To employ these lightweight composite materials in to engineering applications, these materials are to be designed in such a way that they are safe to use and this safety can be predicted by using the Finite Element Analysis simulations. However, to check the reliability of the software simulations, a coupon level testing of the said fiber reinforced composites must be performed under varying strain rate conditions. Finally, it is evident that there is no specific method for performing high strain rate testing. However, already existing methods might not yield correct test data pertaining to the high strain rate testing due to several reasons like the effect of inertia, the complexity of the test setup etc. Due to this reason, a standard test methodology for high strain rate testing and data analysis is needed. This work aims to investigate the mechanical properties like modulus, ultimate tensile strength and failure strength under high strain rate loading conditions. Also, the global and local deformations and overall strain distribution will be studied.

1.8 Objectives

The purpose of this thesis work is to characterize the high strain rate tensile properties of 2x2 twill woven Carbon fiber and 8HS (8-Harness Satin) woven Glass fiber reinforced composite materials provided by the Roush Industries. 3K 2x2 twill woven Carbon fiber, 12K 2x2 twill woven Carbon fiber and 8HS 7781 Glass fiber with ply orientations of 0° and 45° are investigated at various strain rates. The samples will be tested at different strain rates of 0.0025 s^{-1}, 0.25 s^{-1}, 10s^{-1}, 100 s^{-1}, 500 s^{-1}, 1000 s^{-1}. In addition, global and local deformations, strain distributions within the materials will be examined using a high resolution non-contact strain measurement system. Following this, the effect of an open hole on the Carbon fiber and Glass fiber specimens for a ply orientation of 0° subjected to tensile loading conditions will be investigated. The slow strain rate/quasi static testing will be performed using Instron 5767 Universal Testing Machine. The High strain rate testing will be carried out on a hydraulic MTS test machine and an in-house developed pneumatic system.

References

[1] Chawla, K.K.,1998, *Composite materials: Science and Engineering*, Springer, New York 2nd Edition.

[2] Kaw, A.K.,2006, *Mechanics of Composite Materials*, CRC Press, Boca Raton FL,2nd Edition.

[3] Palucka, Tim., and Bensaude-Vincent, B., 2002, *Composites Overview.*

[4] Pierson Hugh, O., 1993, *Handbook of Carbon, Graphite, Diamond and Fullerenes – Properties, Processing and Application*, Noyes Publications,1st Edition.

[5] Henrici-Olive, G., 2015, "The Chemistry of Carbon Fiber Formation from Polyacrylonitrile," Journal of Advances in Polymer Science, Springer link, Vol.51, pp. 1-6.

[6] Mallick, P.K., 2007, *Fiber-Reinforced Composites- Material, Manufacturing and design*, CRC Press, Boca Raton FL,3rd Edition.

[7] Gibson, Ronald F., 2011, *Principles of Composite Material Mechanics*, CRC Press, Boca Raton FL,3rd Edition.

[8] Busico, Vincenzo., and Cipullo, Roberta., 2001, "Microstructure of Polypropylene," Journal of Progress in Polymer Science, Elsevier, Vol. 26, Issue 3, pp.443-533.

[9] Zikidis, Konstantinos., Skondras, Alexios., and Tokas, Charisios., 2014, "Low Observable Principles, Stealth Aircraft and Anti-Stealth Technologies," Journal of computations and modelling, Scienpress Ltd, Vol. 4, pp.129-165.

[10] Pora, Jerome., 2001, "Composite Materials in the Airbus A380-From History to Future," 13th International Conference on Composite Materials, Beijing, China.

[11] Roncz, J., 1989, "Propeller development for the Rutan Voyager," SAE Technical Paper No. 891034.

[12] Gay, Daniel., 2014, *Composite Materials: Design and Applications*, CRC Press, Boca Raton FL,3rd Edition.

[13] Heimb S., 2009, "Crash Simulation of an F1 Racing Car Front Impact Structure," 7th LS-Dyna Conference, Stuttgart.

[14] Mouritz, A.P., Gellert, E., Burchill, P and Challis, K., 2001, "Review of Advanced Composite Structures for Naval Ships and Submarines," Elsevier - Composite Structures, Vol.53, pp.21-42.

[15] Van Forest, Arnold., and Sippel, Martin., 2008, "The Logistical Challenges of Spaceliner Concept," 1st International Academy of Astronautics Symposium on Private Human Access to Space.

[16] Mohite P.M., "A course on Composite Materials," NPTEL.

[17] Jacob, C.G., Michael Starbuck, J., Fellers, J.F., Simunovice, Srdan., Boeman, R.G., 2004, "Strain Rate Effects on the Mechanical Properties of Polymer Composite Materials," Journal of Applied Polymer Science, Vol.94, pp.296-301.

[18] Barre, S., Chotard, T., and Benzeggagh, M.L., 1996, "Comparitive Study of Strain Rate Effects on Mechanical Properties of Glass Fiber-Reinforced Thermoset Matrix Composites," Journal on Composites-Elsevier, Vol. 27, pp.1169-1181.

[19] Hosur, M.V., Alexander, J., Vaidya, U.K., and Jeelani, S., 2001, "High Strain Rate Compression Response of Carbon/Epoxy Laminate Composites," Journal of Composite Structures, Vol.52, pp. 405-417.

[20] Harding, J., Welsh, L.M., 1983, "A Tensile Testing Technique for Fiber-reinforced Composites at Impact Rates of Strain," Journal of Materials Science, Vol.18, pp. 1810-1826.

[21] Chorcron Benloulo, I.S., Rodriguez, J., Martinez, M.A., and Sanchez Galvez, V., 1997, "Dynamic Tensile Testing of Aramid and Polyethylene Fiber Composites," International Journal of Impact Engineering, Vol.19, pp. 135-146.

[22] Hoggatt, C.R., and Recht, R.F., 1969, "Stress-Strain Data Obtained at High Rates Using an Expanding Ring," Journal of Experimental Mechanics, Vol. 9, pp.441-448.

[23] Borsutzki, M., Cornette, D., Kuriyama, Y., Uenishi, A, Yan, B., and Opbroek, Ed., 2005, "Recommendations for Dynamic Tensile Testing of Sheet Steels," International Iron and Steel Institute.

[24] Melin, L.G., Asp, L.E., 1998, "Effects of Strain Rate on Transverse Tension Properties of a Carbon/Epoxy Composite: Studied by Moiré Photography," Journal of Composites, Vol. 30, pp.305-316.

[25] Welsh, L.M., and Harding, J., 1985, "Effect of Strain Rate on the Tensile Failure of Woven Reinforced Polyester Resin Components," Journal De Physique, Vol. 46, pp. 405-414.

[26] Daniel, I.M., and Hsiao, H.M., 1998, "Strain Rate Behavior of Composite Materials," Journal of Composites Engineering, Vol. 29, pp. 521-533.

[27] Chiem, C.Y., and Liu, Z.G., 1988, "Modeling of Dynamic Behavior of Composite Materials," Proceedings of IMPACT 87, Impact Loading and Dynamic Behavior of Materials, pp. 579-586.

[28] Norihiko, Taniguchi., Tsuyoshi, Nishiwaki., Hiroyuki, Kawada., 2007, "Tensile Strength of Unidirectional CFRP Laminate under High Strain Rate," Journal of Advanced Composite Materials, Vol. 16, pp. 167-180.

[29] Staab, G.H., and Gilat, Amos., 1995, "High Strain Rate Response of Angle-Ply Glass/Epoxy Laminates," Journal of Composite Materials, Vol. 29.

[30] Shokrieh, M.M., and Omidi, M.J., 2009, "Tension Behavior of Unidirectional Glass/Epoxy Composites Under Different Strain Rates," Journal of Composite Structures, Vol. 88, pp. 595-601.

[31] Hamouda, A.M.S., and Hashmi, M.S.J., 1998, “Testing of Composite Materials at High Rates of Strain: Advances and Challenges”, Journal of Materials Processing Technology, Vol.77, pp. 327-336.

[32] Rotem, A., Lifshitz, J.M., 1971, “Longitudinal Strength of Unidirectional Fibrous Composites Under High Rate of Loading,” Journal of Materials Science, Vol. 7, pp. 861-869.

[33] Pickerd, Vanessa., 2013, “Optimization and Validation of the ARAMIS Digital Image Correlation System for use in Large-Scale High Strain Rate Events,” Defense Science and Technology Organization, Technical Paper TN-1203.

[34] Powell, L.A., Luecke, W.E., Merzkirk, Matthias., Avery, Katherine., and Foecke, Tim., 2017, “High Strain Rate Mechanical Characterization of Carbon Fiber Reinforced Polymer Composites Using Digital Image Correlations,” Journal of Materials and Manufacturing-SAE International, Journal Article 2017-01-0230.

[35] Reyes, G., and Sharma, U., 2009, “Mechanical Behavior of Woven Thermoplastic Composites under Varying Strain Rates,” SPE Automotive Composites, Conference and Exhibition.

[36] Tarfaoui, M., Choukri, S., and Neme, A., 2007, “Effect of Fiber Orientation on Mechanical Properties of the Laminated Polymer Composites Subjected to Out-of-Plane High Strain Rate Compressive Loadings,” Journal of Composites Science and Technology, Vol. 68, pp.477-497.

[37] Eskandari, H., and Nemes, J.A., 1999, “Dynamic Testing of Composite Laminates with a Tensile Split Hopkinson Bar”, Journal of Composite Materials, Vol. 34, pp. 260-273.

[38] Okoli, O.I., and Smith, G.F., 2000, “High Strain Rate Characterization of Glass/Epoxy Composite,” Journal of Composites Technology and Research, Vol.22, pp. 3-11.

[39] Makarov, G., Wang, W., and Shenoi, R.A., 2005, “Deformation and Fracture of Unidirectional GFRP Composites at High Strain Rate Tension,” Journal of Composite Structures, Vol. 69, pp. 45-54.

[40] Peijs, Ton., 2000, “Natural Fiber Based Composites,” Journal of Materials Technology, Vol. 15, pp. 281-285.

CHAPTER 2. EXPERIMENTAL PROCEDURE

2.1 Quasi Static Tensile Testing

Initially, the quasi-static tensile properties of thermosetting based woven composites were evaluated in this research work. The composite materials that are used in this study are:

- Carbon Fiber/Epoxy (CFE) 3K 2x2 twill woven composite prepreg
- Carbon Fiber/Epoxy (CFE) 12k 2x2 twill woven composite prepreg
- Glass Fiber/Epoxy (GFE) 8HS-7781

Panels with dimensions of 0.9mx1.8m were manufactured and provided by Roush Industries. From these panels, rectangular specimens with dimensions 24mmx100mm were cut along 0° (along warp yarn) and 45° (perpendicular to both fill and warp yarns). Specimens of each material and orientation were cut using a Diamond coated circular disc cutter as shown in Figure 12.

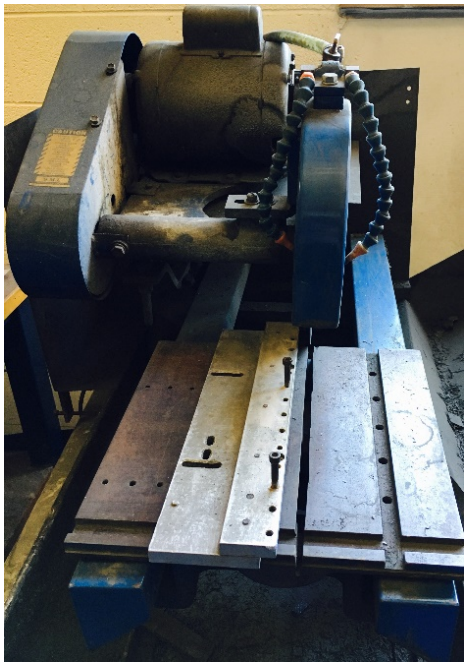

Figure 12 Diamond coated circular disc cutter.

These strips were further machined to achieve a dog-bone shape. Figure 13 shows low magnification images of machined samples of the composite materials, studied in this project. A schematic representation of a typical sample along with dimensions is also included.

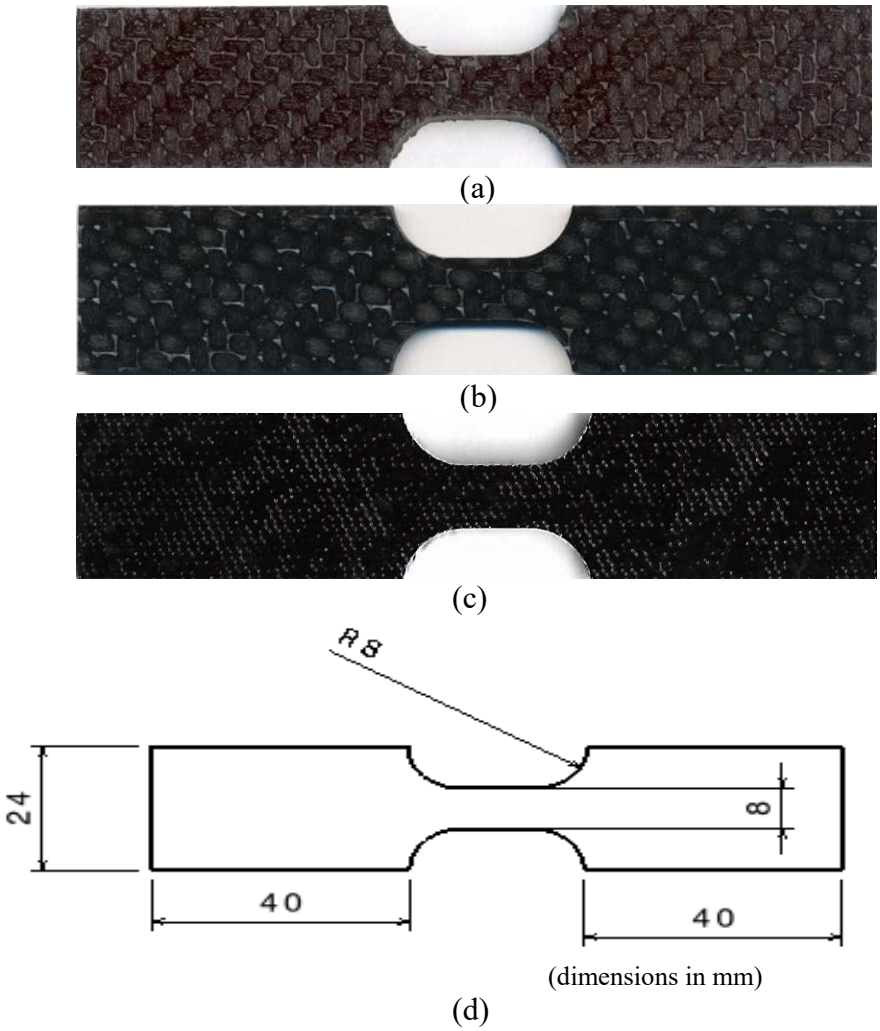

Figure 13 Low magnification images of the specimens under test (a) CFE 12K (b) CFE 3K (c)GFE–8HS 7781 (d) schematic representation.

The prepared specimens were loaded in tension on a universal testing machine and monotonic loading rates of 0.0025 s^{-1}(Cross head speed of 1.5mm/min) and 0.25 s^{-1}(Cross head speed of 150mm/min) were applied to the specimen. The universal testing machine shown in Figure 14 recorded the load and time of the test.

Figure 14 Instron 5597 universal test machine for rates of 0.0025s^{-1} and 0.25s^{-1}.

A number of specimens of each of the orientation were tested at the aforementioned loading rates. In addition, a non-contact strain measurement system was used to evaluate global and local strain distribution patterns.

2.1.1 Introduction to DIC

Digital Image Correlation (DIC) is a non-contact 3D optical deformation measuring system that analyzes deformations in a material. Here, the pixel is defined as the smallest element of an image [1]. DIC recognizes the surface of the specimen that is under test and allocates coordinates to the pixels. The surface of the specimen is crucial for the measurement and analysis using the digital image correlation software. The surface of the specimen should be printed with a stochastic pattern so that allocation of the pixels to the digital images that are captured during the event of the test would be easy. To have a better contrast and to facilitate the ease of facet identification, the specimen under test is usually illuminated using a fiber optic light. Figure 15 shows the speckle pattern printed on the specimens in preparation for tensile testing.

Figure 15 Specimen speckle pattern for DIC analysis.

The DIC software requires a collection of pixels called facets to compute the displacement in the specimen. This displacement can later be used to calculate the strain in the test specimen. The technique of digital image correlation requires a series of images over a period during which the specimen is tested. For correlation purposes, the software requires two sets of images of the specimen under test taken at separate camera angles. The digital image correlation technique can also be used in high-speed events such as blast and ballistic impact because of the advancement of the high-speed cameras in the recent years [1]. The following steps were carried out to measure local and global strains of the composite materials under tensile loading conditions.

- Determining the measuring volume and preparation of specimen
- Calibration of measuring volume
- Creating a new project
- Setting the image recording mode
- Recording the tensile test event
- Defining a start point for computation
- Computing project and visualizing the required result (like epsilon Y, major strain etc.,)
- Transformation of the project in to a defined coordinate axis
- Defining analysis elements like sections, stage points etc.,
- Post Processing
- Documentation

In addition, special care should be taken in order to obtain reliable results. Here, prior to the measuring process, the specimen under test must be within the measuring volume of the cameras, the measuring volume must be selected in such a way that the measuring area or the measuring object remains within the measuring volume throughout the deformation of the specimen under test. The printed surface pattern should not break early. It must follow the deformation of the specimen. The printed pattern must be dull in order to avoid reflections which usually hinders the measurement. Once the measuring volume is determined, the DIC system must be calibrated to ensure accurate measurements. The correct choice of the sensors (camera lens) also contributes to successful calibration. The DIC system was calibrated each time if the camera lenses were adjusted or the position of the cameras was changed [2]. A suitable calibration object was to be

selected such that it covers the entire measuring volume during the calibration steps. Figure 16 shows the calibration panel that has been used to calibrate the measuring volume.

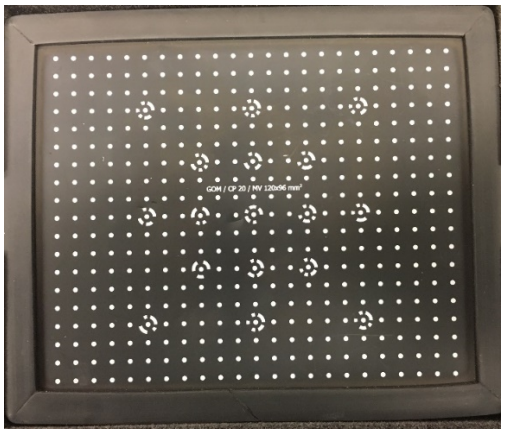

Figure 16 Digital image correlation calibration object.

The distance between the cameras and the test object and the angle between the cameras depended entirely upon the type of sensor and the calibration panel used. Figure 17 shows the typical arrangement of the 3D sensor with respect to the measuring volume of the specimen under test [1] and the test setup for quasi-static tensile testing.

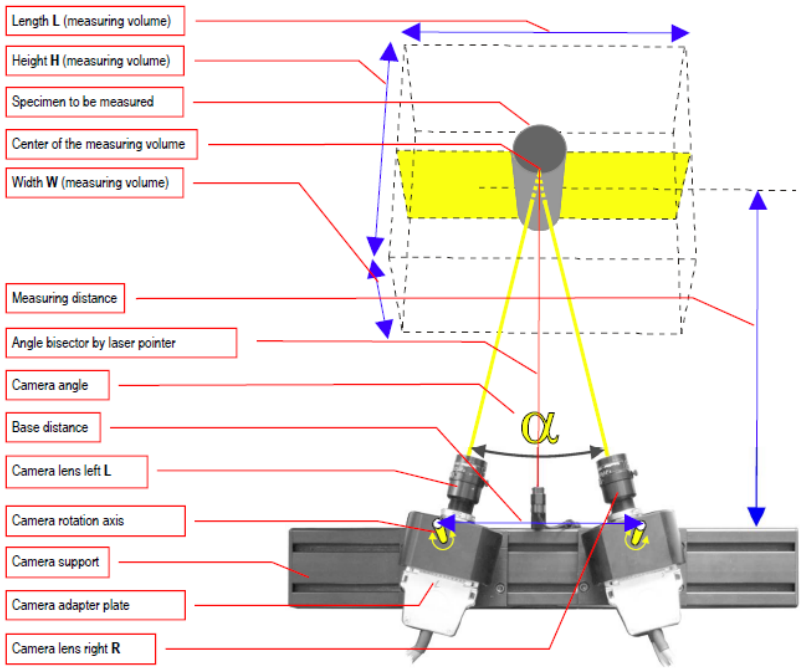

(a)[1]

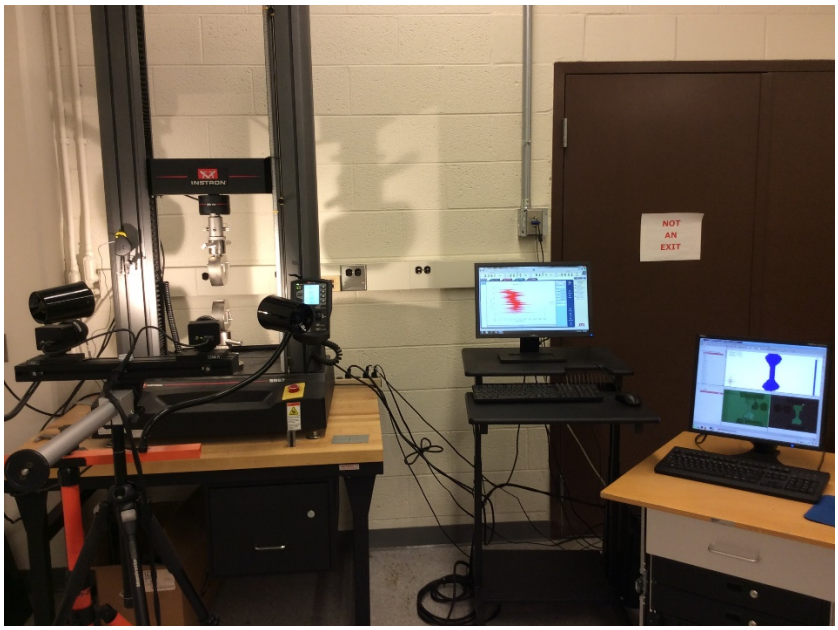

(b)

Figure 17(a) & (b) Representation of GOM Sensors (a) with respect to specimen under test [1] and (b) the test setup for quasi-static tensile loading.

The focal length of the lens used was 50mm, the measuring distance was 800mm and the camera angle was around 25°. The following steps were followed in order to calibrate the measuring volume.

- The calibration object was placed at the center of the measuring volume so that the sensor recorded the entire calibration object.
- Shutter (usually 61ms-64ms) was adjusted such that the calibration object is not over exposed.
- The calibration images were recorded by following the instructions given by the DIC software.
- Once the recording was done and after successful computation, the calibration deviation was less than 0.04.

After the successful calibration, in order to store all the images of the material deformation, a measurement project was needed. The shutter time was defined as the time interval during which the camera recorded the event images. For the sensors to sense the stochastic pattern, it was necessary to use a light source. The light source illuminated the specimen uniformly thus avoiding any dark regions. The Recording mode is activated in order to record the events of the test once the specimen was loaded in the universal testing machine. Each image that was recorded by the

sensors corresponded to a stage in DIC software. Once the recording was done, all the images were ready for computing. For the facet computation, it was required to identify the same facet across all the stages. This recognition process could be termed as identification of start point. The position of a coordinate system depended entirely on the cameras and had no logical relation with the specimen [1]. Therefore, it was necessary to define the coordinate axis of the specimen based on the geometry. Hence a 3-2-1 transformation should be applied to the specimen. After computation, the results could be viewed in the evaluation mode where displacement and strain fields could also be visualized. The DIC software could help cut the computed 3D data in to sections. Filters could also be used to eliminate any unwanted noise within the specimen pattern. Interpolation may be done in order to fill any void 3D spaces. Analysis elements could also be used to evaluate the deformation in a material. Point to point distance analysis elements was usually used to calculate the deformations in the specimen under test. Following this, a brief report which included the stage images, strain maps, plots and analysis elements were generated. Figure 18 shows a sample report generated by the DIC software which shows the strain map, stage images, and plots along with the legend of the visualized result. The DIC software uses the principle of triangulation to compute the 3D points on a surface of the specimen under test. A strain value computed is a function of the stretch ratio which can be defined as the ratio of the current length to the original length. The deformation of the specimen under test may be assumed as a solid which changes its form in space over time [1]. This change of a function is its gradient.

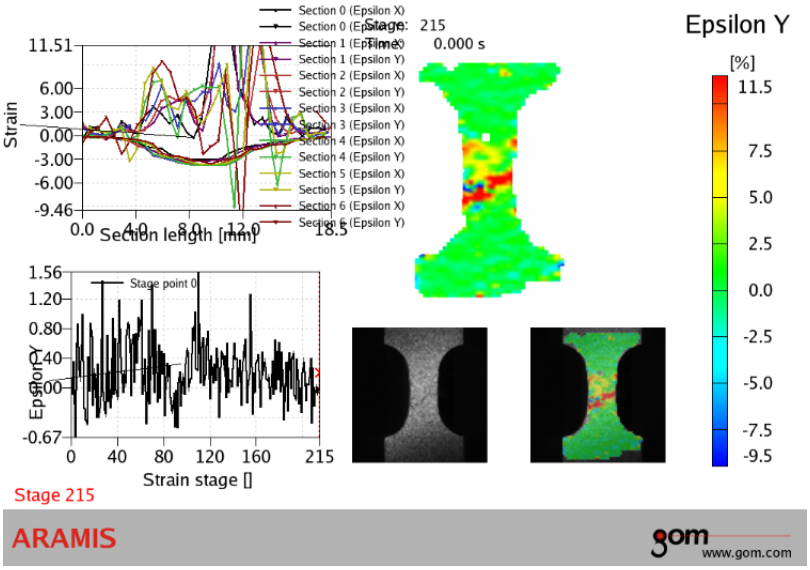

Figure 18 Sample report generated by the DIC software.

This gradient can be represented as a tensor F. The tensor F transforms the element $d\vec{X}$ from its original state to the current state $d\vec{x}$ because of the deformation. Therefore, the deformation gradient can also be represented as

$$d\vec{x} = F.\ d\vec{X} \tag{2.1}$$

In the DIC software, the deformation gradient tensor is modeled to have a single rotation and a stretch matrix. This is surpassed by splitting the deformation tensor into a rotational and a stretch tensor. Therefore

$$F = R.U \tag{2.2}$$

where R contains rotation and U is the stretch tensor.

The stretch tensor usually contains stretch ratios and thus the displacements and strains. It may be represented as

$$U = \begin{pmatrix} U_{11} & U_{12} \\ U_{21} & U_{22} \end{pmatrix} = \begin{pmatrix} \Lambda_{11} & \Lambda_{12} \\ \Lambda_{21} & \Lambda_{22} \end{pmatrix} \text{[2]} \tag{2.3}$$

Values of strains in x and y directions like ε_x and ε_y may be directly read from the stretch tensors [1].

2.2 Dynamic Tensile Testing

The processed composite specimens were subjected to high rates of loading. Strain rates of 10 s^{-1}, 100s^{-1}, 500 s^{-1} and 1000 s^{-1} were considered for the test. Specimens with fiber orientations 0° and 45° were tested at the aforementioned rates of strain. The strain on the surface of the specimen was captured by using a pair of Photron APX-RS high speed cameras. The images were captured in a software called Photron FASTCAM viewer (PFV) and analyzed carefully using the DIC system for the strain maps and Photron FASTCAM analysis (PFA) for additional strain values. Composite specimens were subjected to a tensile loading of 10 s^{-1} and 100 s^{-1} on a servo hydraulic MTS test machine with the capacity of the force transducer as 50 KN. Servo hydraulic machines can be either closed or open loop systems. The actuator in a closed loop system moves at a constant speed where as there is no specific speed that is determined in an open loop system. For the actuator to achieve the specified velocity, a special device called slack adapter is designed to initially provide the free traveling distance [3]. The maximum level of the actuator displacement,

error detectors etc., are usually controlled by a software that communicates with the test system. Figure 19 shows the servo hydraulic test system that was used for testing the specimens under dynamic loading conditions.

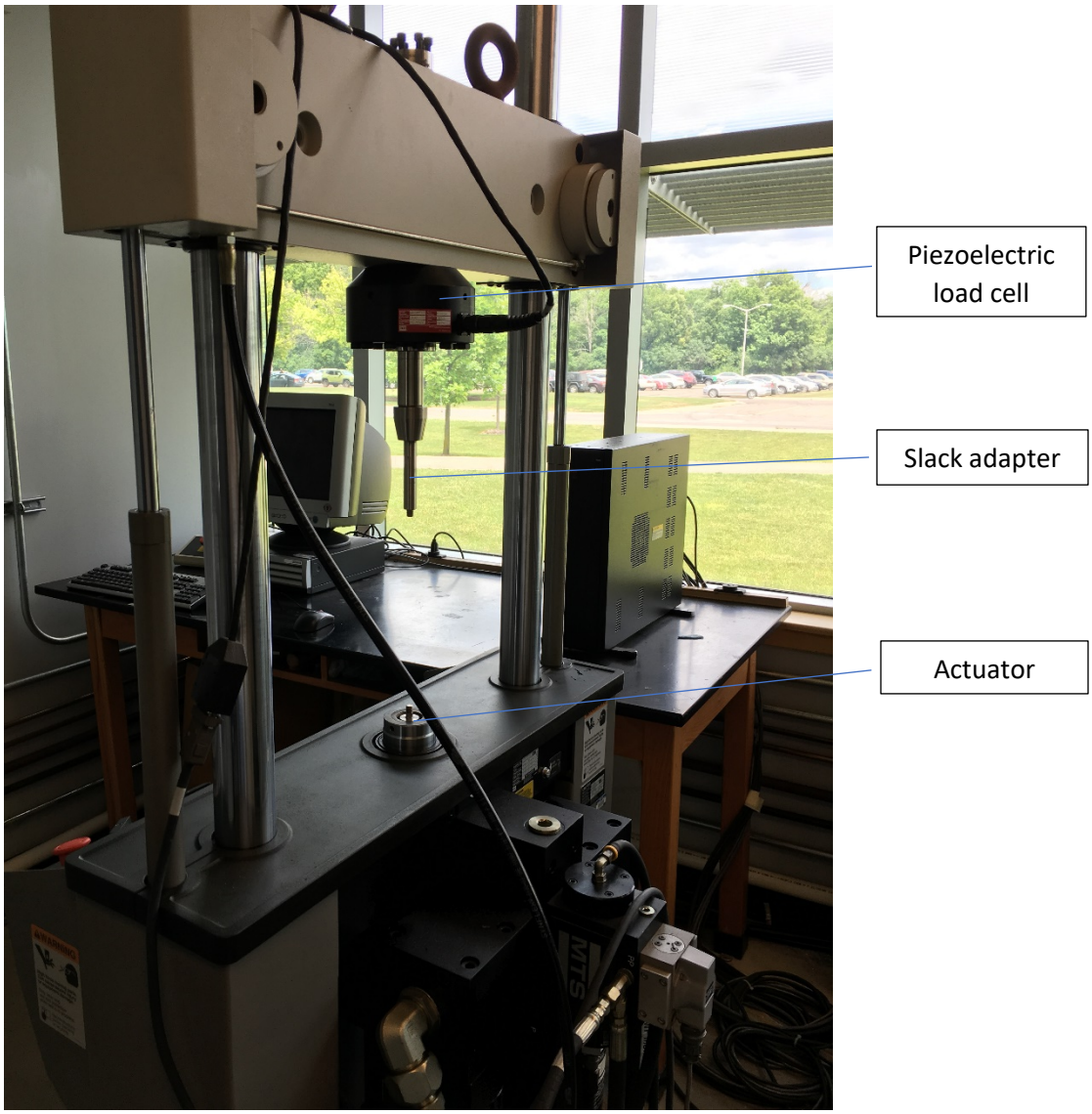

Figure 19 MTS servo hydraulic test system.

The above test system uses a basic MTS testware which has inbuilt procedures and test configurations which controls the test system. A special procedure was specifically designed for running tensile tests at higher rates. The software usually contains different processes in a process palate which can be arranged sequentially to run the desired test. Since the specimens were to be tested at a higher strain rate, the process was designed per the flow chart below.

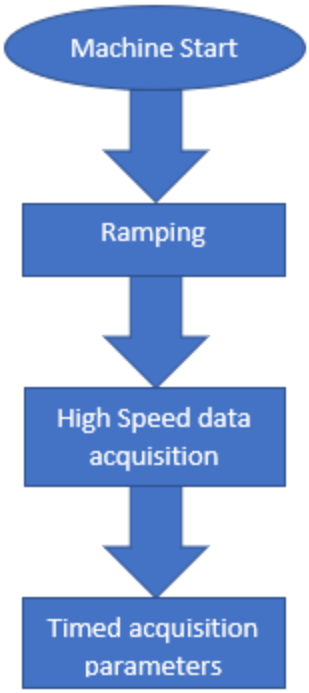

Figure 20 Procedure designed for high strain rate testing.

The ramping step specifies the velocity of the test i.e., the velocity of the actuator and displacement of the actuator. The high-speed data acquisition process has the sampling frequency which is set to 6144 Hz and a sampling duration which depends upon the rate used for testing. The timed acquisition parameters specify the time step for capturing the data points like time, load and displacement of the actuator [8].

2.2.1 Photron Fastcam Viewer (PFV)

A pair of Photron APX-RS cameras were used and were connected to a laptop using an IEEE 1391 cable. Initially, camera 1 was set to be the master camera and camera 2 as the slave so that they both capture the images synchronously [4]. Suitable lenses with an appropriate focal length, which serve the purpose of imaging are generally mounted on to the body of the camera. Photron Fastcam viewer has an inbuilt feature to perform the shading correction also known as calibration. Proper care should be taken while handling the camera and the lenses during calibration. At the time of the calibration, the image sensor should be properly covered with lens cap placed on the lens. Once the calibration is complete, a proper frame rate was selected which generally suits the needs for the high-speed testing. An apt resolution and shutter speed should be selected such that the cameras would record the entire test event. Once the image sensor was calibrated, the measuring volume

was calculated to cover the area in which the material under test can be clearly viewed in the captured images. A frame rate of 30000 fps and a resolution of 256 x 256 was chosen to suit the requirement of the high-speed testing and the geometry of the specimen under testing. Since the captured images were to be analyzed using a DIC system for corresponding strain maps, the surface of the specimens was printed stochastically and was illuminated using a high intensity fiber optic light. The measuring volume was also calibrated in accordance with the calibration procedure within the DIC software. A trigger mode of "random" was selected from the dropdown in the settings menu of the PFV and calibration images were acquired. These images were further transferred into DIC software using Import→Stage Data→ from external image series. The camera that was used for capturing of these images was to be specified prior to adding of the image series. Figure 21 shows the schematic layout of the high strain rate test setup.

Figure 21 Test setup for high speed tensile testing.

A separate pair of fixtures were used to clamp the specimen on to the MTS test system. They included a slot to accommodate wedges which hold the specimen firmly without any slip. Figure 22 shows the test fixture clamped on to the MTS test system.

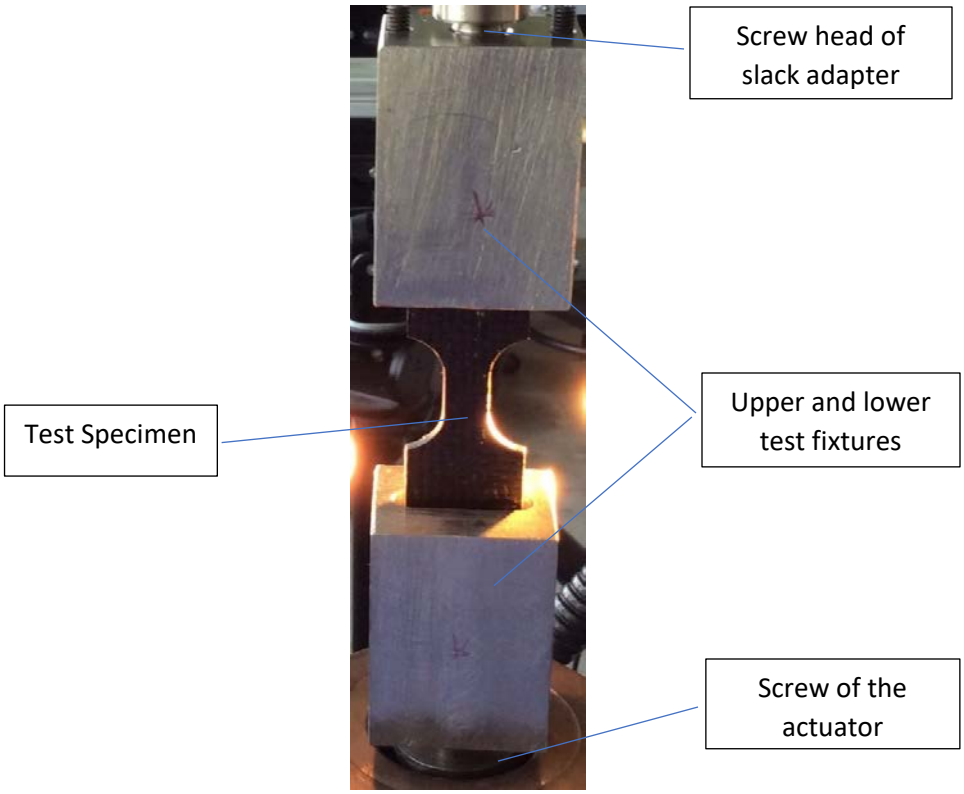

Figure 22 Test fixture for high strain rate testing.

Once the test fixture was clamped on to the test system, the surface of the test specimen was illuminated, and a pretest was performed on the specimen by capturing a couple of images and processing them in the DIC software. Once the strain patterns from the pretest were obtained, the trigger mode could be changed to "start" in the settings. Whenever the frame rate/trigger/resolution was altered, it was necessary to check the gray scale of the image sensor. Once the image sensor was calibrated, the MTS test system is checked for any warnings before turning it on. Limits and error detectors were set such that the test system does not stop in between the event of the test. The cameras started recording the event when the "start" trigger mode in PFV was pressed. The cameras continued to record until the memory was full. It was mandatory to run the MTS test system and cameras simultaneously during the event of the test. Once the recording was complete, all the images were saved to the memory of the camera. A suitable playback area which covered the entire event desirable for further analysis was saved (approximately 200-300 images). The saved images were imported into Photron Fastcam analysis (PFA) for calculations of displacement and the strain.

2.2.2 Photron Fastcam Analysis

With Photron fastcam analysis (PFA), it was possible to analyze the image sequence that was imported from PFV to obtain the values of displacement, velocity, and acceleration. These can be exported to a .csv (comma separated value) file [5]. Upon importing the image sequence into the PFA, the frame rate that was used during the recording event should be specified. Once the images were ready for the analysis, tracker points which are similar to the points in a coordinate system were created. In addition, a scale was created and the distance between the tracker points was specified so that all the further analysis was carried out with respect to the scale that was set. Once the analysis is concluded, a csv file which contains the coordinates for the tracker points, velocity, and acceleration for each of the images in the image sequence was exported for further calculations. The following method was used for the calculation of strain.

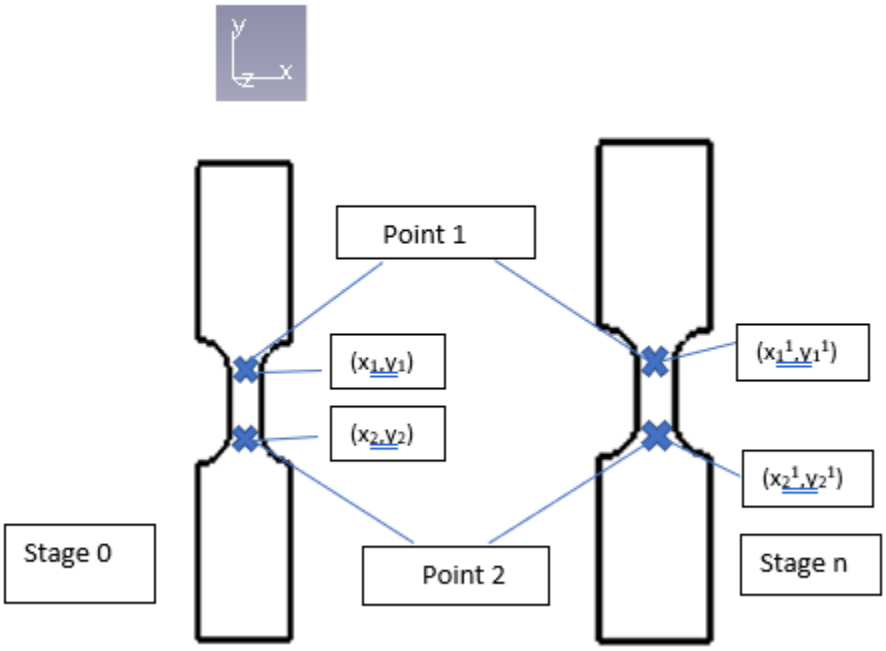

Figure 23 Stage representation in PFA.

Figure 23 shows the stage representation of the tensile test event. Once the file containing the displacements was exported, it contained the coordinates of point 1 and point 2 across all the images in the image series. Here, Strain was defined as the ratio of change in length over an original length. Stage 0 was considered as where the specimen is not under deformation. Therefore, two

trackers were placed in the gage section of the specimen. The distance between these two points was given by

$$D = \sqrt{(y_2-y_1)^2+(x_2-x_1)^2} \tag{2.4}$$

Upon deformation of the specimen, there would be a change in the co-ordinates of the tracker points because of a very little elongation. The distance between the tracker points after deformation was given by

$$D1 = \sqrt{(y_2^1-y_1^1)^2+(x_2^1-x_1^1)^2} \tag{2.5}$$

Therefore, from the equations (2.4) and (2.5), the strain was calculated as

$$\varepsilon = (D^1 - D)/D \tag{2.6}$$

2.2.3 Pneumatic Tensile Testing System

For strain rates, higher than $100s^{-1,}$ an inhouse built pneumatic tensile testing system was used. The system comprises of a pressure vessel with a pressure capacity of 1,600 psi and a volume of 2,250 cm^3 connected through a high speed-high pressure solenoid valve that is connected to an approximately 1.8m long thick steel barrel. The system is coupled to a gas booster which boosts the air pressure from 80 psi to 1200 psi. The machine also has a high pressure digital meter along with a valve to let the pressurized air into the pressure vessel. It is equipped with a safe release valve to let the pressurized air out of the chamber. A striker bar as shown in Figure 24 was pushed through the steel barrel, to hit the tensile testing fixture.

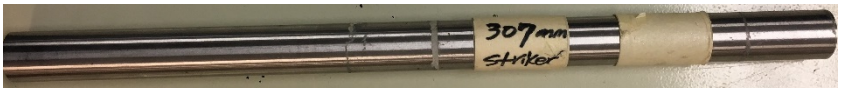

Figure 24 Striker bar used for impact tests.

The pressure that is needed to achieve the required rate of loading was pre-calibrated. Figure 25 shows the typical layout of the pneumatic tensile test system.

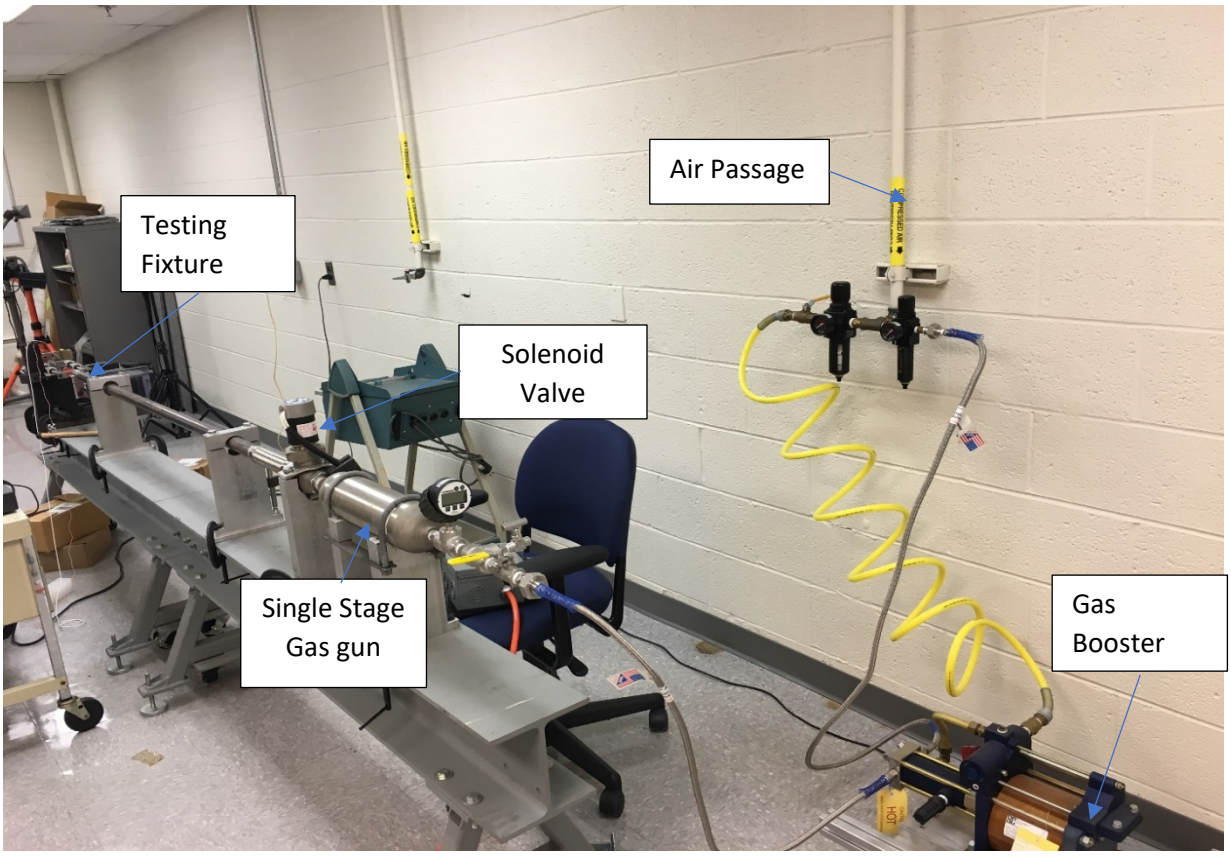

Figure 25 Pneumatic tensile testing system (PTTS)

The PTTS was also equipped with an integrated circuit piezoelectric (ICP) sensor to measure load and another ICP sensor which gives an acceleration output. The ICP sensor contains a material made of piezoelectric material which converts the mechanical signal into an electrical signal. Figure 26 shows the load sensor and accelerometer used for measurement of load and acceleration.

Figure 26 accelerometer and a load sensor. [6]

2.2.4 LMS Testlab

The ICP sensors were connected to the front end of LMS Scadas V8 which consists of 4 input ports. The signals were tracked using the LMS Testlab 14.0 software in the signature acquisition module. The LMS scadas data acquisition system has a sampling rate of 100 kHz. Before measuring the project in the signature testing module of the Testlab, the sensitivity and the range

of the sensors were specified. The measure worksheet in the signature testing module accommodates the measurement for the required parameters in the test. Prior to the data acquisition, the sensors were armed for the measurement. After the measurement started, the trigger for the PTTS and the remote trigger of the camera were simultaneously pressed so that the entire event of the test was recorded. The measurement in the LMS Testlab should be stopped immediately after the test was concluded. The system was disengaged before making any further analysis. The force vs time and acceleration vs time plots were obtained from the navigator pane in the Testlab. For this, time domain integration must be done which is possible by enabling the time data editor-advanced add-in in the tools option of the Testlab. To ensure accurate displacement values, double integration of the acceleration vs time data was done. However, the obtained acceleration vs time data needs to be subjected to a set of conditions to achieve an accurate displacement vs time. Any low frequency components in the acceleration vs time were filtered to avoid variations in the data while integrating it. To remove the linearization errors in the data, it was up- sampled by four times the original sampling frequency (=4 x 2048,000Hz). A bandwidth of 1024,000 Hz was used for the data acquisition; hence the sampling frequency was twice the bandwidth (=2 x 1024,000Hz). Once the data linearization was done, it must be double integrated to obtain the displacement vs time curve. This was followed by resampling the data back to the original sampling frequency and filtering the data to remove any constants that were obtained because of the double integration [7].

References

[1] GOM mbh, 2009, *ARAMIS V 6.1 User manual.*

[2] GOM mbh, “Technical document on strain computation”.

[3] Borsutzki, Michael., 2005, “Recommendations for dynamic tensile testing of steel sheets,” International Iron and Steel Institute.

[4] Photron Limited, 2005, *Photron FASTCAM Viewer Operation Manual V2.431*

[5] Photron Limited, 2013, *Photron FASTCAM Analysis Operation Manual V1.3.1*

[6] PCB Inc., Specification sheets of load sensor and accelerometer.

[7] Siemens PLM., “Technical Document on Time Domain Integration.

[8] MTS test manual.

CHAPTER 3. RESULTS & DISCUSSIONS

3.1 Quasi Static Tensile Properties

In this research project, the tensile properties that include peak stress and maximum strain at failure were investigated on carbon and glass fiber reinforced composites. Specimens were subjected to tensile loading on a universal testing machine. Figure 27 shows some of the common failure modes that can be expected when a composite test coupon is subjected to a tensile loading.

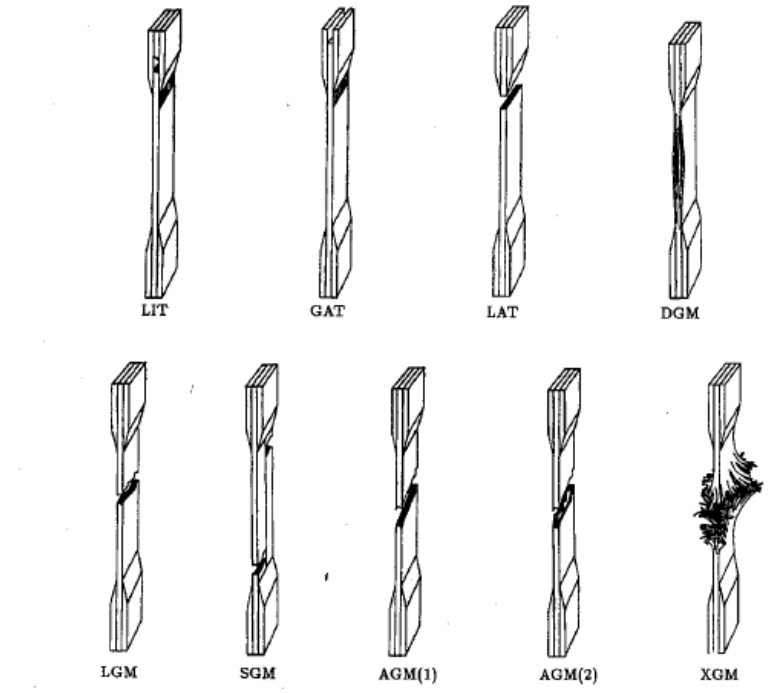

First Character

Failure Type	Code
Angled	A
edge Delamination	D
Grip/tab	G
Lateral	L
Multi-mode	M(xyz)
long. Splitting	S
eXplosive	X
Other	O

Second Character

Failure Area	Code
Inside grip/tab	I
At grip/tab	A
<1W from grip/tab	W
Gage	G
Multiple areas	M
Various	V
Unknown	U

Third Character

Failure Location	Code
Bottom	B
Top	T
Left	L
Right	R
Middle	M
Various	V
Unknown	U

Figure 27 Different types of failure modes of fiber reinforced composites subjected to tensile loading. [1]

3.1.1 3K 2x2 twill woven carbon fiber

A woven composite usually consists of two components used in weaving: warp and weft. In a fabric loom, the warp yarns are usually held in tension and the weft yarns usually go above and below the warp yarns. The specimens that are loaded along the warp direction is 0° in this investigation. As a result, the specimens along 0° direction has the higher load bearing capacity and hence are subjected to higher stresses. Figure 28 shows a typical stress-strain behavior of the test coupon tested at a rate of 0.0025 s^{-1}. The coupon was tested until it experiences a complete fracture.

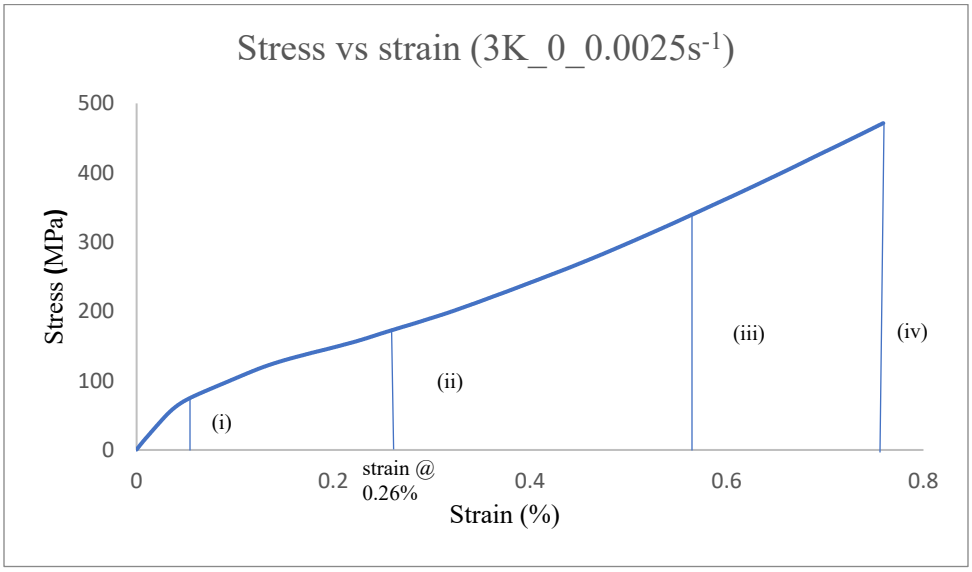

Figure 28 Tensile stress-strain behavior of 3K 2x2 twill woven carbon fiber based composite tested along the 0° orientation at a rate of 0.0025 s^{-1}.

The 3K 2x2 twill woven carbon fiber coupons exhibited an average peak stress of 468 MPa and average strain to failure is 0.75%. The modulus of elasticity was evaluated from the slope of the stress-strain curves. Figure 29 shows low magnification optical micrographs of a 3K-0° test coupon after failure when subjected to a tensile loading at a strain rate of 0.0025 s^{-1}.

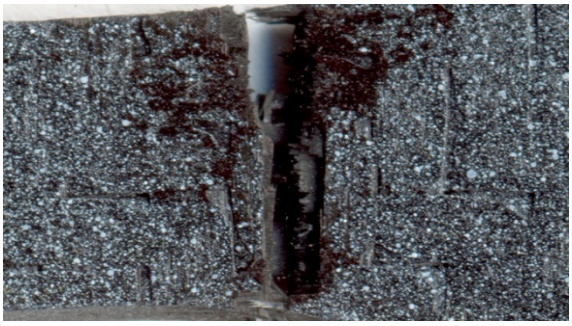

(a)

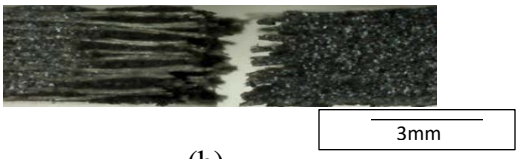

(b)

Figure 29 Low magnification 3K- 0° optical micrograph of specimens under tensile loading at a rate of 0.0025 s^{-1} (a) front view (b) thickness view.

From the Figure 29 and types of failure suggested in Figure 27, it is evident that the failure is of type Lateral (L), Gage (G) area and in the middle (M). Therefore, this is considered as LGM failure mode according to the ASTM 3039 test standards [1]. In addition, it can be seen from the optical micrographs that the failure of the coupon is not explosive, but there was a considerable amount of fiber breakage and pullout resulting in the failure of the test coupon. Figure 29 (b) shows that there is no considerable delamination that has taken place beyond the fracture location and through the length of the specimen. Figure 30(a) and (b) shows the strain evolution and strain distribution pattern of the test coupon prior to failure that is computed using the DIC system. From Figure 30 (a), it is evident that the gage area of the test coupon is subjected to a higher failure strain.

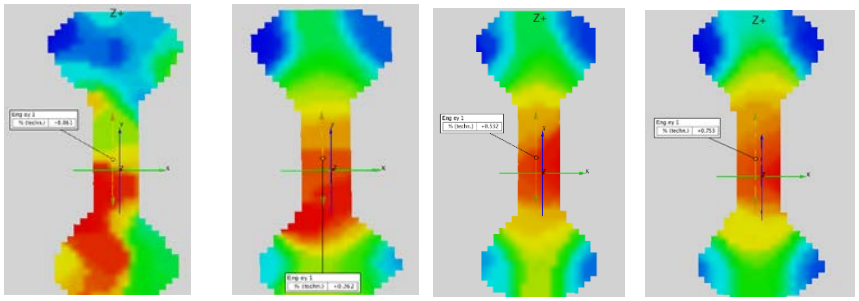

(i) (ii) (iii) (iv)

(a)

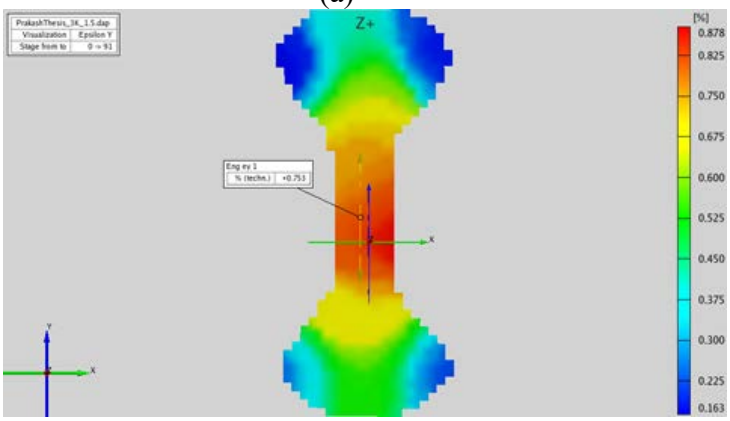

(b)

Figure 30 (a) and (b) DIC strain evolution and distribution pattern for 3K-0° specimen subjected to loading at a rate of 0.0025s^{-1}.

From the above figure, the portion of the gauge at which the failure has occurred has a maximum strain of 0.753 %.

Figure 31 shows a typical stress-strain plot of 3K 2x2 twill woven test coupons subjected to a tensile loading at a strain rate of 0.25 s^{-1}.

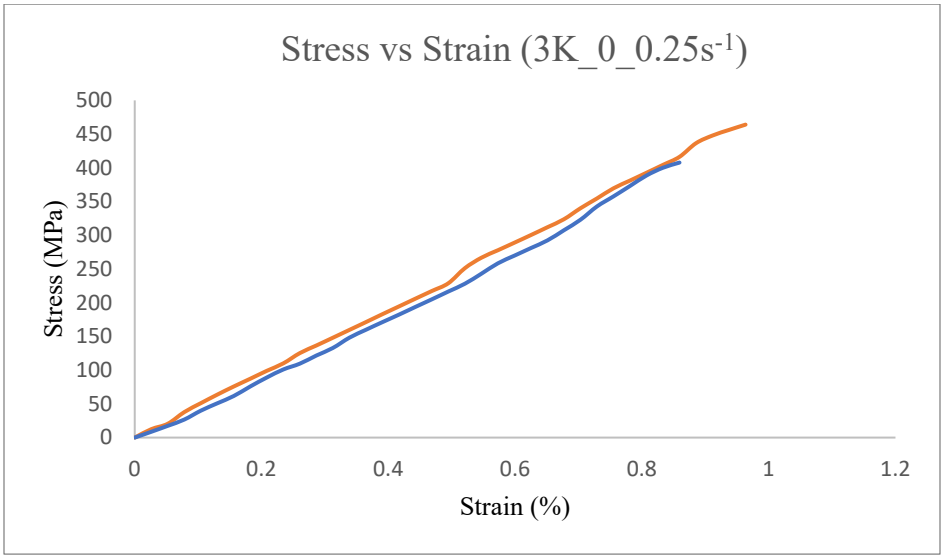

Figure 31 Tensile stress-strain behavior of 3K 2x2 twill woven carbon fiber based composite tested along the 0° orientation at a rate of 0.25 s^{-1}.

The 3K 2x2 twill woven carbon fiber test coupons exhibited an average peak stress of 428 MPa and an average strain to failure of 0.9%. Figure 32 (a) & (b) shows low magnification optical micrograph of 3K-0º 2x2 twill woven carbon fiber after the failure that is subjected to a tensile loading at a rate of 0.25s^{-1}.

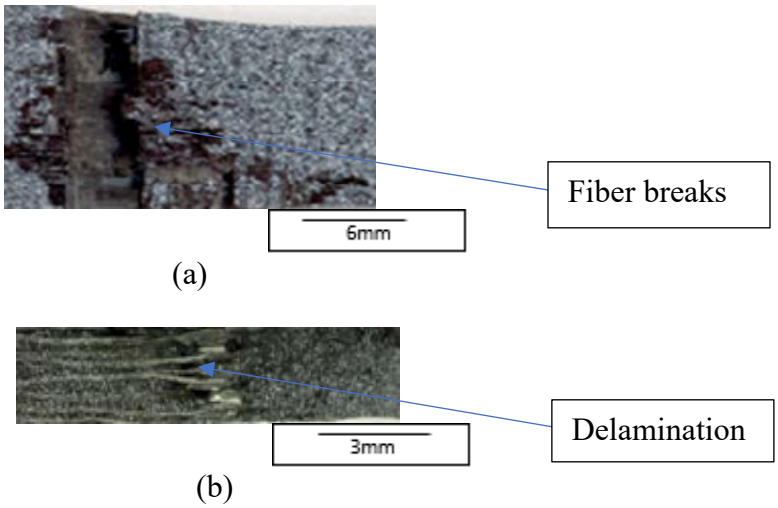

Figure 32 Low magnification 3K- 0° optical micrograph of specimens under tensile loading at a rate of 0.25 s^{-1} (a) front view (b) thickness view.

From Figure 32 (b), a small amount of delamination is observed as the test coupons are subjected to higher loading rates. A little amount of fiber breakage and pullout can also be seen. In addition, it can be observed from the Figure 32 (a) that the mode of failure is Lateral(L), occurred in the Gage area (G) and in the middle (M). This is considered as an LGM failure mode as per the ASTM 3039 test standards [1].

Figure 33 shows a typical strain distribution pattern of a test coupon just before the failure. From the figure, it is evident that the portion of the gage at which the failure occurred has a maximum strain and is the location of failure.

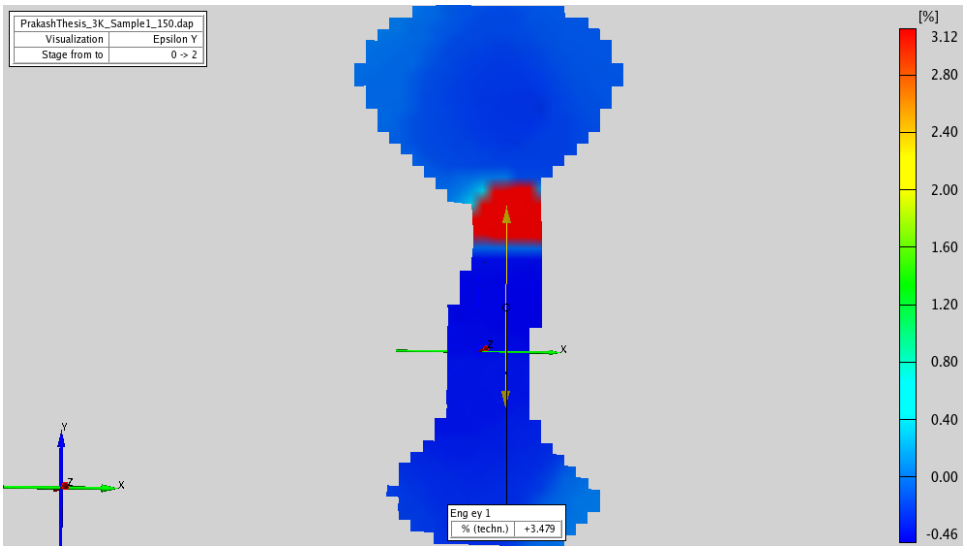

Figure 33 DIC strain distribution pattern at failure for a test coupon subjected to a tensile rate of 0.25 s^{-1}.

Figure 34 shows a typical stress-strain behavior of a 3K 2x2 twill woven carbon fiber composite tested along 45°.

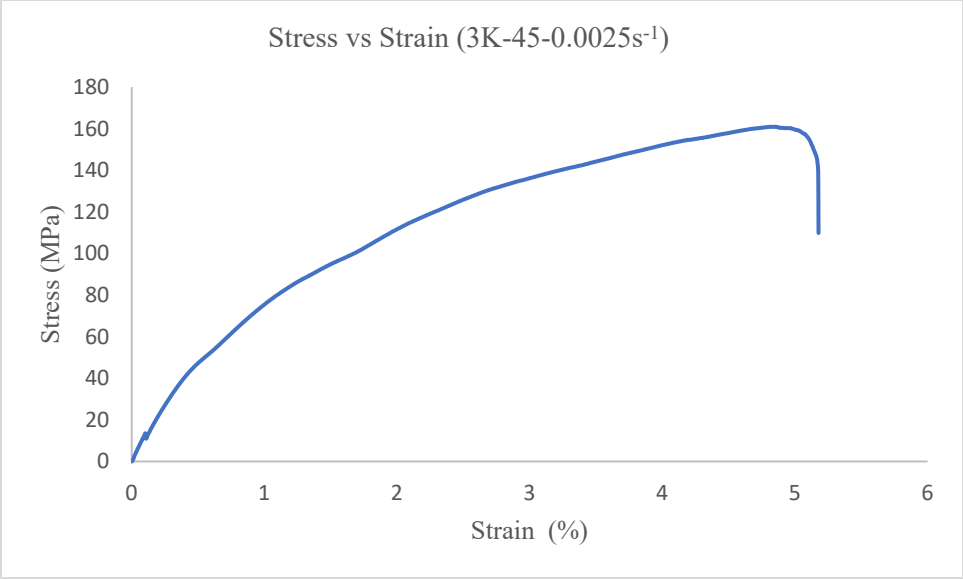

Figure 34 Tensile stress-strain behavior of 3K 2x2 twill woven carbon fiber based composite tested along the 45° orientation at a rate of 0.0025s^{-1}.

The 3K 2x2 twill woven carbon fiber coupons exhibited a peak stress of 161 MPa and an average strain to failure is 5.17%. Figure 35 (a) and (b) shows low magnification optical micrographs of a 3K-45° test coupon after failure when subjected to a tensile loading at a strain rate of 0.0025 s^{-1}.

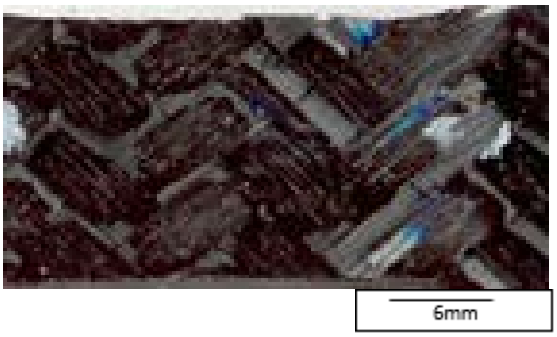

(a)

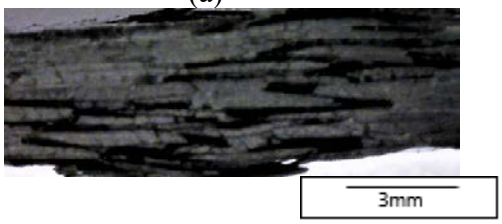

(b)

Figure 35 (a) and (b) Low magnification 3K- 45°optical micrograph of specimens under tensile loading at a rate of 0.0025 s^{-1} (a) front view (b) thickness view.

From the Figure 35 and types of failure suggested in Figure 27, it is evident that the failure is of type Angular (A), occurred in Gage Area (G) and in the middle of the Gage (M). Therefore, this is considered as AGM failure mode according to the ASTM 3039 test standards. Figure 35 (b) shows that there is a considerable delamination that has taken place at the fracture location. Figure 36 shows a typical stress-strain plot of 3K 2x2 twill woven test coupons subjected to a tensile loading at a strain rate of 0.25 s^{-1}.

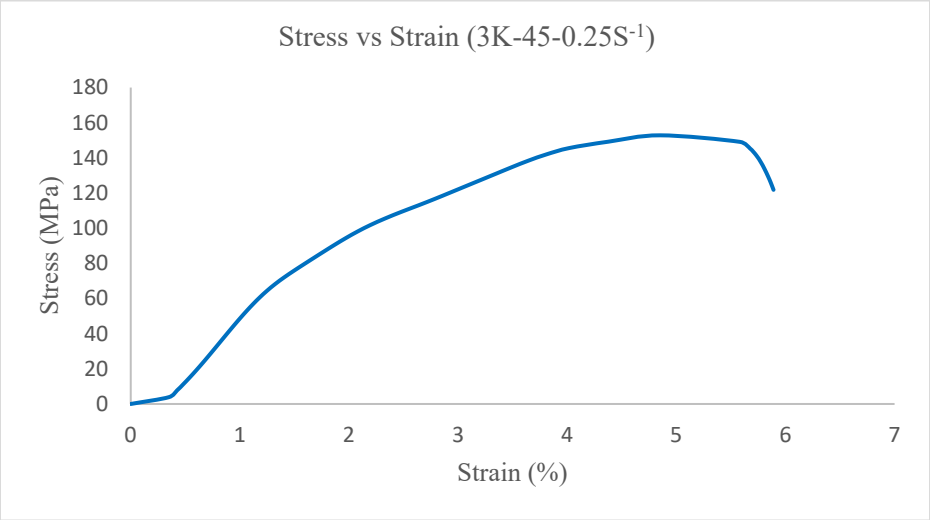

Figure 36 Tensile stress-strain behavior of 3K 2x2 twill woven carbon fiber based composite tested along the 45° orientation at a rate of 0.25s^{-1}.

The 3K 2x2 twill woven carbon fiber test coupon exhibited a peak stress of 153 MPa and a strain to failure of 5.7 %. Figure 37 shows low magnification optical micrographs of a 3K-45° test coupon after failure when subjected to a tensile loading at a strain rate of 0.25 s^{-1}.

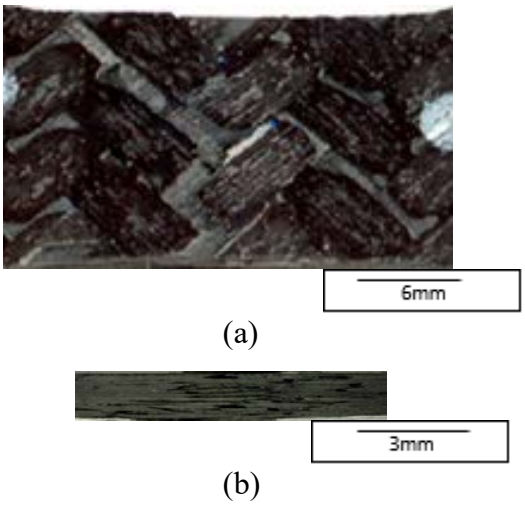

Figure 37 Low magnification 3K- 45°optical micrograph of specimens under loading at a rate of 0.25 s^{-1} (a) front view (b) thickness view.

From the Figure 37 and the types of failures suggested in Figure 27, it is evident that the failure is of type Angular (A), occurred in the gage Area (G) and in the middle of the gage section (M). Therefore, this is considered as AGM failure mode according to the ASTM 3039 test standards. There is a considerable amount of delamination in the region of the fracture.

3.1.2 12K 2x2 twill woven carbon fiber

The 12K carbon fiber test coupon contains 12000 filaments/fibers in a tow thus making it stronger than 3K. Specimens with fibers oriented along the warp direction are considered as 0° in this investigation. Figure 38 shows the stress-strain curve for 12K 2x2 twill woven carbon fiber test coupon when subjected to a tensile loading at a strain rate of 0.0025 s^{-1}.

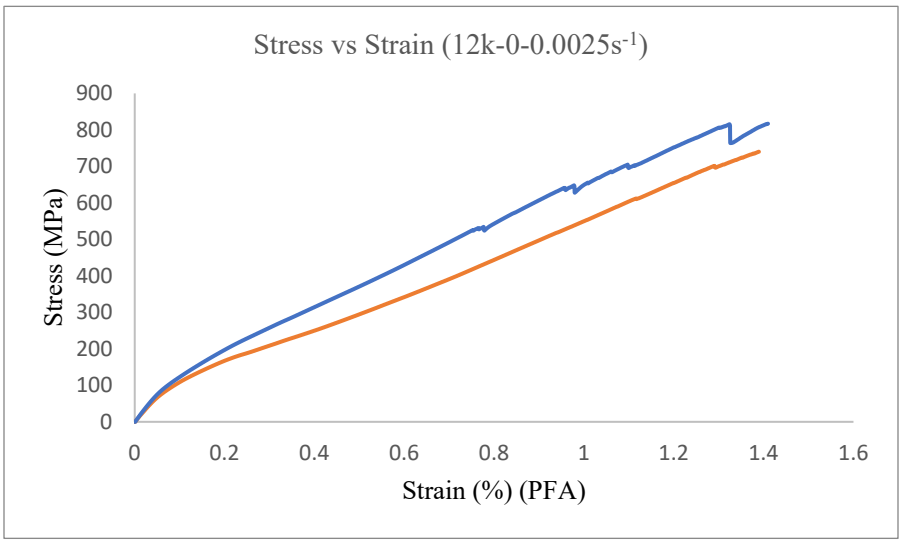

Figure 38 Tensile stress-strain behavior of 12K 2x2 twill woven carbon fiber based composite tested along the 0° orientation at a rate of 0.0025s^{-1}.

The variations in the graph are because of the intermittent failure of the fibers and the matrix. Because of the presence of higher number of fibers in the tow, the maximum stress that the test coupon can withstand is relatively higher thus making these test coupons suitable for manufacturing structural components that require higher strength. The 12K 2x2 twill woven carbon fiber exhibited an average peak stress of 778 MPa and an average strain to failure of 1.39% Figure 39 (a) & (b) shows a low magnification optical micrograph of 12K-0º after failure when the test coupons are subjected to a tensile loading condition at a rate of 0.0025 s^{-1}.

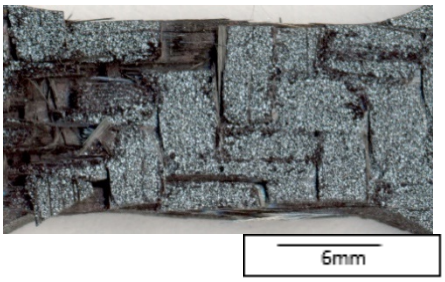

(a)

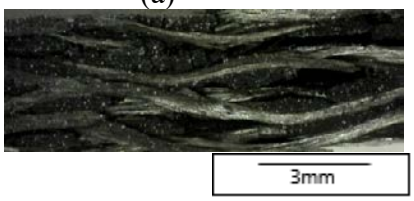

(b)

Figure 39 (a) & (b) Low magnification 12K- 0° optical micrograph of specimens under tensile loading at a rate of 0.0025 s^{-1} (a) front view (b) thickness view.

It is evident from the micrograph that the mode of failure is lateral (L), occurs in gage section (G) and in the middle of the specimen (M). Hence it is considered as LGM failure mode as per the ASTM 3039 standards [1]. Also, there is a notable amount of delamination within the test coupon and also some amount of fiber pullout as represented in Figure 39 (b). There are also several micro cracks and fiber breaks as observed in Figure 39 (a). Figure 40 shows the DIC strain distribution pattern prior to failure.

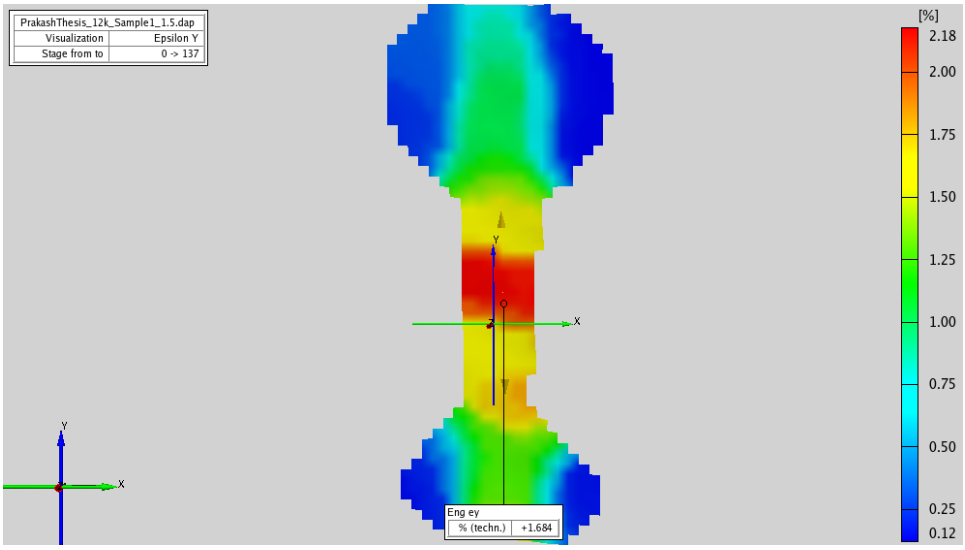

Figure 40 DIC strain pattern for a test coupon at failure subjected to a tensile loading at a rate of 0.0025s^{-1}.

Figure 40 shows the area at which the test coupon has undergone a maximum strain of 1.6% prior to failure.

Figure 41 shows the linear stress strain behavior of a 12K 2x2 twill woven carbon fiber test coupon subjected to a tensile loading at a rate of 0.25 s^{-1}. The material exhibits a linear behavior until the onset of fracture.

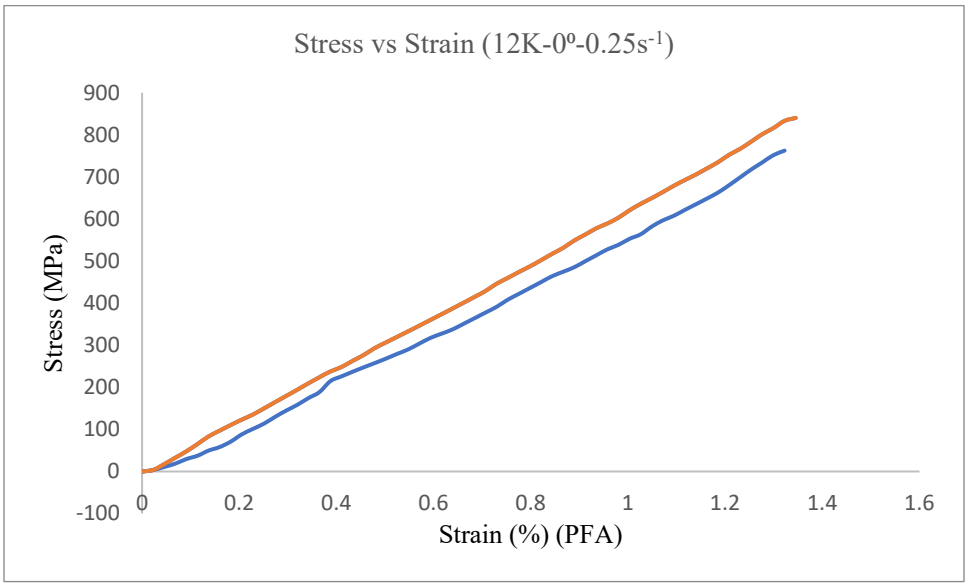

Figure 41 Tensile stress-strain behavior of 12K 2x2 twill woven carbon fiber based composite tested along the 0° orientation at a rate of 0.25 s^{-1}.

The 12K test coupon exhibits an average peak stress of 801 MPa and an average peak strain of 1.33 %. Figure 42 represents the low magnification optical micrograph of 12K-0º 2x2 twill woven carbon fiber test coupon after failure subjected to a tensile loading at a rate of 0.25 s^{-1}.

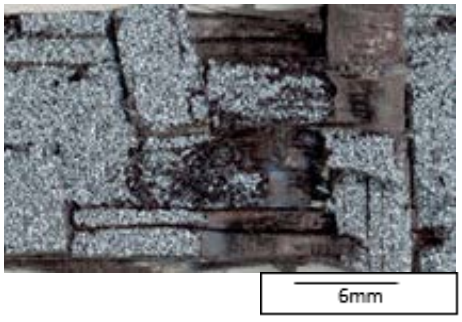

(a)

(b)

Figure 42 Low magnification 12K- 0° optical micrograph of specimens under tensile loading at a rate of 0.25 s^{-1} (a) front view (b) thickness view.

Figure 42 (a) shows the damage of the test coupon. From the micrograph and from the Figure 27, it is evident that the failure mode is explosive (X), occurred in the gage (G) and in the middle of the specimen (M). Hence it is an XGM failure mode per the ASTM 3039 test standards. Figure 42 (b) shows a significant amount of damage caused by delamination and fiber pullout as well. Figure 43 shows the strain distribution pattern at failure that was computed using DIC software.

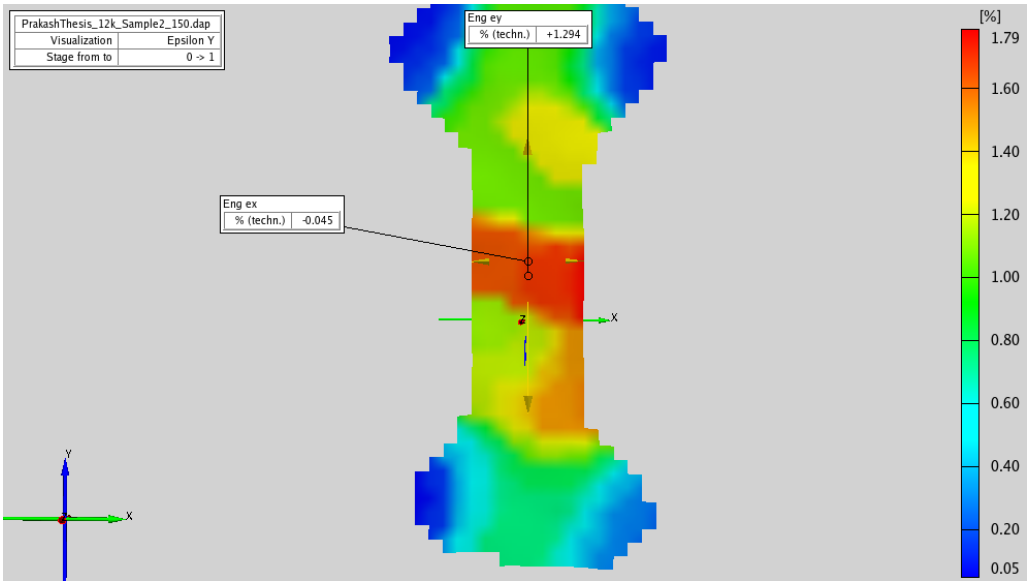

Figure 43 DIC strain pattern for a test coupon at failure subjected to a tensile loading at a rate of 0.25s^{-1}.

It can be seen from the Figure 43 that the strain is more localized and is greater at the area of failure with a maximum strain of 1.29%.

Figure 44 shows typical stress-strain curves for 12K 2x2 twill woven carbon fiber oriented at 45° subjected to a tensile strain rate of 0.0025 s^{-1}.

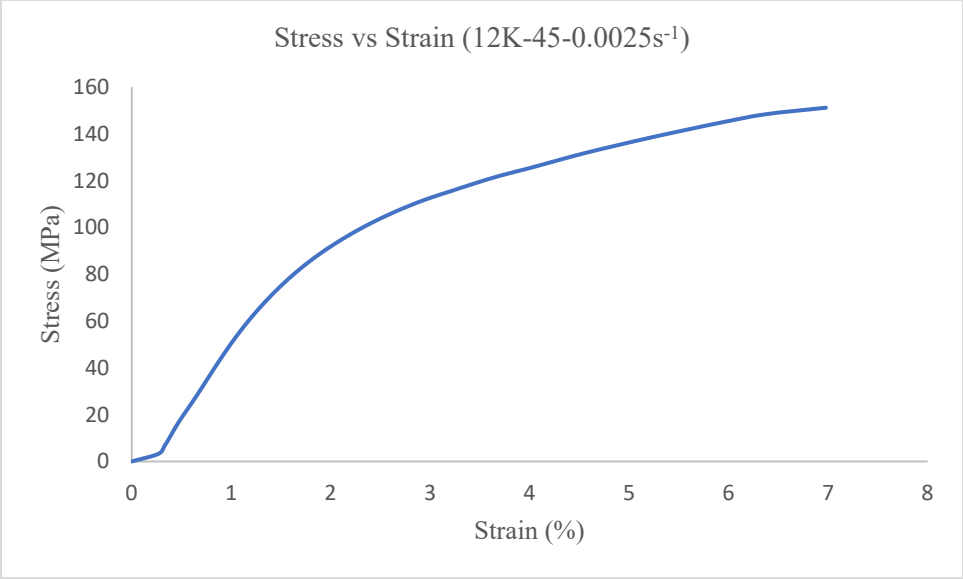

Figure 44 Tensile stress-strain behavior of 12K 2x2 twill woven carbon fiber based composite tested along the 45° orientation at a rate of 0.0025s^{-1}.

The 12K 2x2 twill woven carbon fiber exhibited a peak stress of 151 MPa and an average strain to failure of 6.97%. Figure 45 (a) and (b) show low magnification optical micrographs of 12K - 45° after failure when subjected to a tensile loading at a strain rate of 0.0025 s^{-1}.

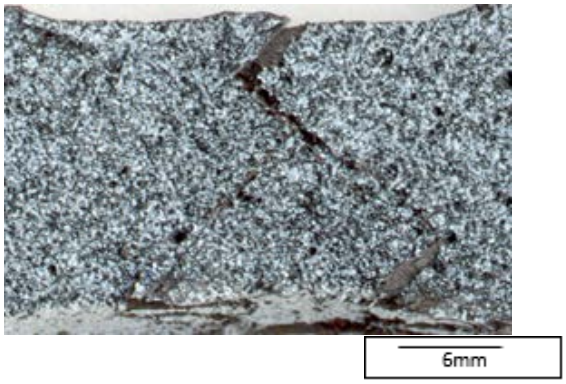

(a)

(b)

Figure 45 Low magnification 12K- 45° optical micrograph of specimens under tensile loading at a rate of 0.0025 s^{-1} (a) front view (b) thickness view.

From the Figure 45 and types of failure suggested in Figure 27, it is evident that the failure is of type Angular (A), in the Gage area (G) and in the Middle of the gage location (M). Therefore, this

is considered as AGM failure mode according to the ASTM 3039 test standards. In addition, it can be seen from the micrographs that the failure of coupon occurs due to a little amount of delamination in the region of fracture. Figure 46 shows typical stress-strain curve for 12K 2x2 twill woven carbon fiber oriented at 45°subjected to a tensile strain rate of 0.25 s^{-1}.

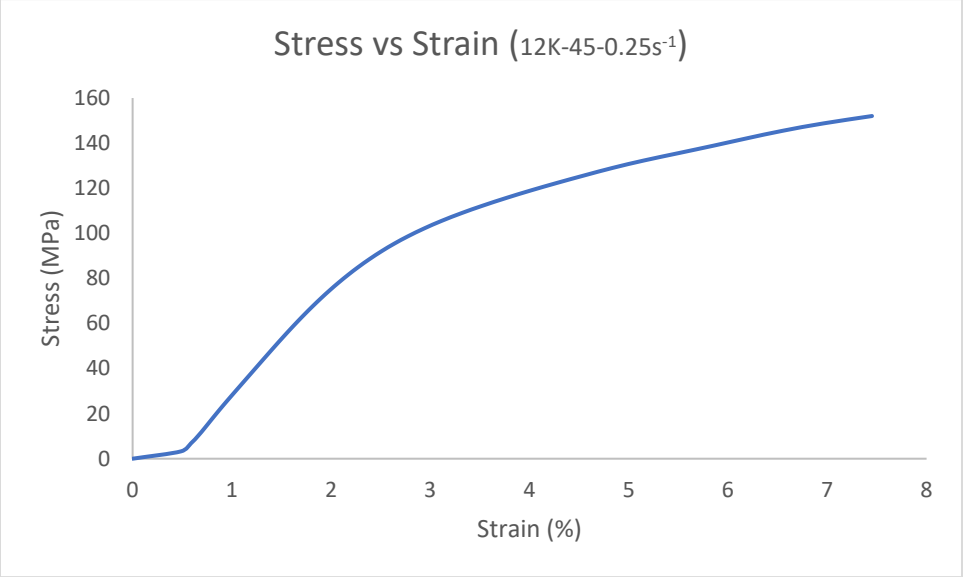

Figure 46 Tensile stress-strain behavior of 12K 2x2 twill woven carbon fiber based composite tested along the 45° orientation at a rate of 0.25s^{-1}.

The 12K 2x2 twill woven carbon fiber composite has a peak stress of 152 MPa and a strain to failure of 7.45%. Figure 47 shows low magnification optical micrographs of a 12K-45° test coupon after failure when subjected to a tensile loading at a strain rate of 0.25 s^{-1}.

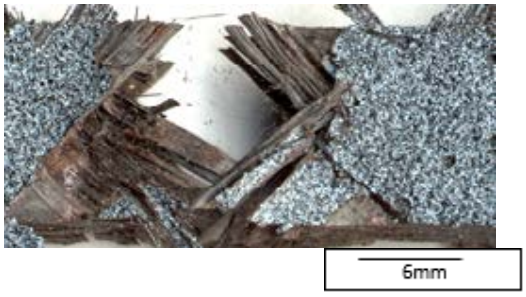

(a)

(b)

Figure 47 Low magnification 12K- 45° optical micrograph of specimens under tensile loading at a rate of 0.25s^{-1} (a) front view (b) thickness view.

From the Figure 47 (a) and types of failure suggested in Figure 27 it is evident that the failure is of type Angular (A), occurred in the Gage (G) and in middle (M) of the specimen. Therefore, this is considered as AGM failure mode according to ASTM 3039 standards. It is evident from Figure 47 (b) that there is a considerable amount of delamination with fiber pullout.

3.1.3 Glass fiber 8HS – 7781

The glass fiber satin weave generally has less folds in the intersection of warp and weft because of the pattern of the weave hence making it easier to distort as compared to that of a normal plain weave pattern. Figure 48 shows a typical stress-strain behavior of glass fiber 8HS 7781 test coupon subjected to a tensile loading along the warp direction at a loading rate of 0.0025 s^{-1}.

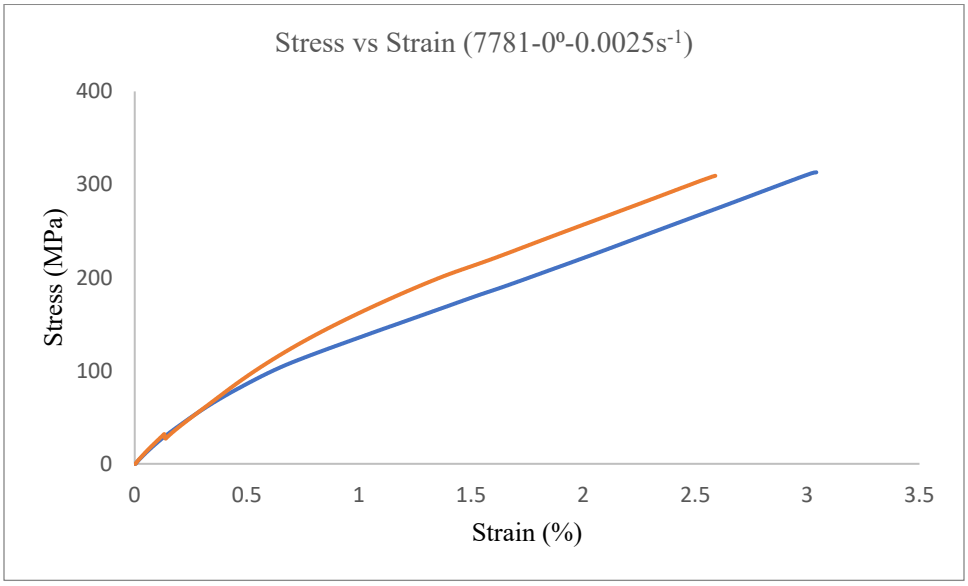

Figure 48 Tensile stress-strain behavior of 8HS 7781 glass fiber based composite tested along the 0° orientation at a rate of 0.0025s^{-1}.

The 8HS Glass fiber 7781 test coupon exhibits an average stress of 311 MPa and an average failure stress of 2.81 %. The higher strain to failure is because of the distortion of the fibers along warp and weft directions. Figure 49 (a) & (b) represents the low magnification optical micrographs at failure when the test coupons are subjected to a tensile loading at a rate of 0.0025s^{-1}.

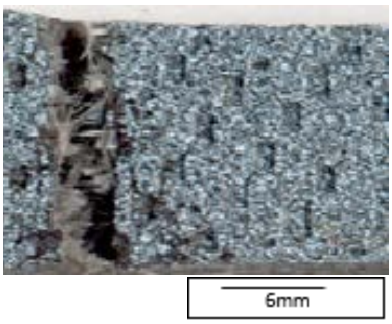

Figure 49 (a) & (b) Low magnification 7781 8HS glass fiber 0° optical micrograph of specimens under tensile loading at a rate of 0.0025 s^{-1} (a) front view (b) thickness view.

It is evident from the figure 49 (a) that the failure mode is of lateral (L) type. Occurred in the gage (G) and in the middle (M). Hence it can be summarized as an LGM failure mode per ASTM 3039 test standards for fiber reinforced composites. Figure 49 (b) shows a little delamination at the area of the fracture. The gage section of the test coupon shows a higher strain in the DIC strain map as shown in Figure 50.

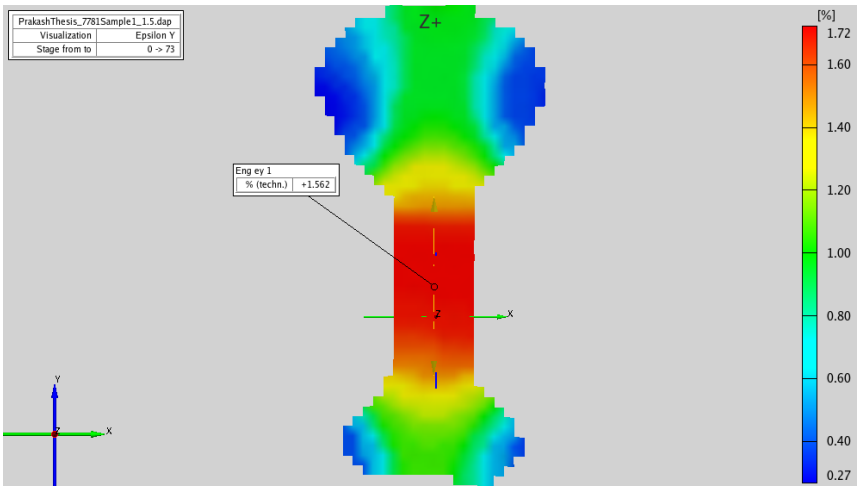

Figure 50 DIC strain distribution of glass fiber 8HS 7781 test coupon prior to failure subjected to a tensile strain rate of 0.0025 s^{-1}.

Figure 51 shows a typical stress-strain relationship of glass fiber 8HS 7781 test coupon subjected to a tensile loading at a strain rate of 0.25 s^{-1}.

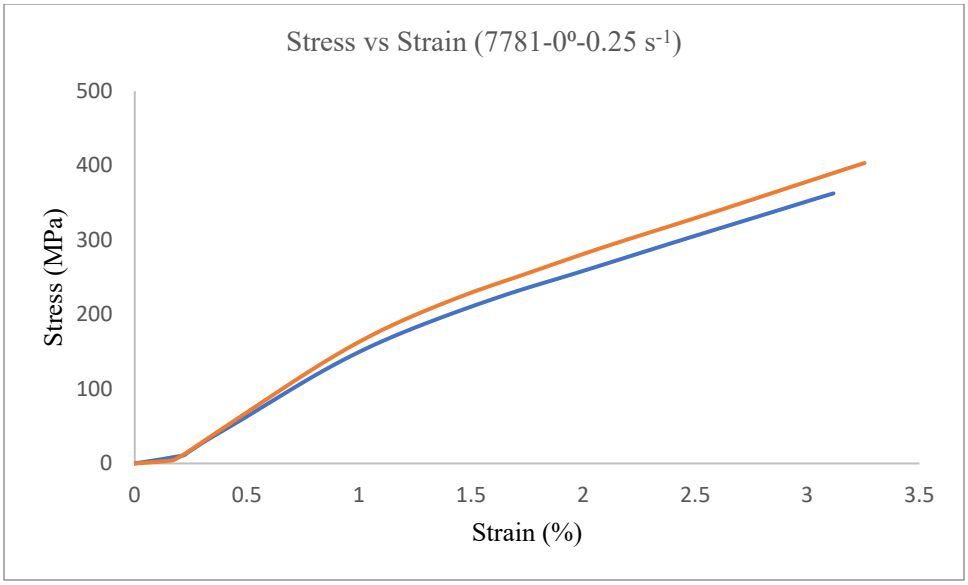

Figure 51 Tensile stress-strain behavior of 8HS 7781 glass fiber based composite tested along the 0° orientation at a rate of 0.25s^{-1}.

It is evident from the above graph that the glass fiber 7781 has an average peak stress of 382 MPa and an average maximum strain at failure as 3.18 %. Figure 52 (a) & (b) shows low magnification optical micrographs of glass fiber 8HS 7781 test coupons after failure when subjected to a tensile loading at a rate of 0.25s^{-1}.

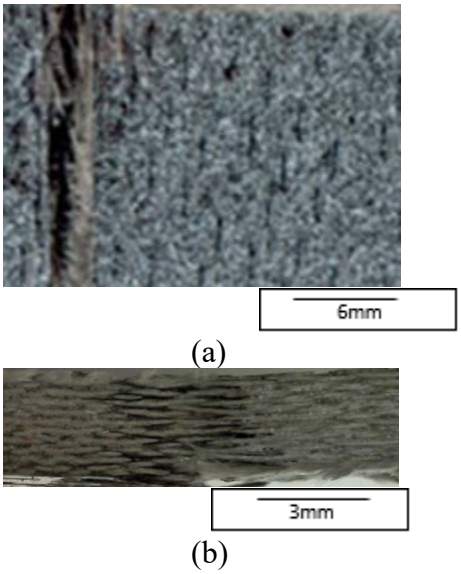

Figure 52 (a) & (b) Low magnification 7781 8HS glass fiber 0° optical micrograph of specimens under tensile loading at a rate of 0.25 s^{-1} (a) front view (b) thickness view.

It can be observed from the micrographs that there is a minimal amount of fiber pull out and also a little amount of delamination surrounding the area of fracture. It can be observed from the

micrographs that the failure mode is lateral (L), occurred in the gage section (G) and in the middle (M) of the test coupon. Hence it may be termed as a LGM failure per the ASTM 3039 standards. Figure 53 shows the DIC strain distribution map indicating the maximum strain at the region of failure.

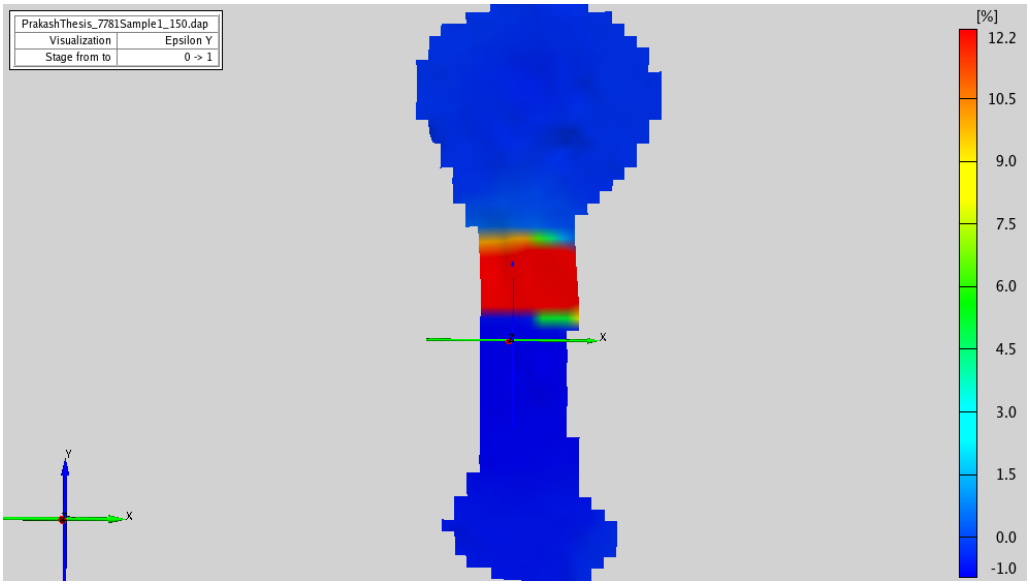

Figure 53 DIC strain distribution of glass fiber 8HS 7781 test coupon prior to failure subjected to a tensile loading at a rate of 0.25 s^{-1}.

Figure 54 shows a typical stress-strain behavior of 8HS 7781 glass fiber oriented at 45° subjected to a tensile strain rate of 0.0025 s^{-1}.

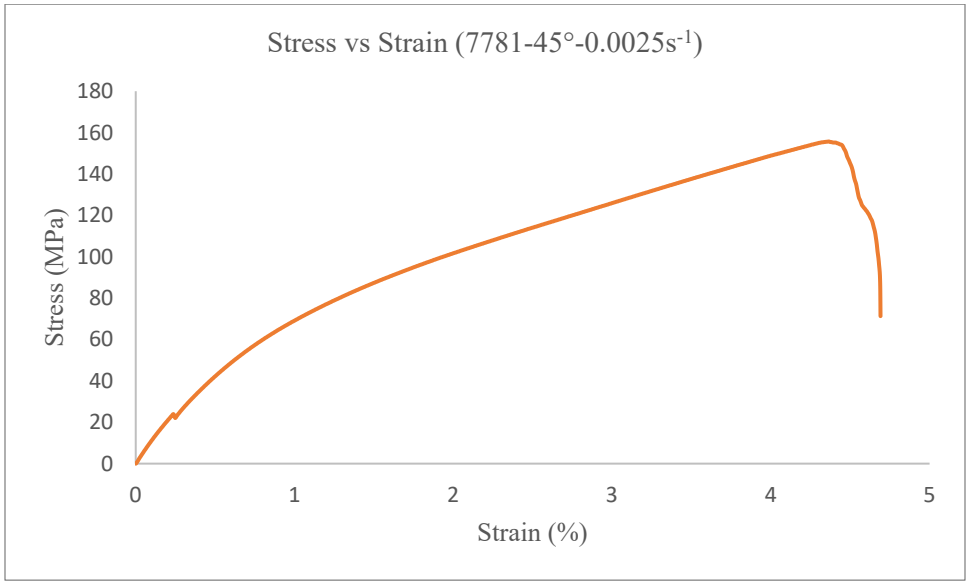

Figure 54 Tensile stress-strain behavior of 8HS 7781 glass fiber based composite tested along the 45° orientation at a rate of 0.0025s^{-1}.

The 8HS 7781 glass fiber based composite exhibited a peak stress of 156 MPa and a strain to failure of 4.69 %. Figure 55 (a) & (b) shows low magnification optical micrographs of an 8HS 7781-45° test coupon after failure when subjected to a tensile loading strain rate of $0.0025s^{-1}$.

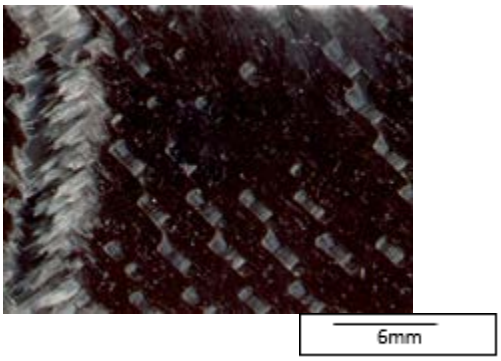

(a)

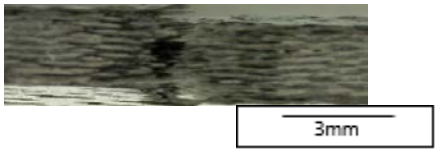

(b)

Figure 55 (a) & (b) Low magnification 7781 8HS glass fiber 45° optical micrograph of specimens under tensile loading at a rate of 0.0025 s^{-1} (a) front view (b) thickness view.

From the Figure 55 (a) and types of failure suggested in Figure 27, it is evident that the failure is of type Lateral (L), Gage (G) area and in the middle (M) of the specimen. Therefore, it is considered as a LGM failure mode according to the ASTM 3039 standards. It is evident from the Figure 55 (a), the failure occurred because of fiber breakage and there is considerable amount of delamination in the region of fracture, which is evident in the Figure 55 (b).

Figure 56 shows a typical stress-strain behavior of 8HS 7781 glass fiber based composite subjected to a tensile loading at a rate of 0.25 s^{-1}.

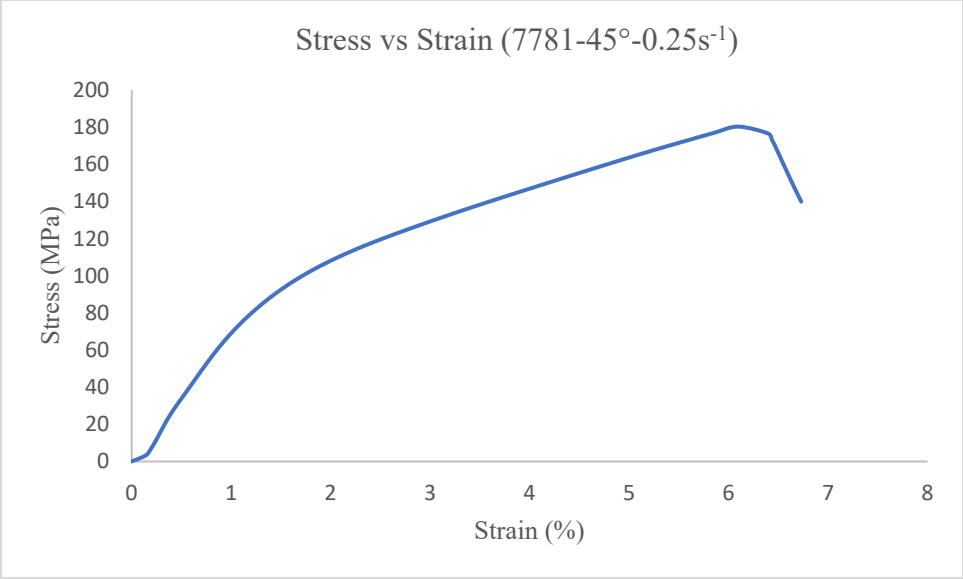

Figure 56 Tensile stress-strain behavior of 8HS 7781 glass fiber based composite tested along the 45° orientation at a rate of 0.25s^{-1}.

The 8HS 7781 glass fiber based composite test coupon exhibited a peak stress of 180MPa and a strain to failure of 6.09%. Figure 57 (a) & (b) shows low magnification optical micrographs of a 7781-45° test coupon after failure when subjected to a tensile loading at a strain rate of 0.25s^{-1}.

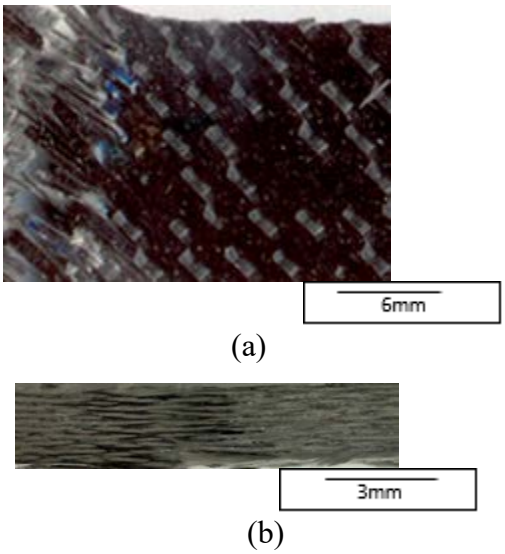

Figure 57 (a) & (b) Low magnification 7781 8HS glass fiber 45º optical micrograph of specimens under tensile loading at a rate of 0.25 s^{-1} (a) front view (b) thickness view.

From the Figure 57 (a) and the types of failure suggested in Figure 27, it is evident that the type of failure is lateral (L), occurred in Gage (G) and in middle of the specimen. Therefore, it is considered as LGM failure mode according to the ASTM 3039 test standards. It is also evident from the micrographs that fiber breakage is the main reason for the failure of coupon with little

amount of delamination that occurred in the region of the fracture. Table 1 shows the summarized results of static tensile testing of the three different composite test coupons.

Composite Type	Rate (s^{-1})	Orientation	Young's Modulus (GPa)	Peak Stress (MPa)	Peak Strain(%)
3K 2x2 twill woven CFE	0.0025	0°	46.73	468.46	0.75
	0.25		44.36	428	0.92
	0.0025	45°	10.52	161	5.17
	0.25		11.02	153	5.7
12k 2x2 twill woven CFE	0.0025	0°	52.98	778.51	1.39
	0.25		57.29	801.07	1.34
	0.0025	45°	11.73	151	6.97
	0.25		12.41	152	7.45
8HS 7781 GFE	0.0025	0°	17.26	311.23	2.81
	0.25		18.25	382.95	3.18
	0.0025	45°	9.05	156	4.69
	0.25		8.69	180.35	6.09

Table 1 Mechanical properties of different types of composite test coupons with different fiber orientations subjected to a tensile loading at different quasi static rates.

Composite structures are carefully designed and analyzed by comparing the stress and strains in the structure due to applied loads with permissible limits of stress and strains of the material being used [5]. There are several failure prediction models specially designed for unidirectional composites. The following are some of the failure models/theories that are used.

1) Maximum Stress Theory
2) Maximum Strain Theory
3) Azzi-Tsai-Hill Theory
4) Tsai-Wu Failure Theory

However, the predictions for woven composites made using the above theories were just an approximation. The 3D structure of the woven composites makes the failure prediction a little complicated. Advanced failure theories should be modeled to predict the failure criterion for the woven fiber reinforced composites [7]. Since, the failure prediction for the woven composites is not in the scope of this thesis, this could be a potential recommendation for future work.

3.2 Dynamic Tensile Testing

3.2.1 3K 2x2 twill woven carbon fiber

3K 2x2 twill woven carbon fiber is subjected to a dynamic tensile loading in the direction of the warp at a loading strain rate of $10s^{-1}$ (equivalent to a cross head speed of 6000 mm/min). Since many of the fibers are oriented lengthwise along the warp direction, the test coupon can usually endure higher loads before the onset of the failure. Figure 58 shows a typical stress-strain behavior of the 3K 2x2 twill woven carbon fiber test coupon subjected to a tensile loading at a loading rate of $10s^{-1}$.

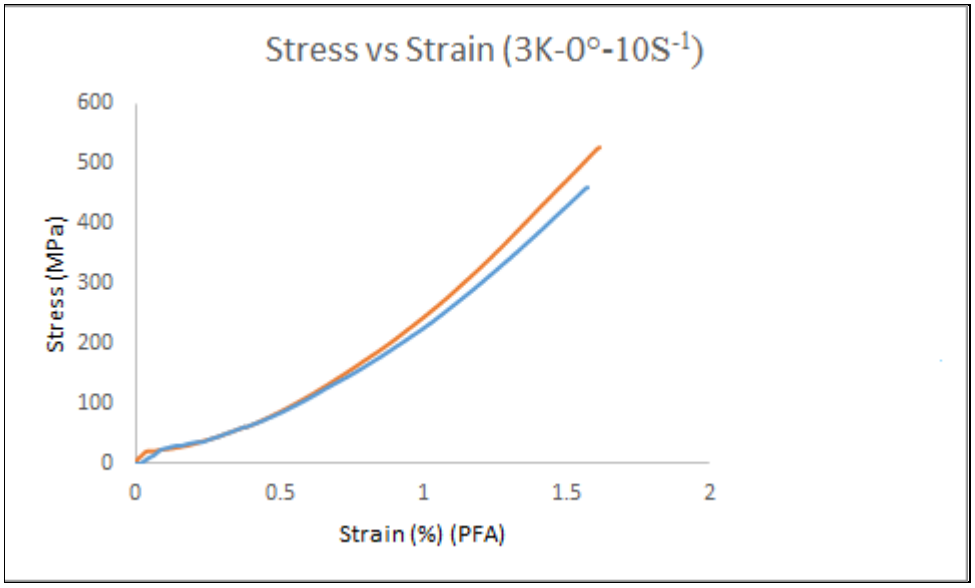

Figure 58 Tensile stress-strain behavior of 3K carbon fiber based composite tested along the 0° orientation at a rate of $10s^{-1}$.

It is evident from the graph that the coupons under test does not follow any linear behavior under impact loading conditions. This may be due to the settling of the specimen in the grip region of the fixture, once the tensile load was uniformly applied to the specimen. The test coupon exhibited an average peak stress of 494 MPa and an average strain to failure of 1.59 %. Figure 59 (a) & (b) shows the low magnification optical micrographs of the test coupons after the failure.

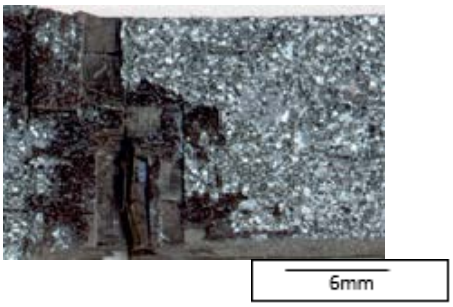

(a)

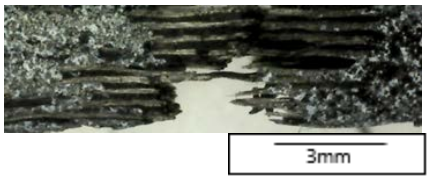

(b)

Figure 59 (a) & (b) Low magnification 3K-0° carbon fiber optical micrograph of specimens under tensile loading at a rate of 10 s^{-1} (a) front view (b) thickness view.

From the above micrographs, there is a noticeable amount of delamination that has occurred in the test coupon. The mode of failure is lateral (L), in the gage section (G) and in the middle of the specimen (M). Hence the failure mode can be summarized as a LGM as per the ASTM 3039 standards. Since impact rates of loading is used, the damage is therefore severe, and type of failure can be identified. Figure 60 shows the strain distribution pattern obtained from the DIC prior to the failure.

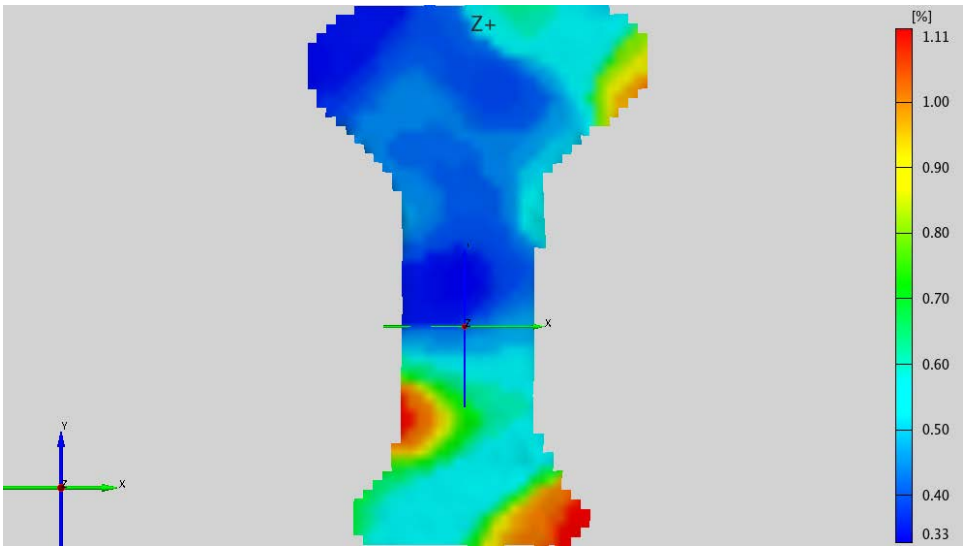

Figure 60 DIC strain distribution plot of 3K 2x2 twill woven carbon fiber subjected to an impact rate of loading of 10s^{-1}.

Figure 61 shows a typical stress-strain behavior of the 3K 2x2 twill woven carbon fiber test coupon subjected to a tensile loading along the warp direction at an impacting loading rate of 100 s^{-1}.

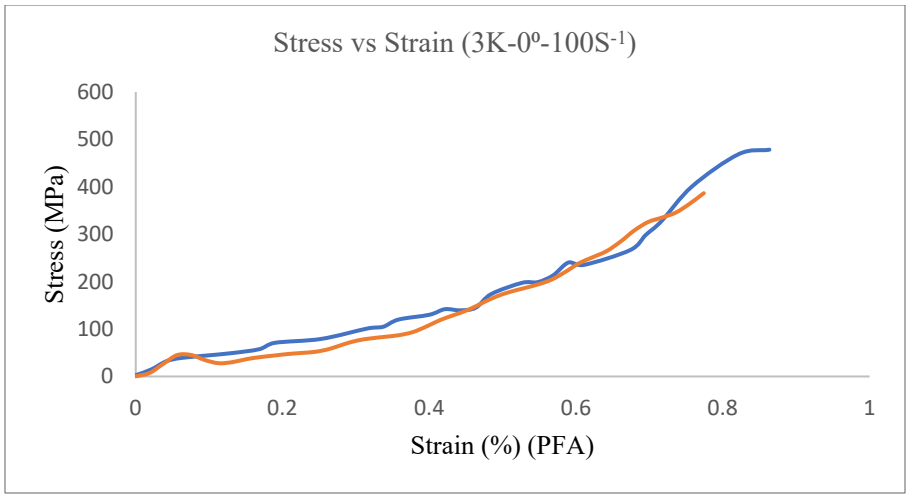

Figure 61 Tensile stress-strain behavior of 3K carbon fiber based composite tested along the 0° orientation at a rate of 100s^{-1}.

It is clear from the above plot that the stress strain plots at higher loads of rating are no longer linear, however there may be certain challenges in data acquisition which results in the fluctuations and noticeable amount of noise in the data. The test coupon subjected to the said tensile loading rate exhibited an average peak stress of 419 MPa and an average peak strain to failure as 0.83 %. Figure 62 (a) & (b) shows the low magnification optical micrographs of 3K 2x2 twill woven carbon fibers at failure.

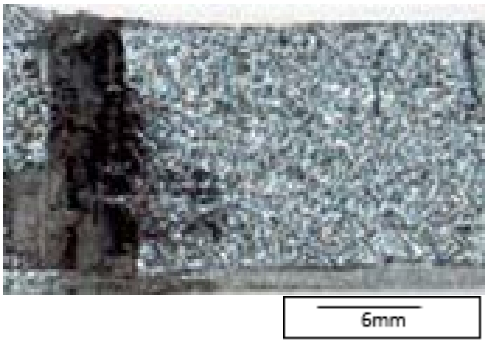

(a)

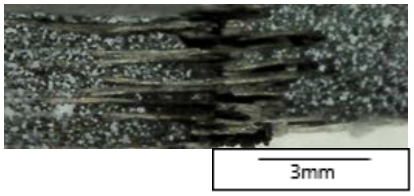

(b)

Figure 62 (a) & (b) Low magnification 3K-0° carbon fiber optical micrograph of specimens under tensile loading at a rate of 100 s^{-1} (a) front view (b) thickness view.

It can be seen from the above micrographs that the mode of failure is lateral (L), occurred in the Gage (G) area and in the middle (M) of the specimen. There is a considerable amount of delamination between the layers that is evident from the above micrographs. Hence, it is a LGM failure according to the ASTM 3039 standards.

Figure 63 shows the DIC strain distribution map at a point prior to the failure.

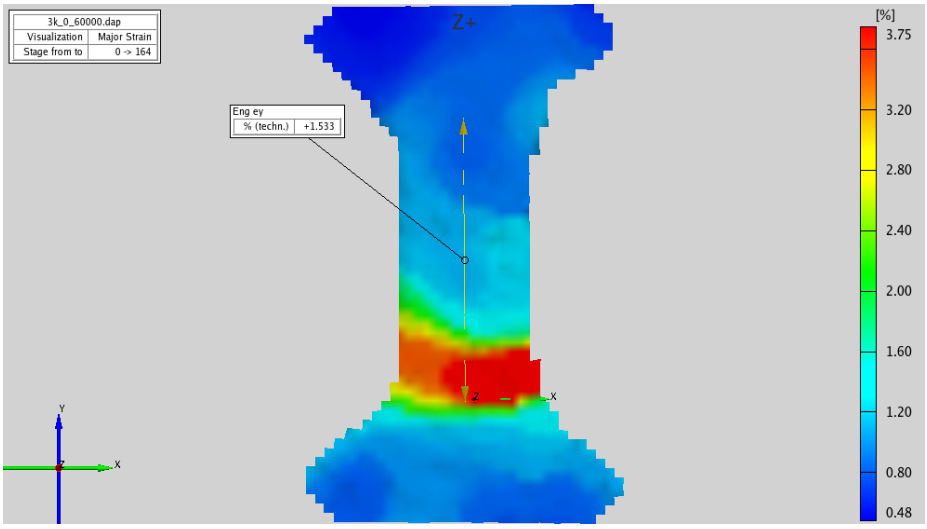

Figure 63 DIC strain distribution map of 3K 2x2 twill woven carbon fiber based composite subjected to a loading rate of $100s^{-1}$.

Figure 64 shows a typical stress-strain behavior of 3K 2x2 twill woven carbon fiber base composite subjected to a tensile loading along 0° at a rate of $500s^{-1}$.

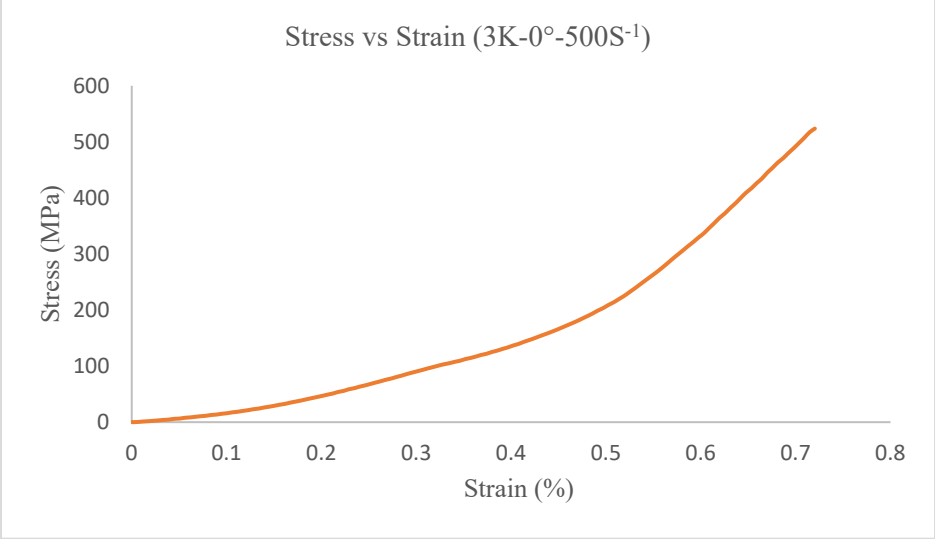

Figure 64 Tensile stress-strain behavior of 3K carbon fiber based composite tested along the 0° orientation at a rate of $500s^{-1}$.

The 3K 2x2 twill woven carbon fiber based composite exhibited a peak stress of 523 MPa and a strain to failure of 0.7%.

Figure 65 shows low magnification optical micrographs of 3K 2x2 twill woven carbon fiber test coupon after failure when subjected to a tensile loading at a strain rate of 500 s^{-1}.

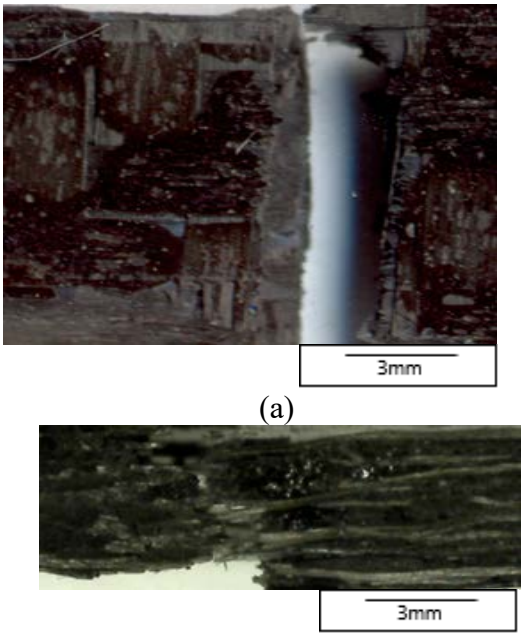

Figure 65 (a) & (b) Low magnification 3K-0° carbon fiber optical micrograph of specimens under tensile loading at a rate of 500 s^{-1} (a) front view (b) thickness view.

From the Figure 65 and types of failure suggested in Figure 27, it is evident that the failure is of type lateral (L), occurred in the Gage (G) and in the middle of the specimen (M). Therefore, this is considered as LGM failure mode according to the ASTM 3039 standards.

Figure 66 shows a typical stress-strain behavior of a 3K 2x2 twill woven composite fiber subjected to a tensile loading at a rate of 1000 s^{-1}.

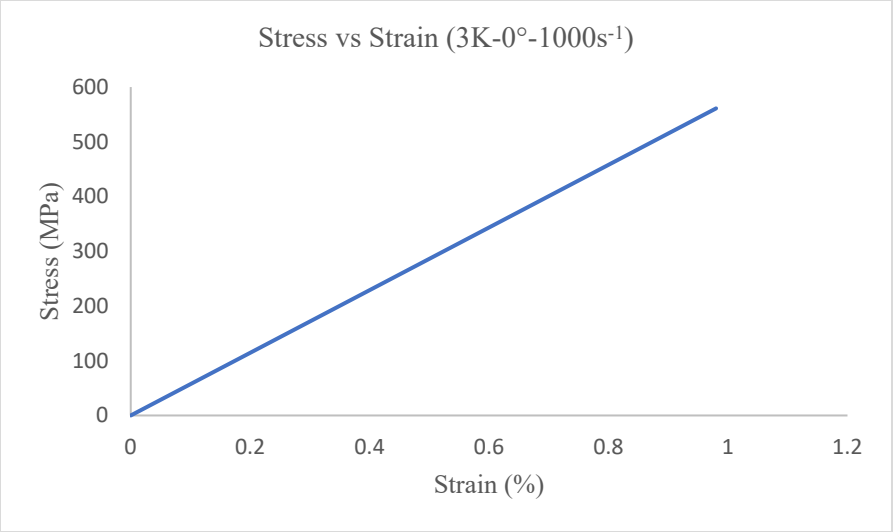

Figure 66 Tensile stress-strain behavior of 3K carbon fiber based composite tested along the 0° orientation at a rate of 1000s^{-1}.

The 3k 2x2 twill woven composite exhibited a peak stress of 560 MPa with an average strain to failure of 0.98%.

Figure 67 (a) & (b) shows low magnification optical micrographs of a 3K 2x2 twill woven carbon fiber based composite after failure when subjected to a tensile loading at a strain rate of 1000 s^{-1}.

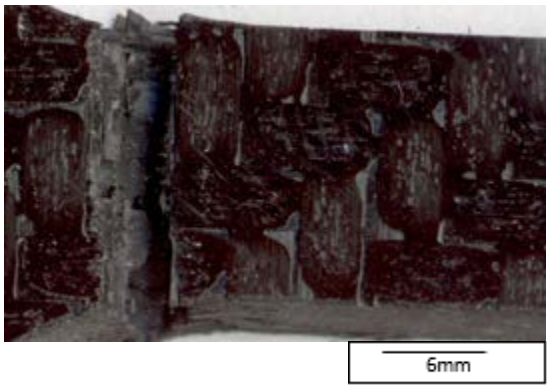

(a)

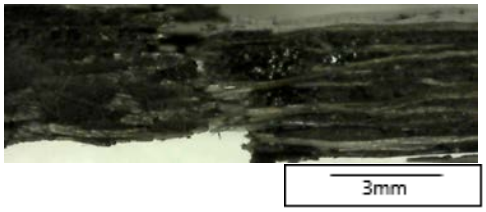

(b)

Figure 67 (a) & (b) Low magnification 3K-0° carbon fiber optical micrograph of specimens under tensile loading at a rate of 1000 s^{-1} (a) front view (b) thickness view.

From Figure 67 and the types of failure suggested in the Figure 27, the failure is of type lateral (L), occurred in the Gage (G) and in the middle (M) of the specimen. Therefore, this is considered as LGM failure mode according to the ASTM 3039 standards. It can be seen from the optical micrographs that the failure of the coupon is brittle with no much fiber pullout, however, a little amount of delamination is evident at the failure region.

Figure 68 shows a typical stress-strain behavior of 3K 2x2 twill woven carbon fiber test coupon that is subjected to a tensile loading perpendicular to both warp and weft directions. This is the case in which the fibers are said to be oriented along 45º. It can be seen from the below plot that the test coupon can withstand lower amounts of stress as there are no much fibers in this direction which offers more resistance to the pull. When a test coupon oriented along 45º is subjected to a tensile loading, shear forces act on the test coupon because of which it contributes to yielding at lower stress values.

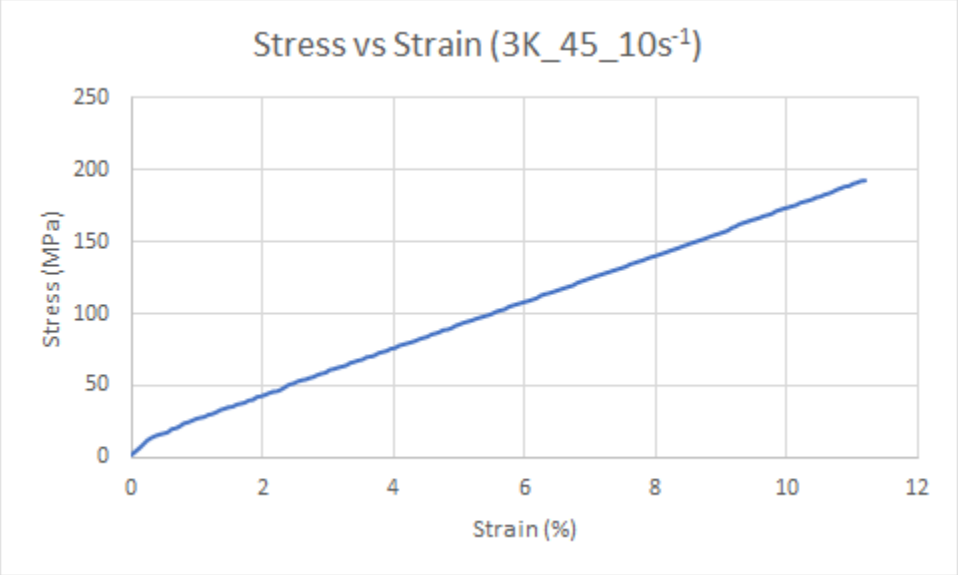

Figure 68 Tensile stress-strain behavior of 3K carbon fiber based composite tested along the 45° orientation at a rate of $10s^{-1}$.

It can be noted from the above graph that the peak stress is 193 MPa and a maximum strain to failure as 11% which is more compared to the tensile loading along 0º.

Figure 69 (a) & (b) shows the low magnification optical micrographs of a 3K-45° test coupon after failure when subjected to a tensile loading at a strain rate of $10s^{-1}$.

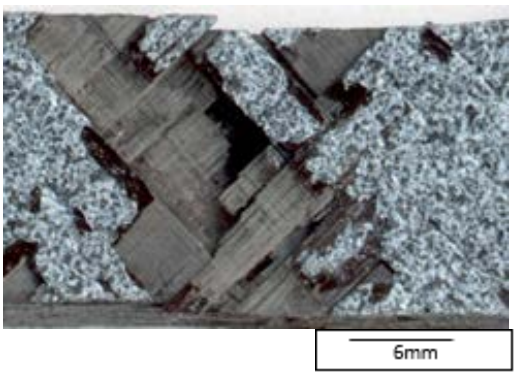

(a)

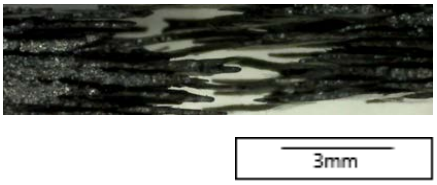

(b)

Figure 69 (a) & (b) Low magnification 3K-45° carbon fiber optical micrograph of specimens under tensile loading at a rate of 10 s^{-1} (a) front view (b) thickness view.

From the above figure, it is clear that the specimen has undergone a considerable amount of shear deformation. The mode of failure is Angular (A), occurred in the gage section (G) and in the middle of the specimen (M). Therefore, it is an AGM failure mode according to the ASTM 3039 standards for testing. It may also be noted that the test coupon is delaminated completely upon failure. Figure 70 shows the DIC strain distribution plot prior to the failure of the test coupon.

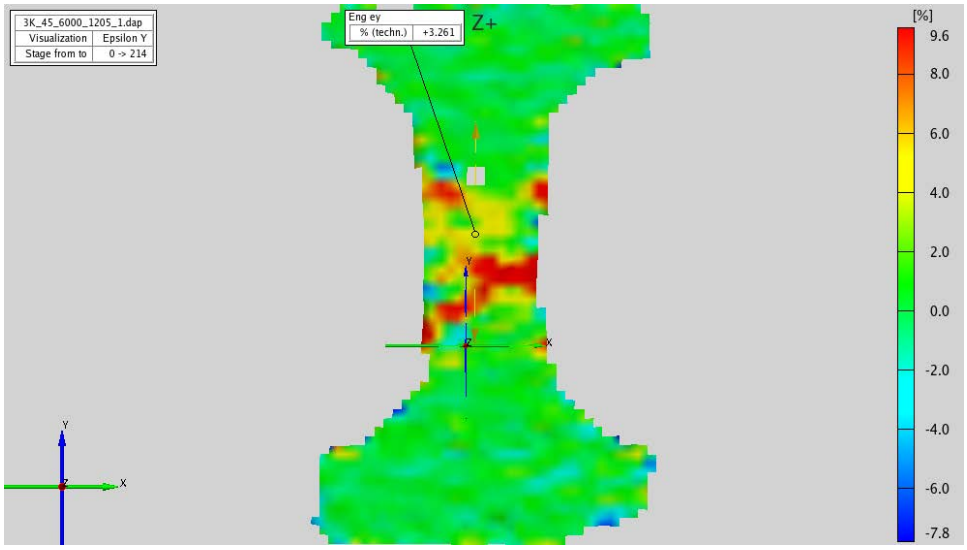

Figure 70 DIC strain distribution of 3K-45° 2x2 twill woven carbon fiber based test coupon prior to failure subjected to a tensile strain rate of 10 s^{-1}.

Figure 71 shows the stress strain behavior of 3K 2x2 45° twill woven carbon fiber test coupon subjected to a tensile loading at a rate of $100s^{-1}$ (60000mm/min).

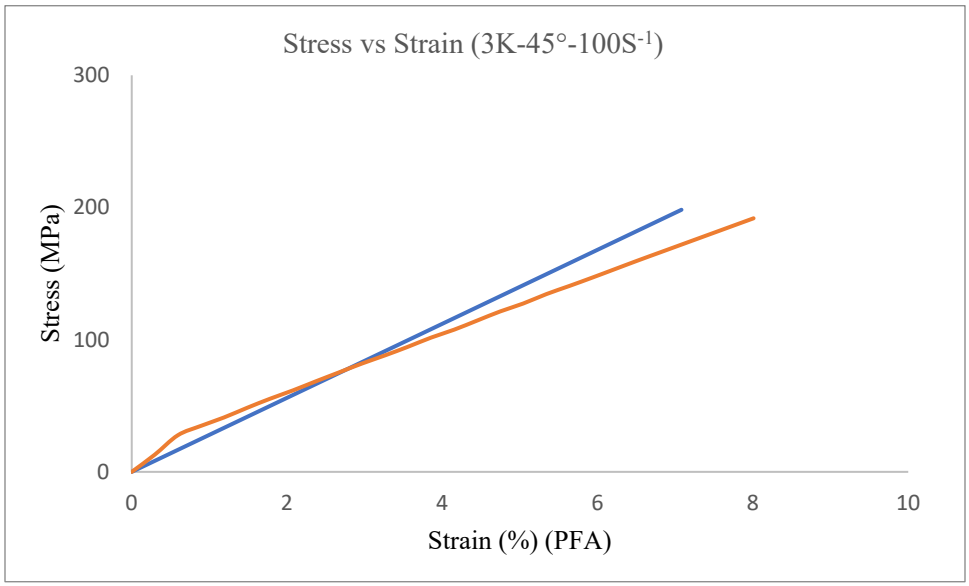

Figure 71 Tensile stress-strain behavior of 3K carbon fiber based composite tested along the 45° orientation at a rate of $100s^{-1}$.

3K 45° 2x2 twill woven carbon fiber composite when subjected to an impact loading yields an average peak stress of 195 MPa and an average maximum strain to failure of 7.75 %. The test coupon in this case is also subjected to a shear loading. Hence, the overall load that the specimen can endure is less overall. Figure 72 (a) & (b) shows a low magnification optical micrograph of a 3K 2x2 twill woven carbon fiber test coupon at failure.

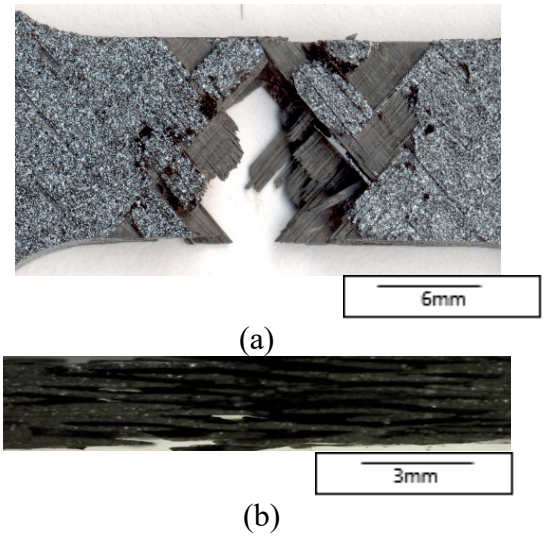

Figure 72 (a) & (b) Low magnification 3K-45° carbon fiber optical micrograph of specimens under tensile loading at a rate of 100 s^{-1} (a) front view (b) thickness view.

It can be seen from the above optical micrographs that there was considerable amount of damage to the test coupon and the failure was basically due to delamination. From the figure, the failure mode is angular (A), occurred in the gage area (G) and in the middle of the specimen (M). Hence, it is an AGM failure mode according to the ASTM 3039 test standards.

Figure 73 shows the DIC strain distribution plot of 3K 2x2 twill woven carbon fiber test coupon subjected to a tensile loading prior to failure.

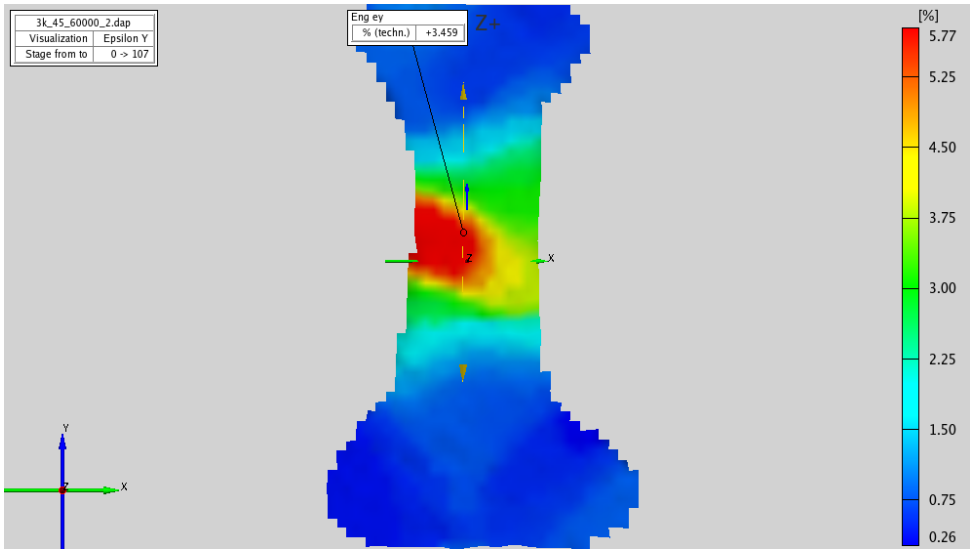

Figure 73 DIC strain distribution of 3K-45° 2x2 twill woven carbon fiber based test coupon prior to failure subjected to a tensile strain rate of 100 s^{-1}.

Figure 74 shows a typical stress-strain behavior of a 3K 2x2 twill woven carbon fiber based test coupon tested at a rate of 500 s^{-1}.

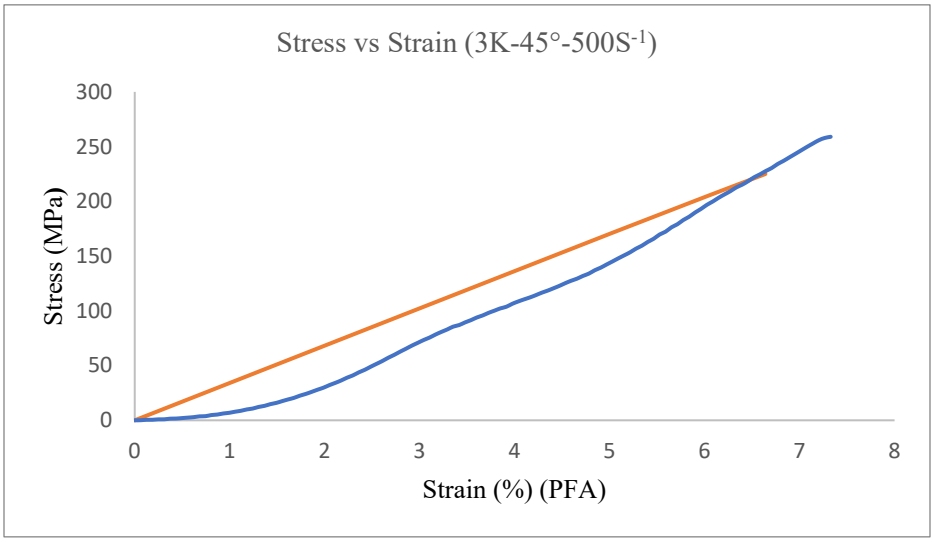

Figure 74 Tensile stress-strain behavior of 3K carbon fiber based composite tested along the 45° orientation at a rate of 500s^{-1}.

The 3K 2x2 twill woven carbon fiber exhibited an average peak stress of 236 MPa and a strain to failure of 7 %. Figure 75 (a) & (b) shows low magnification optical micrographs of a 3K-45° test coupon after failure when subjected to a tensile loading at a strain rate of 500 s^{-1}.

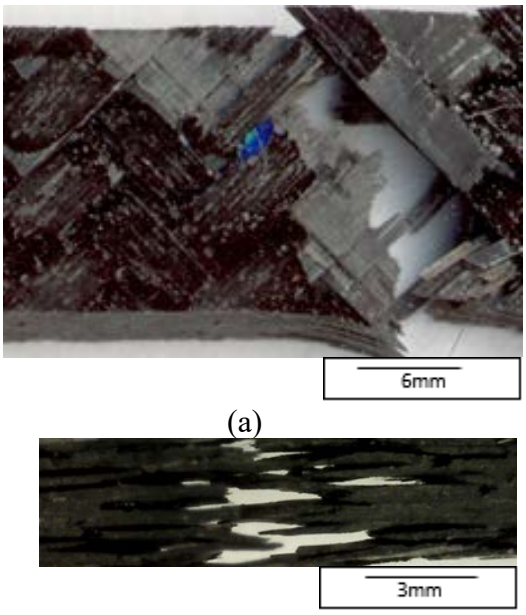

(a)

(b)

Figure 75 (a) & (b) Low magnification 3K-45° carbon fiber optical micrograph of specimens under tensile loading at a rate of 500 s^{-1} (a) front view (b) thickness view.

From Figure 75 (a) and the types of failure suggested in Figure 27, it is evident that the failure is of type angular (A), occurred in the Gage (G) and in the middle of the specimen (M). Therefore, this is considered as LGM failure mode according to the ASTM 3039 standards. It is evident from the Figure 75 (b) that there is considerable amount of delamination in the test coupon.

Figure 76 shows a typical stress-strain behavior of a 3K 2x2 twill woven carbon fiber based test coupon tested at 1000 s^{-1} along 45° orientation.

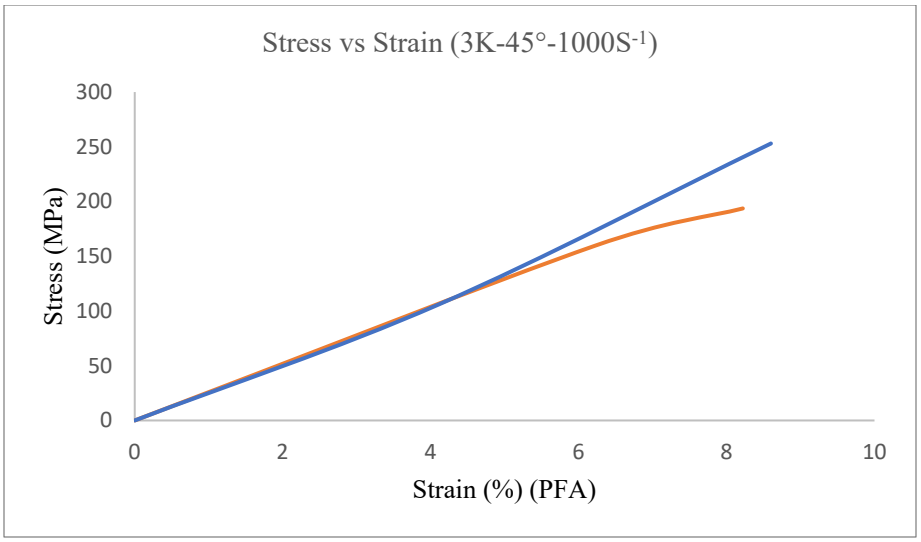

Figure 76 Tensile stress-strain behavior of 3K carbon fiber based composite tested along the 45° orientation at a rate of 1000s^{-1}.

The 3K 2x2 twill woven carbon fiber coupons exhibited an average stress of 273 MPa and an average strain to failure of 8.4 %.

Figure 77 (a) & (b) shows low magnification optical micrographs of 3K 45° test coupon after failure when subjected to a tensile loading at a strain rate of 1000s^{-1}.

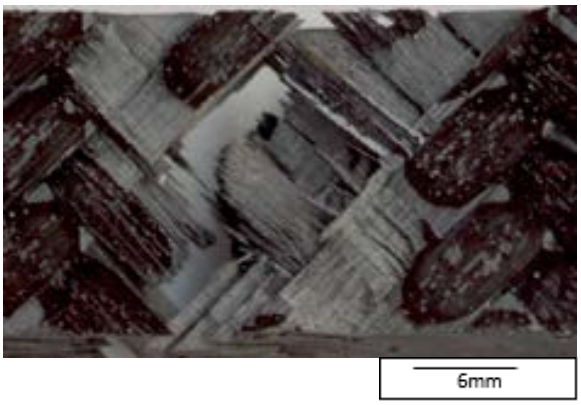

(a)

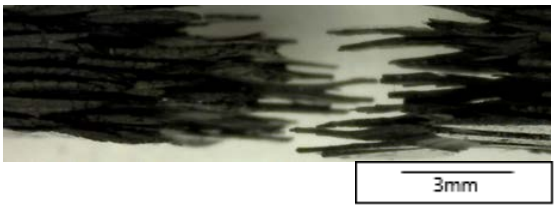

(b)

Figure 77 (a) & (b) Low magnification 3K-45° carbon fiber optical micrograph of specimens under tensile loading at a rate of 100 s^{-1} (a) front view (b) thickness view.

From Figure 77 (a) and the types of failure suggested in Figure 27, it is evident that the failure is of type angular (A), occurred in the Gage (G) and in the middle of the specimen (M). Therefore, this is considered as LGM failure mode according to the ASTM 3039 standards. It is evident from the Figure 77 (a) that there is some amount of fiber breakage and pullout resulting in the failure of the test coupon. Figure 77 (b) shows a clear delamination in the region of the fracture.

3.2.2 12K twill woven carbon fiber

Figure 78 shows a typical stress-strain behavior of 12K 2x2 twill woven carbon fiber based composite test coupon subjected to a tensile loading rates of $10s^{-1}$, loaded along 0°.

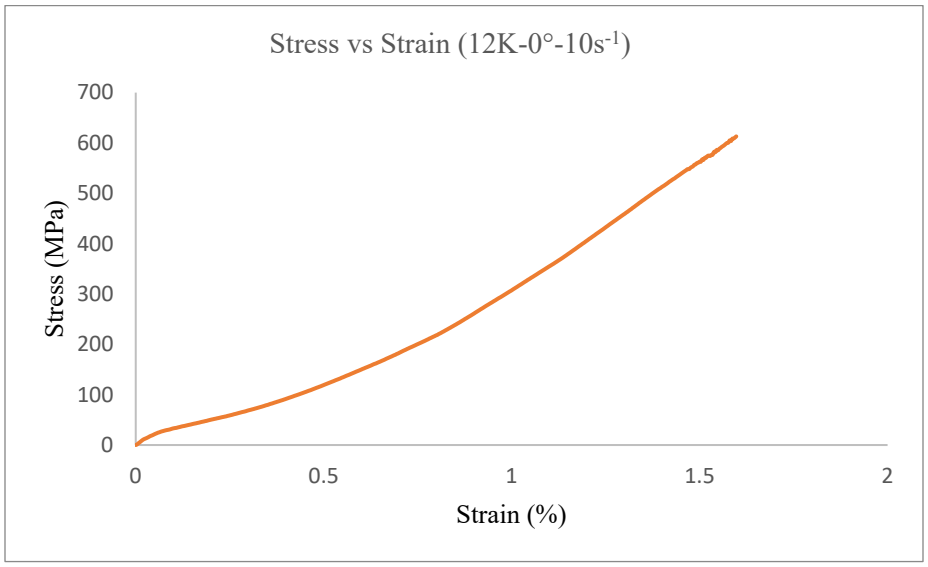

Figure 78 Tensile stress-strain behavior of 12K carbon fiber based composite tested along the 0° orientation at a rate of $10s^{-1}$.

It is evident from the graph that the stress strain behavior is following a nonlinear trend and there is some considerable amount of noise in the data which may be because of the intermediate fiber failure and fiber/matrix failure. Since there are higher number of fibers along the test direction, the test coupon can endure higher loads thus resulting in higher peak stresses. The average peak stress is 679 MPa and an average maximum strain to failure is 1.45 %. Figure 79 (a) & (b) represents the low magnification optical micrographs of 12K 0° 2x2 twill woven carbon fiber test coupon at failure when subjected to a strain rate of 10 s^{-1}.

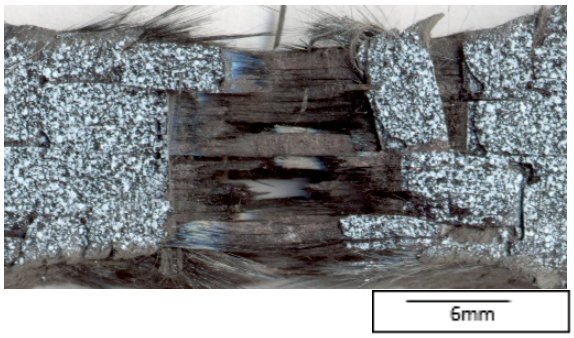

(a)

(b)

Figure 79 (a) & (b) Low magnification 12K-0° carbon fiber optical micrograph of specimens under tensile loading at a rate of 10 s^{-1} (a) front view (b) thickness view.

It is evident from the above micrographs that the mode of failure is explosive (X), occurred in the gage section (G) and in the middle (M) of the specimen. Hence the failure mode is XGM as per the ASTM 3039 test standards. From Figure 79 (b), the damage of the test coupon is accompanied by a good amount of delamination and fiber pull out.

Figure 80 shows the DIC strain distribution map of 12K 0° 2x2 twill woven carbon fiber prior to failure.

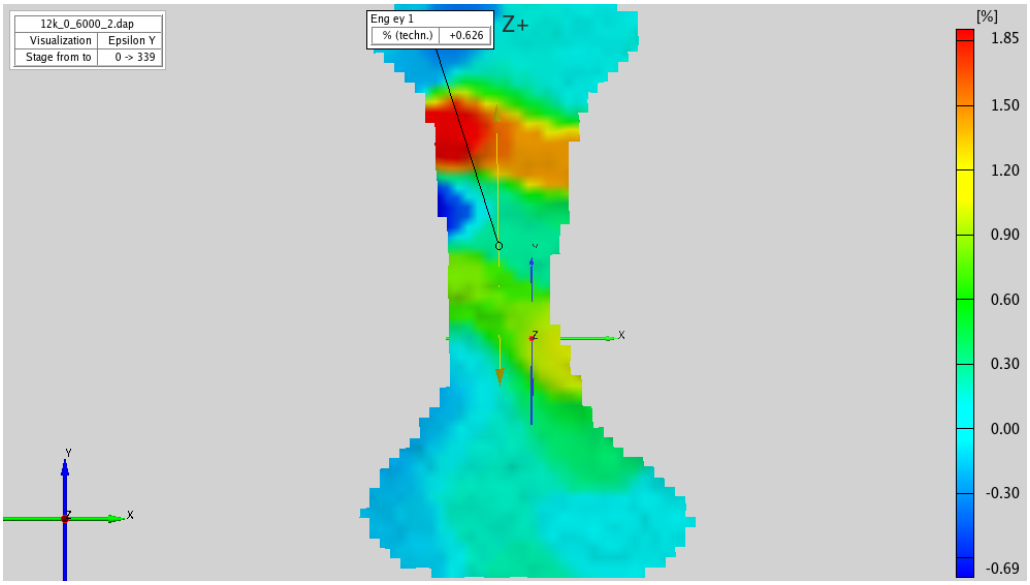

Figure 80 DIC strain distribution of 12-0° 2x2 twill woven carbon fiber based test coupon prior to failure subjected to a tensile strain rate of 10 s^{-1}.

The maximum strain region in the above figure represents the onset of the explosive crack which finally resulted in the total damage of the test coupon.

Figure 81 shows a typical stress-strain behavior of 12K 0° 2x2 twill woven carbon fiber test coupon that is subjected to tensile loading at higher impact rate of $100s^{-1}$ (60000 mm/min).

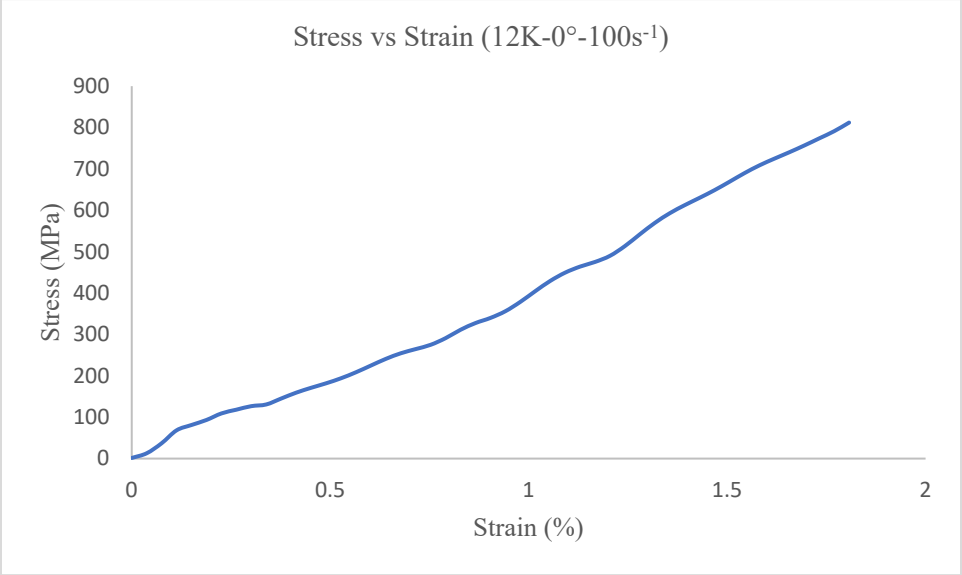

Figure 81 Tensile stress-strain behavior of 12K carbon fiber based composite tested along the 0° orientation at a rate of $100s^{-1}$.

It was experimentally found that an average peak stress endured by the 12K 0° 2x2 twill woven carbon fiber is 812 MPa and an average maximum strain to failure was found to be 1.8 %. Figure 82 (a) & (b) shows the low magnification optical micrographs of the 12K 2x2 twill woven carbon fibers at the failure when subjected to a tensile loading at a rate of $100s^{-1}$.

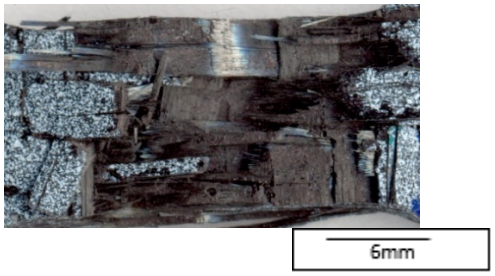

(a)

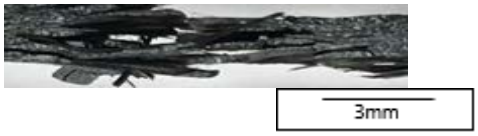

(b)

Figure 82 (a) & (b) Low magnification 12K-0° carbon fiber optical micrograph of specimens under tensile loading at a rate of $100\ s^{-1}$ (a) front view (b) thickness view.

From Figure 82 (a), it is evident that the mode of failure is explosive (X), occurred in the gage section (G) and in the middle of the specimen. Hence it is an XGM mode of failure. From figure 82 (b) delamination of the test coupon and fiber breakage and pullout are the primary reasons for failure. Also, there are some edge cracks present on the test coupon. Figure 83 shows the DIC strain distribution plot of 12K 0° 2x2 twill weave carbon fiber test coupon prior to onset of failure.

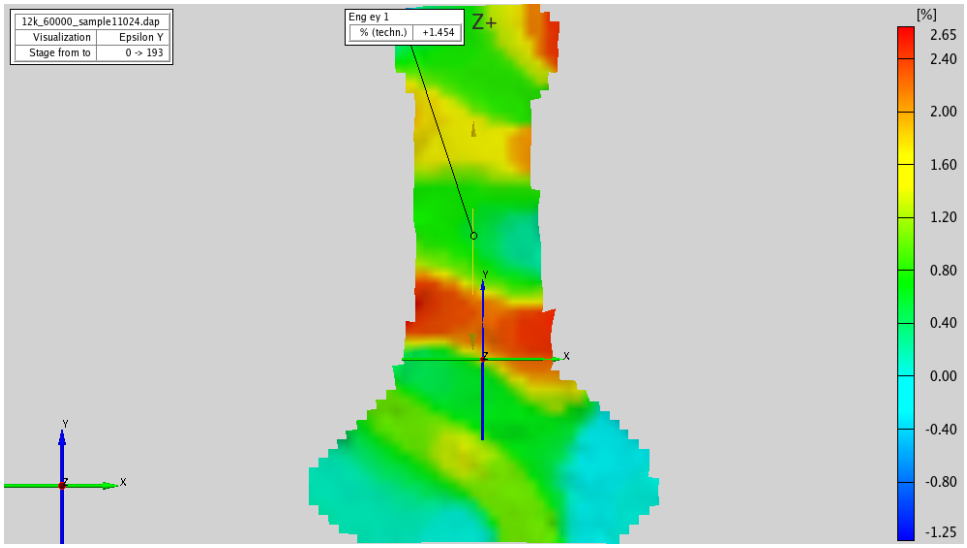

Figure 83 DIC strain distribution of 12-0° 2x2 twill woven carbon fiber based test coupon prior to failure subjected to a tensile strain rate of 100 s^{-1}.

Figure 84 shows a typical stress-strain behavior of 12K 2x2 twill woven carbon fiber tested at a loading rate of 500s^{-1} along 0° fiber orientation.

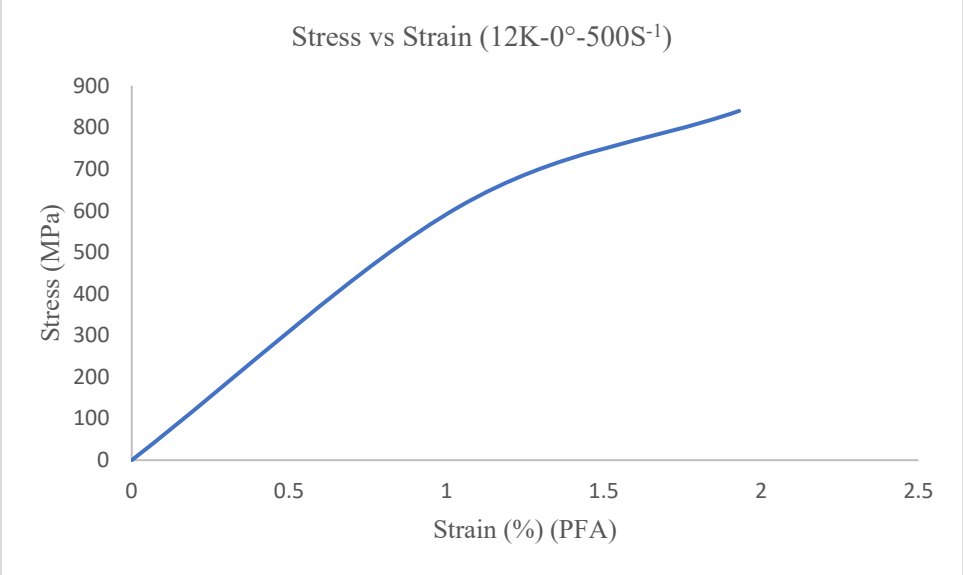

Figure 84 Tensile stress-strain behavior of 12K carbon fiber based composite tested along the 0° orientation at a rate of 500s^{-1}.

The 12K 2x2 twill woven carbon fiber based composites exhibited an average peak load of 839 MPa and an average peak strain of 1.9 %. Figure 85 shows low magnification optical micrographs of a 12K-0° test coupon after failure when subjected to a tensile loading at a rate of 500 s^{-1}.

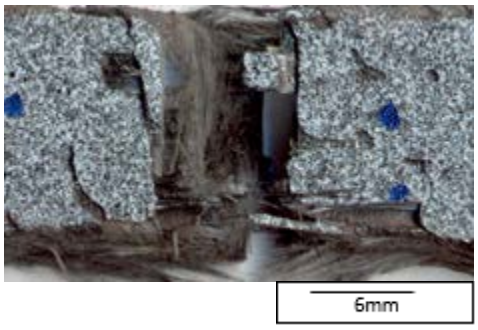

(a)

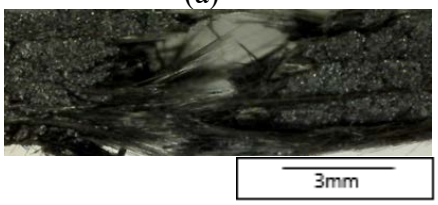

(b)

Figure 85 (a) & (b) Low magnification 12K-0° carbon fiber optical micrograph of specimens under tensile loading at a rate of 500 s^{-1} (a) front view (b) thickness view.

From Figure 85 (a) and types of failure suggested in Figure 27, it is evident that the mode of failure is explosive (X), occurred in the gage section (G) and in the middle (M) of the specimen. Hence it is considered an XGM mode of failure according to ASTM 3039 standards. From Figure 85 (b), it is evident that there is a considerable amount of fiber pullout resulting in the fracture of the test coupon. Figure 86 shows a typical stress-strain behavior of 12K 2x2 twill woven carbon fiber tested at a loading rate of 1000s^{-1} along 0° fiber orientation.

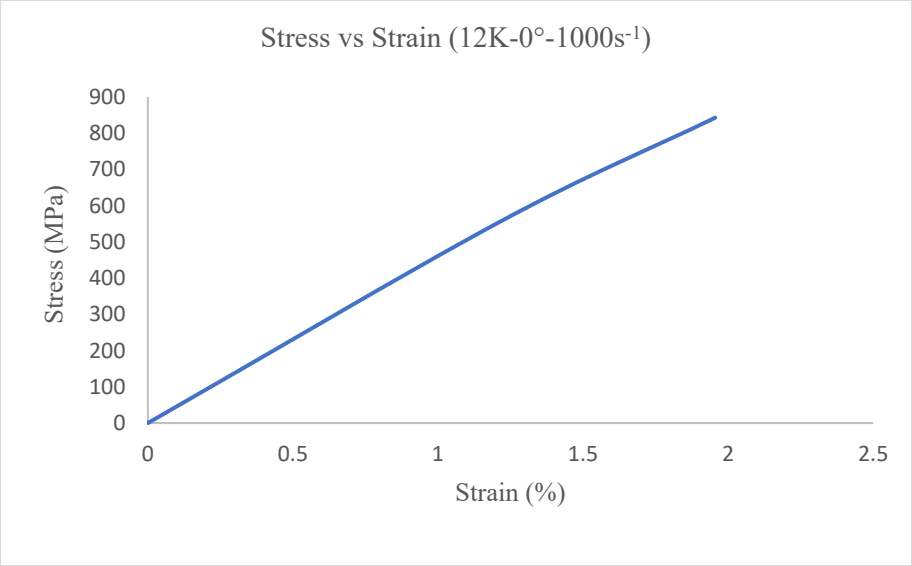

Figure 86 Tensile stress-strain behavior of 12K carbon fiber based composite tested along the 0° orientation at a rate of 1000s^{-1}.

The 12K 2x2 twill woven carbon fiber based composite test coupon exhibited an average peak stress of 843 MPa and an average strain to failure of 1.95 % when tested at a rate of 1000s^{-1}. Figure 87 shows low magnification optical micrographs of a 12K 2x2 twill woven carbon fiber based test coupon after failure when subjected to a tensile loading at a strain rate of 1000s^{-1}.

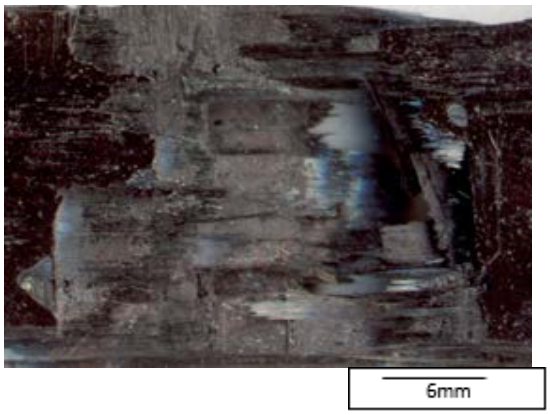

(a)

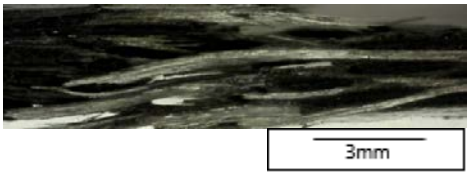

(b)

Figure 87 (a) & (b) Low magnification 12K-0° carbon fiber optical micrograph of specimens under tensile loading at a rate of 1000 s^{-1} (a) front view (b) thickness view.

From the Figure 87 and types of failure suggested in Figure 27, the failure is of type Explosive (X), occurred in Gage (G) and in middle of the specimen. Therefore, this type of failure can be summarized as an XGM as per ASTM 3039 test standards. From the Figure 87 (a) it is evident that there is considerable amount of fiber breakage which contributed to the failure of the test coupon along with delamination and fiber pullout which is evident in Figure 87 (b).

Figure 88 shows a typical stress-strain behavior of 12K 2x2 twill woven carbon fiber test coupon subjected to a tensile loading at a rate of $10s^{-1}$ along the fiber direction of 45°.

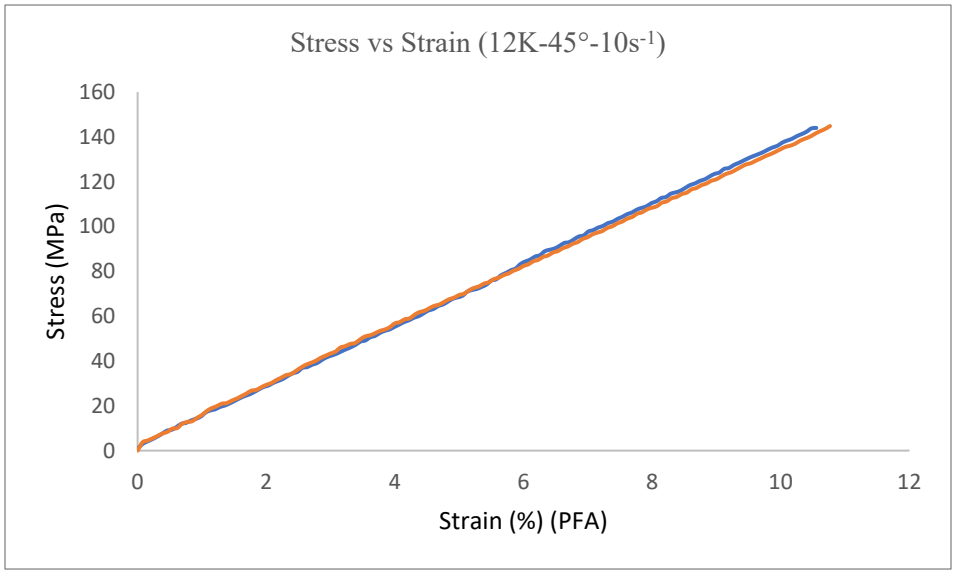

Figure 88 Tensile stress-strain behavior of 12K carbon fiber based composite tested along the 45° orientation at a rate of $10s^{-1}$.

The 12K 2x2 twill woven carbon fiber test coupon exhibits an average stress of 144 MPa and an average peak strain to failure of 10.56 %. A linear stress strain behavior is observed until the onset of failure. Figure 89 (a) & (b) shows the low magnification optical micrographs of 12K 45° twill woven carbon fiber test coupons at the failure when subjected to a tensile loading at a rate of $10s^{-1}$.

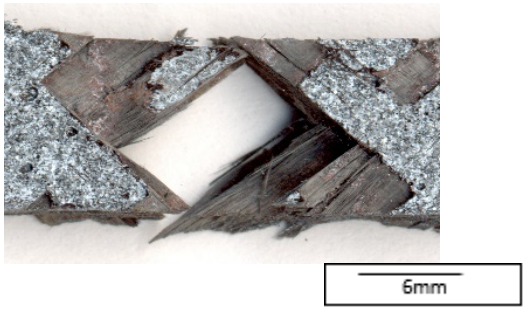

(a)

(b)

Figure 89 (a) & (b) Low magnification 12K-45° carbon fiber optical micrograph of specimens under tensile loading at a rate of 10 s^{-1} (a) front view (b) thickness view.

The mode of failure for 12K 45° 2x2 twill woven carbon fiber test coupon is angular (A), occurs in the gage (G) and in the middle of the specimen (M). Hence the failure is AGM as per the ASTM 3039 test standards. Because of the impact loadings, severe delamination of the test coupon can be seen in the Figure 89 (b). Figure 90 shows the DIC strain distribution map prior to the failure of the test coupon.

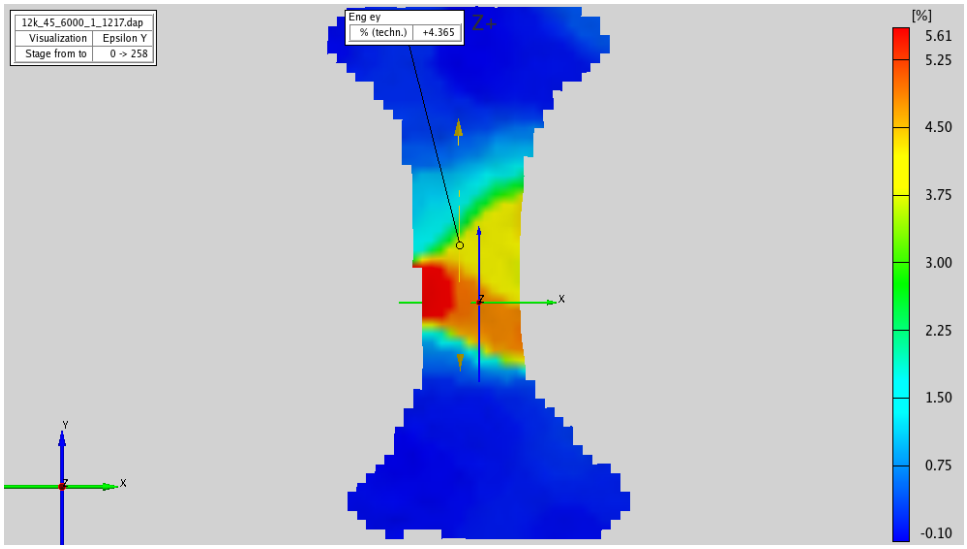

Figure 90 DIC strain distribution of 12-45° 2x2 twill woven carbon fiber based test coupon prior to failure subjected to a tensile strain rate of $10s^{-1}$.

The test coupon is subjected to a shear when subjected to loading perpendicular to both warp and weft. Figure 91 shows a typical tensile stress-strain behavior of 12K 2x2 twill woven carbon fiber subjected to an impact loading rate of $100s^{-1}$ along 45° fiber orientation.

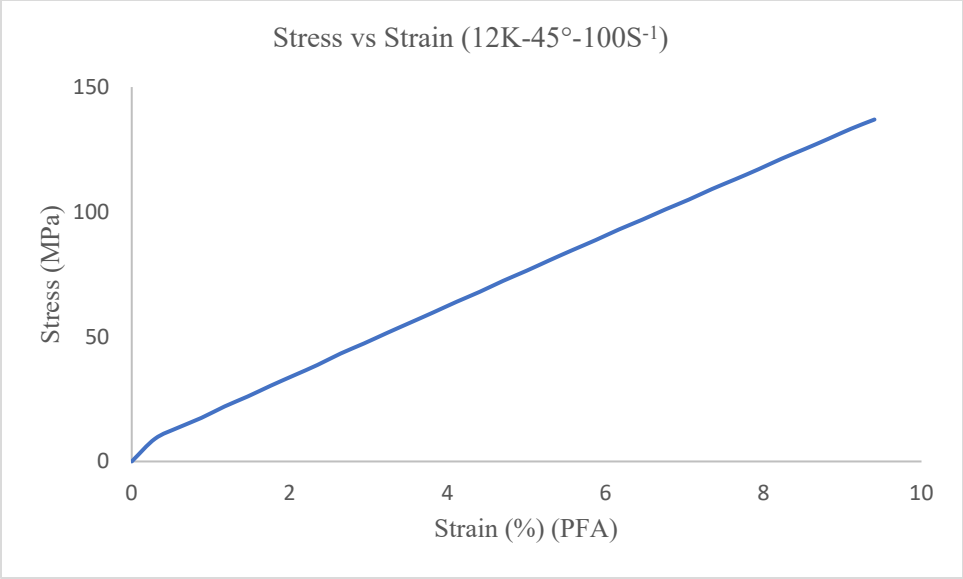

Figure 91 Tensile stress-strain behavior of 12K carbon fiber based composite tested along the 45° orientation at a rate of 100s^{-1}.

The 12K 2x2 twill woven carbon fiber exhibited an average stress of 137MPa and an average strain to failure of 9.4 %. Figure 92 (a) & (b) shows the low magnification optical micrographs of 12K 45° 2x2 twill weave carbon fiber at failure when subjected to a rate of 100s^{-1}.

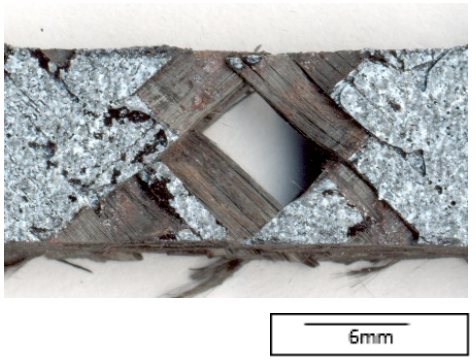

(a)

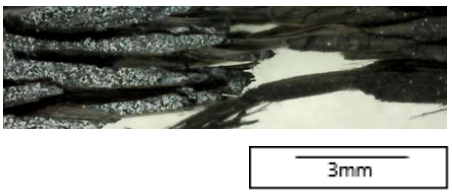

(b)

Figure 92 (a) & (b) Low magnification 12K-45° carbon fiber optical micrograph of specimens under tensile loading at a rate of 100 s^{-1} (a) front view (b) thickness view.

The mode of failure is explosive (X) occurred in the gage (G) section and at the middle of the specimen (M). Hence the failure mode can be XGM as per ASTM 3039 test standards. There is a noticeable amount of fiber pullout accompanied by fiber breakage and delamination as well. Figure 93 shows the DIC strain distribution map for 12K 2x2 twill woven carbon fiber test coupon.

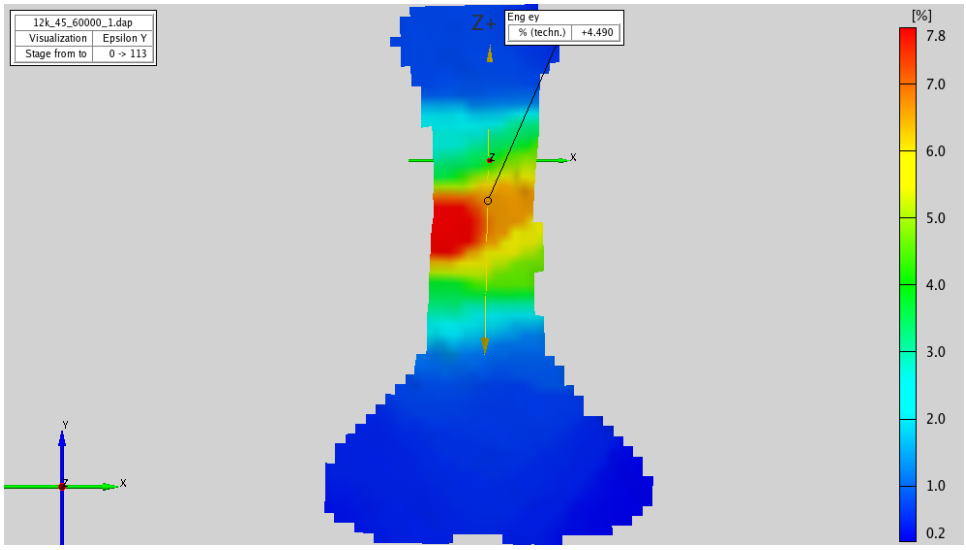

Figure 93 DIC strain distribution of 12-45° 2x2 twill woven carbon fiber based test coupon prior to failure subjected to a tensile strain rate of 100 s^{-1}.

Figure 94 shows a typical stress-strain behavior of the test coupon tested at a rate of 500s^{-1}.

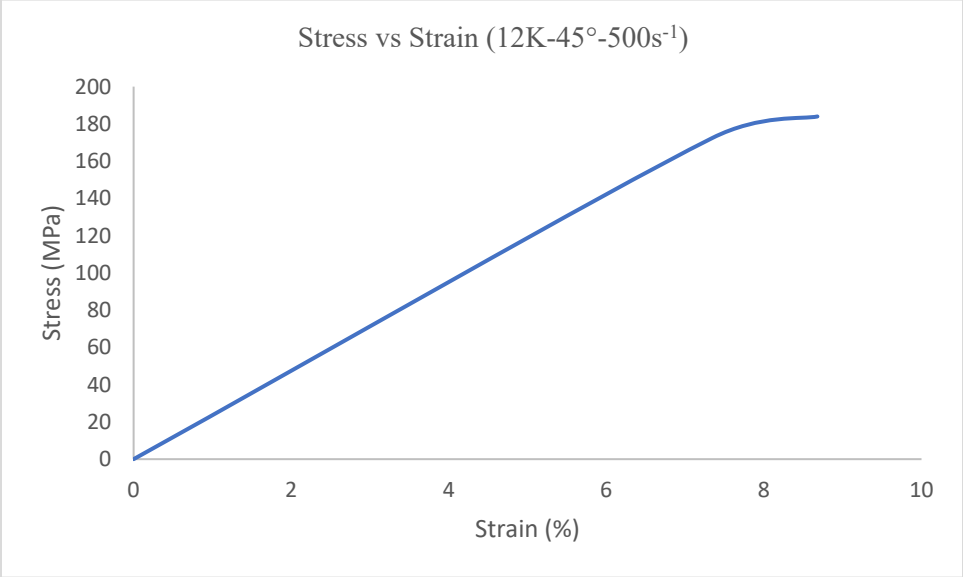

Figure 94 Tensile stress-strain behavior of 12K carbon fiber based composite tested along the 45° orientation at a rate of 500s^{-1}.

The 12K 2x2 twill woven carbon fiber exhibited an average stress of 183 MPa and an average strain to failure of 8.7 %. Figure 95 shows low magnification optical micrographs of 12K 2x2 twill woven carbon fiber based composite subjected to a loading rate of $500s^{-1}$.

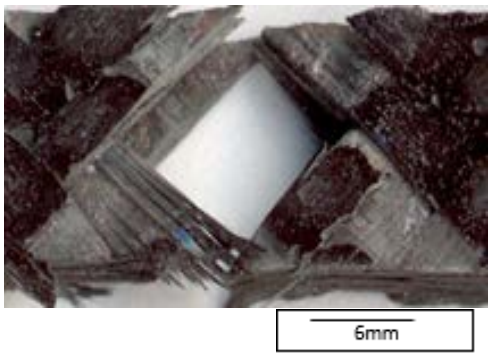

(a)

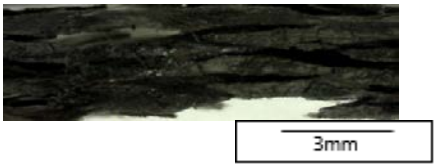

(b)

Figure 95 (a) & (b) Low magnification 12K-45° carbon fiber optical micrograph of specimens under tensile loading at a rate of 500 s^{-1} (a) front view (b) thickness view.

From the Figure 95 and types of failures suggested in the Figure 27 it is evident that the failure is of type Angular (A), occurred in Gage (G) and in the middle (M) of the specimen. Therefore, this is considered as AGM failure mode according to the ASTM 3039 test standards.

Figure 96 shows a typical stress-strain behavior of 12K 2x2 twill woven carbon fiber based composite tested at a rate of $1000s^{-1}$.

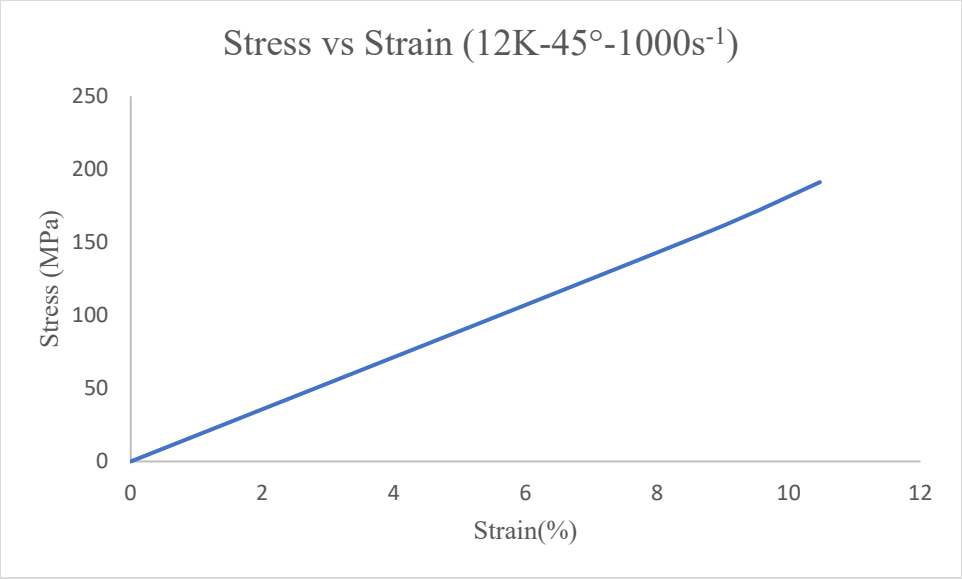

Figure 96 Tensile stress-strain behavior of 12K carbon fiber based composite tested along the 45° orientation at a rate of 1000s^{-1}.

The 12K 2x2 twill woven carbon fiber based composite exhibited an average peak stress of 193 MPa and a strain to failure of 10.4 %.

Figure 97 shows low magnification optical micrographs of 12K 45° test coupon at failure when subjected to a loading rate of 1000 s^{-1}.

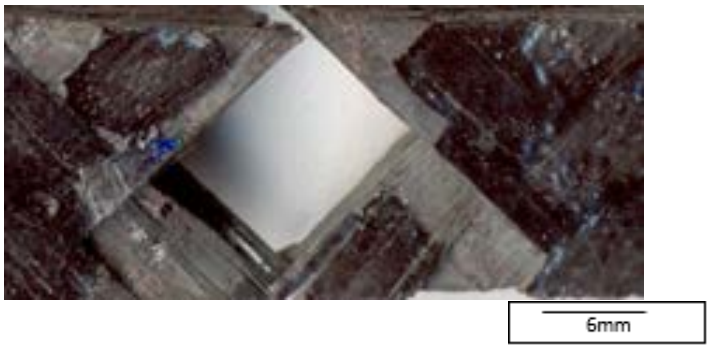

(a)

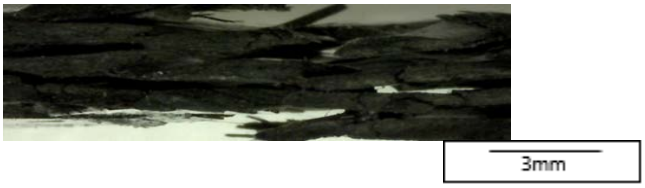

(b)

Figure 97 (a) & (b) Low magnification 12K-45° carbon fiber optical micrograph of specimens under tensile loading at a rate of 1000 s^{-1} (a) front view (b) thickness view.

From the Figure 97 (a) and types of failures suggested in the Figure 27, the type of failure is Angular (A), occurred in Gage (G) and in the middle (M) of the specimen. Therefore, this is an

AGM failure mode according to the ASTM 3039 test standards. The test coupon failed due to an excessive amount of delamination which occurred because of impact loading rates.

3.2.3 Glass fiber 8HS- 7781

Figure 98 shows a typical stress-strain behavior of glass fiber 8HS 7781 subjected to a tensile loading at an impact load rates of $10s^{-1}$ (equivalent to cross head speed of 6000mm/min).

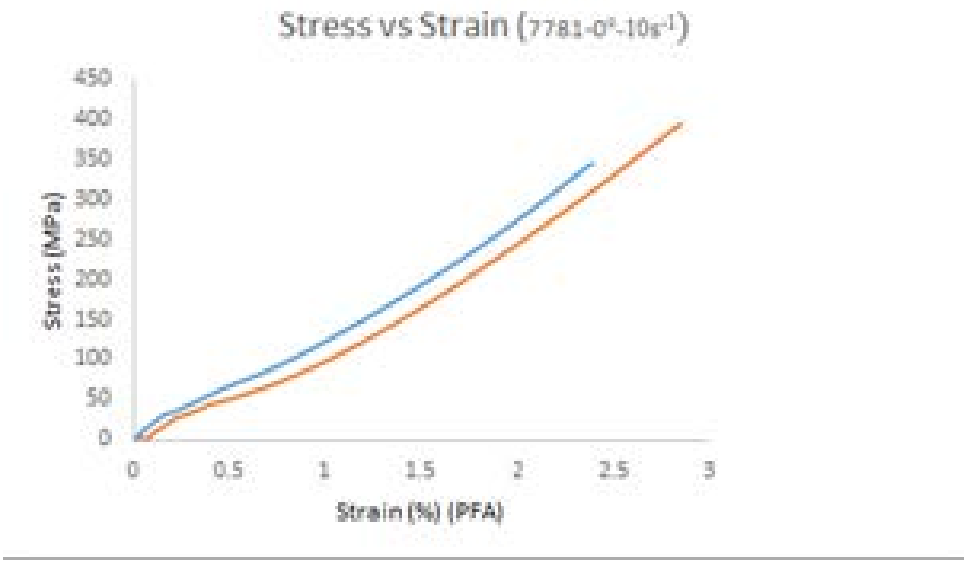

Figure 98 Tensile stress-strain behavior of 8HS 7781 glass fiber based composite tested along the 0° orientation at a rate of $10s^{-1}$.

It is evident from the above graph that the glass fiber 8HS 7781 test coupon endures an average peak stress of 368 MPa and an average maximum strain to failure of 2.62 %. Figure 99 (a) & (b) represents the low magnification optical micrographs of glass fiber 8HS 7781 at failure.

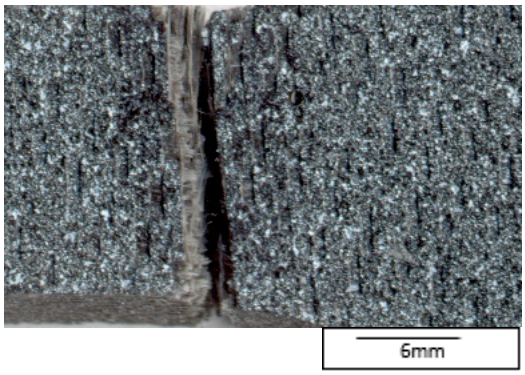

(a)

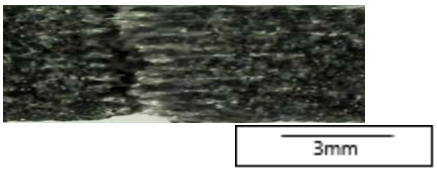

(b)

Figure 99 (a) & (b) Low magnification 8HS 7781 0° glass fiber optical micrograph of specimens under tensile loading at a rate of 10 s^{-1} (a) front view (b) thickness view.

It is evident from the above micrographs that the mode of failure is of lateral (L) type, occurred in the gage (G) area and in the middle of the specimen. Hence it is LGM type of failure according to the ASTM 3039 standards for testing polymers. The type of failure is a brittle one with a little amount of fiber pullout. Figure 100 shows the DIC strain distribution plot of glass fiber 8HS 7781 test coupon prior to failure with a maximum strain of 2.25%.

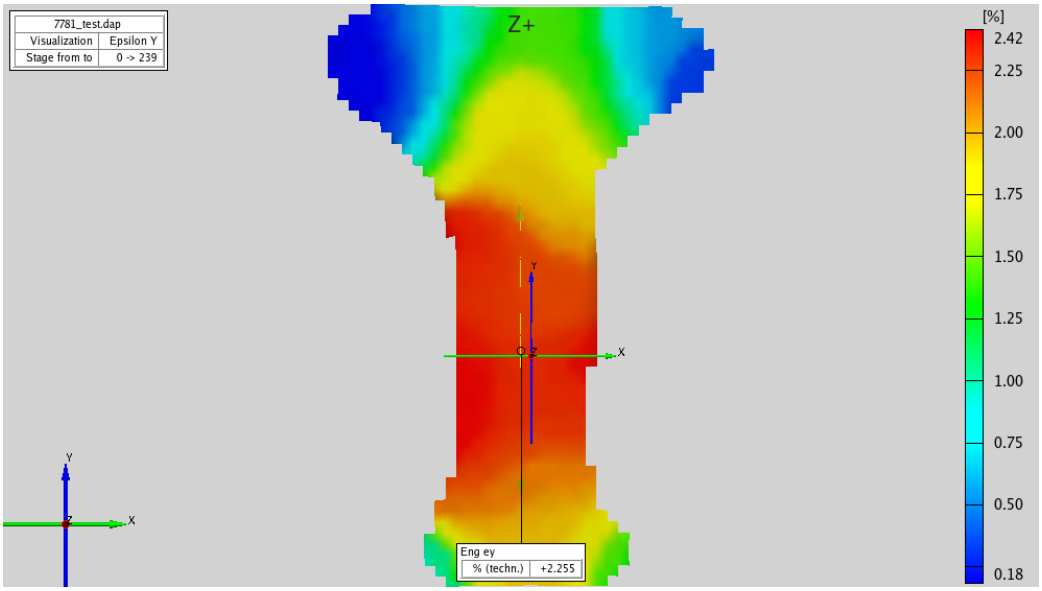

Figure 100 DIC strain distribution of 8HS 7781 glass fiber based test coupon prior to failure subjected to a tensile strain rate of 10 s^{-1}.

Figure 101 shows a typical stress-strain behavior of glass fiber 8HS 7781 test coupon subjected to a tensile loading along the warp direction at a rate of 100s^{-1} (equivalent to actuator speed of 60000 mm/min).

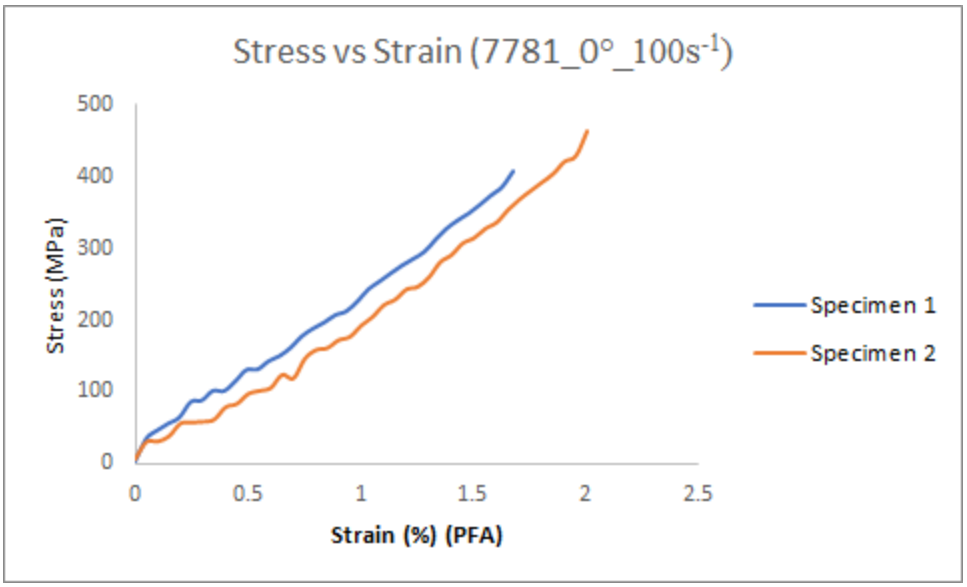

Figure 101 Tensile stress-strain behavior of 8HS 7781 glass fiber based composite tested along the 0° orientation at a rate of 100s^{-1}.

The stress strain relation followed by the glass fiber 8HS 7781 is linear, except for some noise in the data while acquisition. The test coupon endures an average peak strain of 436 MPa and an average strain to failure of 1.84%.

Figure 102 shows the low magnification optical micrographs of glass fiber 8HS 7781 at failure when subjected to a tensile loading at a rate of 100 s^{-1}.

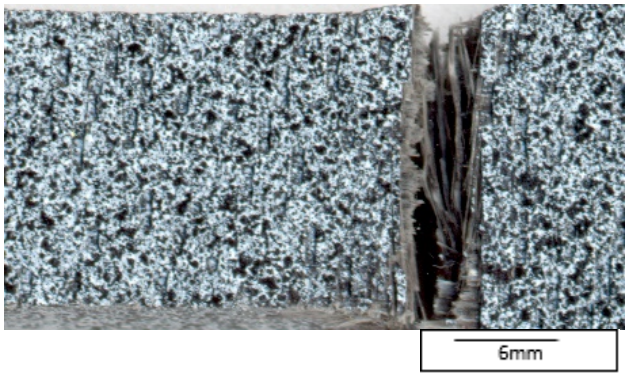

(a)

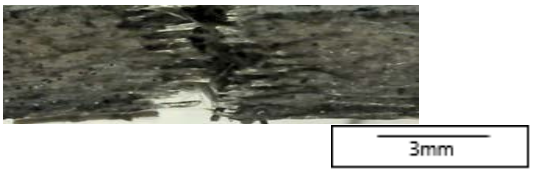

(b)

Figure 102 (a) & (b) Low magnification 8HS 7781 0° glass fiber optical micrograph of specimens under tensile loading at a rate of 100 s^{-1} (a) front view (b) thickness view.

It can be concluded from the above figure that the mode of failure is lateral (L), occurred in the Gage (G) section and in the middle of the specimen (M). Hence the failure is of LGM type as per ASTM 3039 testing standards. It is also evident that the failure is a brittle one with considerable amount of fiber pullout and delamination in the region corresponding to the fracture. Figure 103 shows the DIC strain distribution plot prior to the failure.

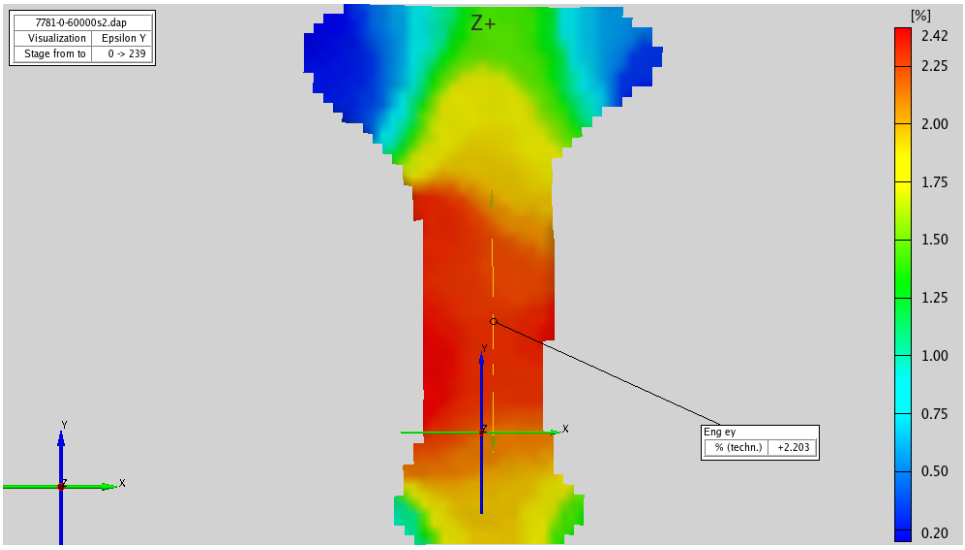

Figure 103 DIC strain distribution of 8HS 7781 glass fiber based test coupon prior to failure subjected to a tensile strain rate of 100 s^{-1}.

Figure 104 shows a typical stress-strain behavior of an 8HS 7781 glass fiber based composite test coupon tested at a strain rate of 500s^{-1}.

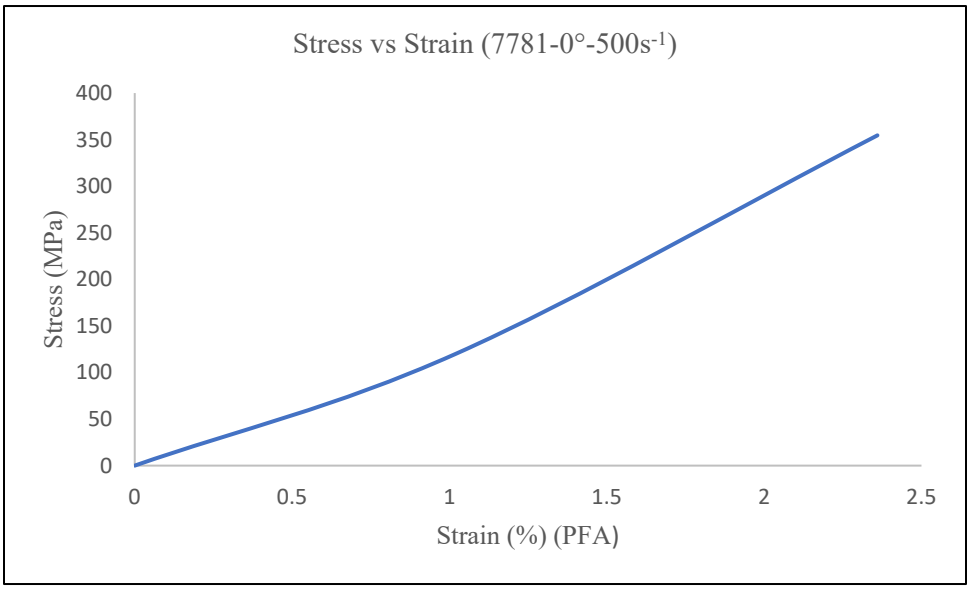

Figure 104 Tensile stress-strain behavior of 8HS 7781 glass fiber based composite tested along the 0° orientation at a rate of 500s^{-1}.

The 8HS 7781 glass fiber based composite exhibited an average peak stress of 354.6 MPa and an average strain to failure of 2.36%. Figure 105 shows low magnification optical micrographs of 8HS 7781 glass fiber based test coupon subjected to a tensile loading at a rate of $500s^{-1}$.

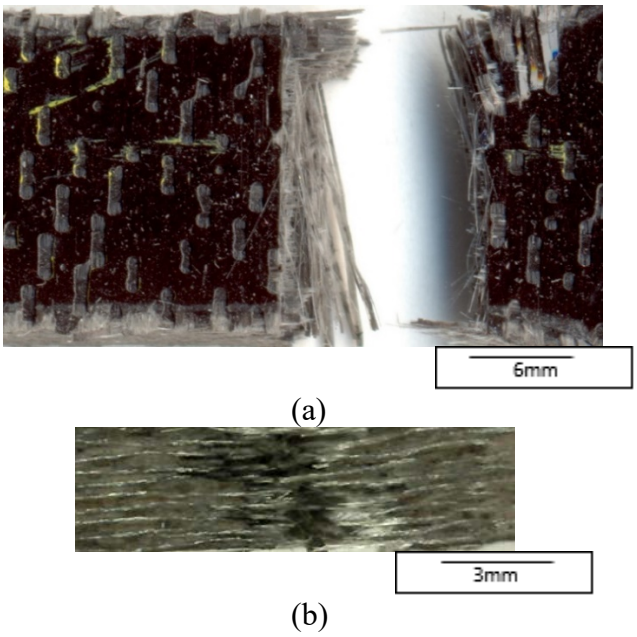

Figure 105 (a) & (b) Low magnification 8HS 7781 0° glass fiber optical micrograph of specimens under tensile loading at a rate of 500 s^{-1} (a) front view (b) thickness view.

From the Figure 105 and the types of failures suggested in the Figure 27, the failure is lateral (L) occurred in the Gage (G) and in the middle (M) of the specimen. Therefore, this is considered as LGM failure according to the ASTM 3039 standards. From Figure 105 (a), the type of failure is brittle and there is very less amount of delamination surrounding the fracture area.

Figure 106 shows a typical stress-strain behavior of 8HS 7781 glass fiber based composite tested at a rate of $1000s^{-1}$.

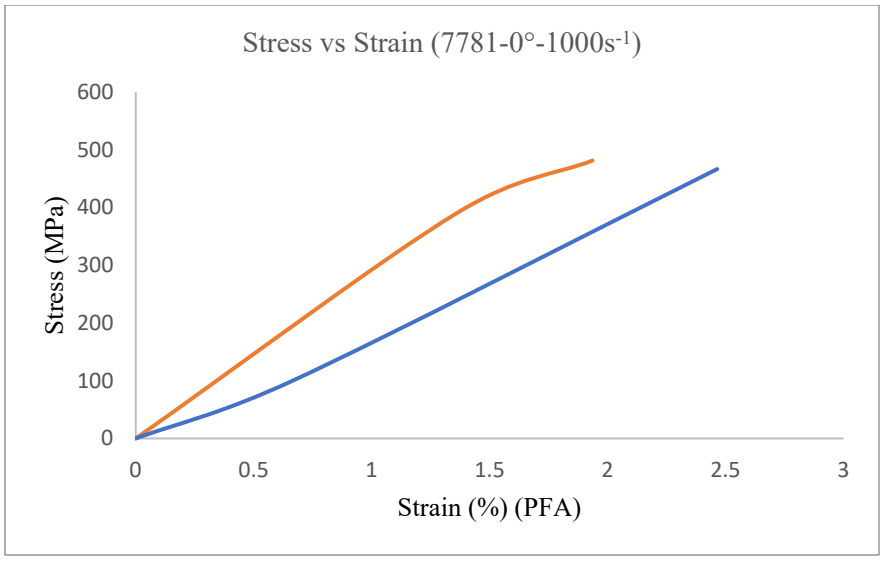

Figure 106 Tensile stress-strain behavior of 8HS 7781 glass fiber based composite tested along the 0° orientation at a rate of 1000s^{-1}.

The 8HS 7781 glass fiber based composite exhibited an average peak stress of 473 MPa and an average strain to failure of 2.3%.

Figure 107 shows low magnification optical micrographs of an 8HS 7781 glass fiber based composite test coupon after failure when subjected to a tensile loading at a rate of 1000 s^{-1}.

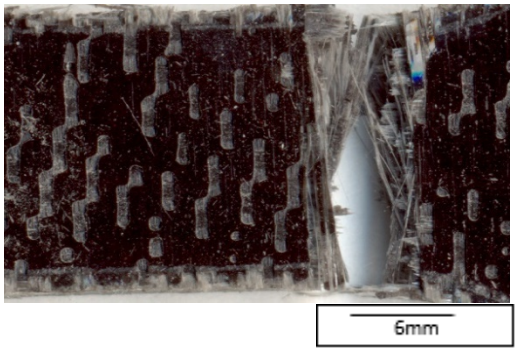

(a)

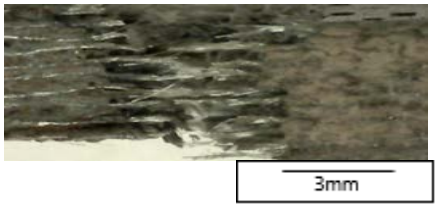

(b)

Figure 107 (a) & (b) Low magnification 8HS 7781 0° glass fiber optical micrograph of specimens under tensile loading at a rate of 1000 s^{-1} (a) front view (b) thickness view.

It is evident from the Figure 107 that the failure is brittle with some amount of fiber pullout and delamination in the region of fracture. From Figure 107 and the types of failure suggested in the Figure 27, it is evident that the failure is of type lateral (L), occurred in the Gage (G) and in the middle of the specimen (M). Therefore, this is considered as LGM failure mode according to the ASTM 3039 test standards.

Figure 108 shows a typical stress-strain behavior of glass fiber 8HS 7781 45° subjected to a tensile loading at a rate of $10s^{-1}$.

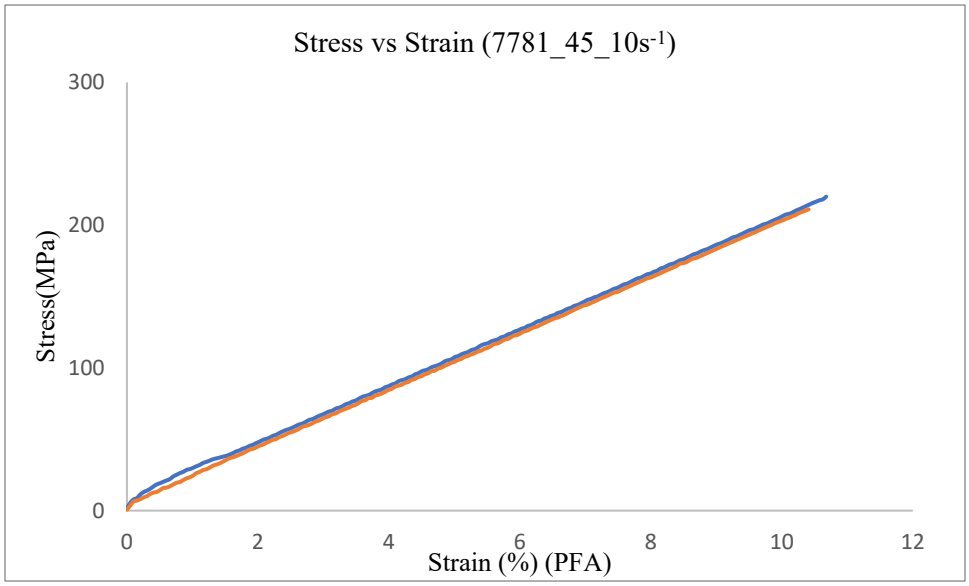

Figure 108 Tensile stress-strain behavior of 8HS 7781 glass fiber based composite tested along the 45° orientation at a rate of $10s^{-1}$.

The glass fiber 8HS 7781 45° exhibited a linear stress strain behavior until failure. The average peak stress endured by the test coupon is 215 MPa and an average peak strain of 10.5 %. Figure 109 (a) & (b) represents the low magnification optical micrographs of glass fiber 8HS 7781 45° at failure.

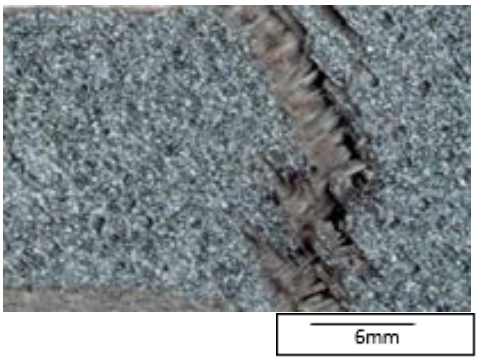

(a)

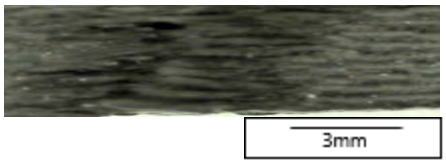

(b)

Figure 109 (a) & (b) Low magnification 8HS 7781 45° glass fiber optical micrograph of specimens under tensile loading at a rate of 10 s^{-1} (a) front view (b) thickness view.

The mode of failure is angular (A), occurred in gage (G) location and in the middle of the specimen (M). Hence the failure is of AGM according to the ASTM 3039 standards. Also, it could be seen the test coupon has undergone a brittle failure with a little amount of fiber pull out. Figure 109 (b) shows delamination of the test coupon surrounding the region of failure and few edge cracks are visible as well. Figure 110 shows the DIC strain distribution pattern prior to the failure.

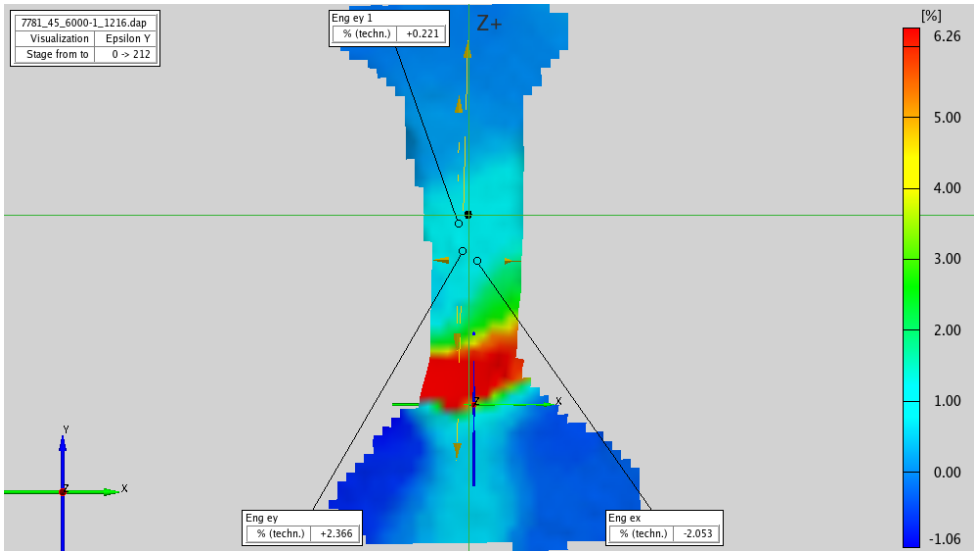

Figure 110 DIC strain distribution of 8HS 7781 glass fiber based test coupon prior to failure subjected to a tensile strain rate of 10 s^{-1}.

Figure 111 shows a typical tensile stress-strain behavior of glass fiber 8HS 7781 45° subjected to a strain rate of $100s^{-1}$.

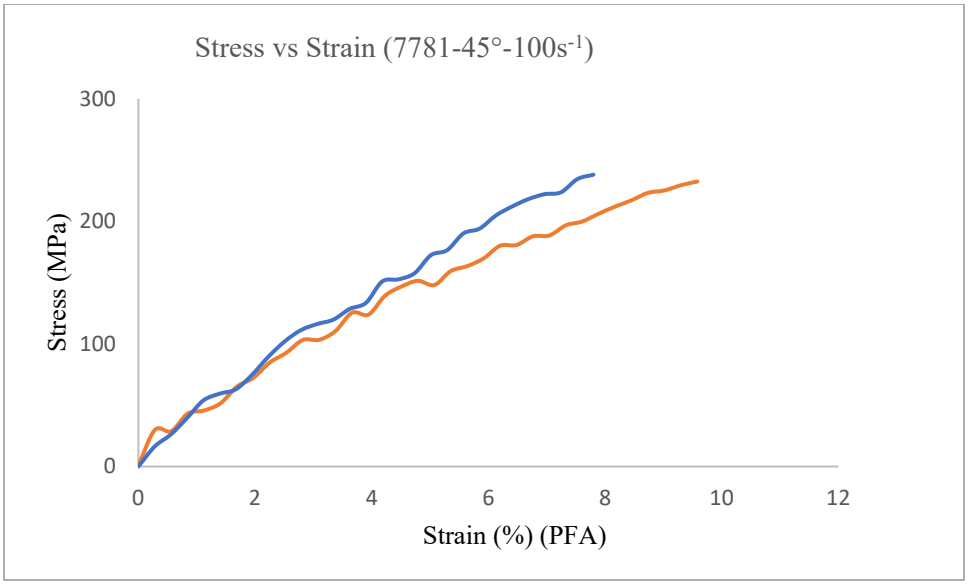

Figure 111 Tensile stress-strain behavior of 8HS 7781 glass fiber based composite tested along the 45° orientation at a rate of 100s^{-1}.

It is evident from the above figure that the test coupon is acted upon by shear forces. Because of these shear forces, the test coupon yields at lower values compared to the test coupons in which the fibers are oriented along warp direction. The stress strain behavior is linear but with some noise in the data acquisition. The average peak stress was found to be 235 MPa and an average strain to failure as 8.69 %. Figure 112 (a) & (b) shows the low magnification optical micrographs of glass fiber 8HS 7781 test coupons at failure when tested at a rate of 100 s^{-1}.

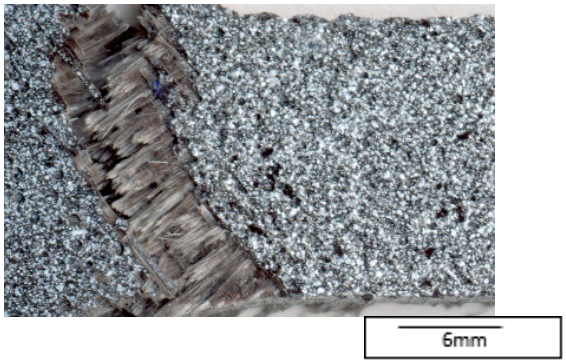

(a)

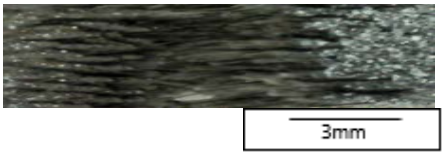

(b)

Figure 112 (a) & (b) Low magnification 8HS 7781 45° glass fiber optical micrograph of specimens under tensile loading at a rate of 100 s^{-1} (a) front view (b) thickness view.

It can be concluded from the above micrographs that the mode of failure is angular (A), occurred in Gage (G) section and in the middle of the specimen (M). Hence the failure mode is AGM as per the ASTM 3039 standards. The failure is a brittle with some amount of fiber pullout and delamination in the region surrounding the failure. Figure 113 shows the DIC strain distribution pattern that has been computed prior to the failure.

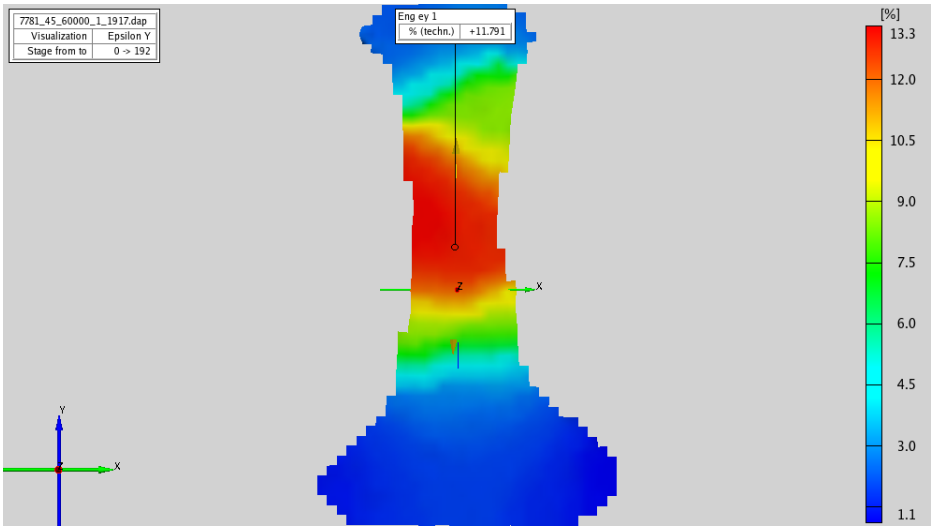

Figure 113 DIC strain distribution of 8HS 7781 glass fiber based test coupon prior to failure subjected to a tensile strain rate of 100 s^{-1}.

Figure 114 shows a typical stress-strain behavior of an 8HS 7781 glass fiber based composite coupon tested at a rate of 500s^{-1} with fibers oriented at 45°.

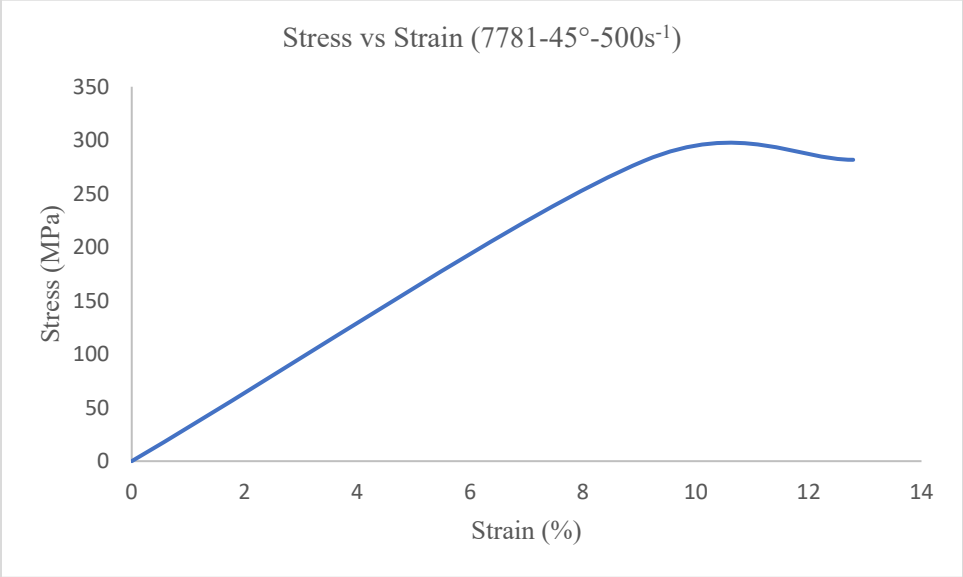

Figure 114 Tensile stress-strain behavior of 8HS 7781 glass fiber based composite tested along the 45° orientation at a rate of 500s^{-1}.

The 8HS 7781 glass fiber based composite test coupon exhibited a peak stress of 281 MPa and a strain to failure of 12%.

Figure 115 shows low magnification optical micrographs of 8HS 7781 glass fiber test coupon after failure when subjected to a tensile loading at a strain rate of $500s^{-1}$.

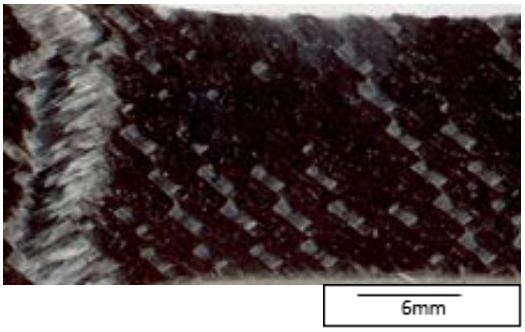

(a)

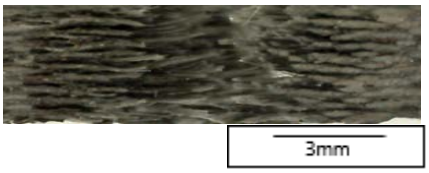

(b)

Figure 115 (a) & (b) Low magnification 8HS 7781 45° glass fiber optical micrograph of specimens under tensile loading at a rate of 500 s^{-1} (a) front view (b) thickness view.

It can be concluded from the above micrographs that the mode of failure is angular (A), occurred in Gage (G) section and in the middle of the specimen (M). Hence the failure mode is AGM as per the ASTM 3039 standards. A little delamination in the region of fracture is evident from the Figure 115 (b).

Figure 116 shows a typical stress-strain behavior of 8HS 7781 glass fiber based composite test coupon subjected to loading at a rate of $1000s^{-1}$ with fibers oriented at 45°.

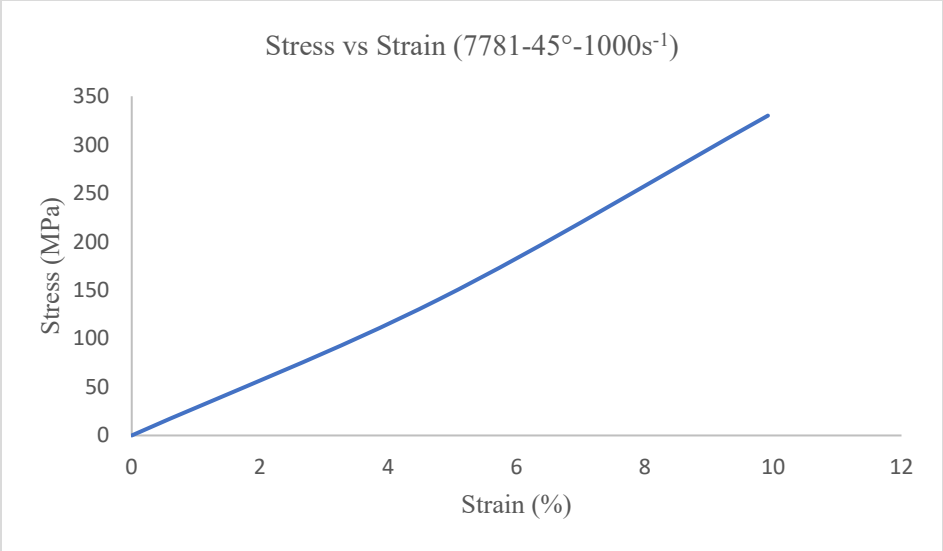

Figure 116 Tensile stress-strain behavior of 8HS 7781 glass fiber based composite tested along the 45° orientation at a rate of 1000s^{-1}.

The 8HS 7781 glass fiber based composite test coupon exhibited a maximum stress of 330 MPa and a strain to failure of 9.9 %. Figure 117 shows low magnification optical micrographs of 8HS 7781 glass fiber based composite at failure when subjected to a tensile loading at a rate of 1000 s^{-1}.

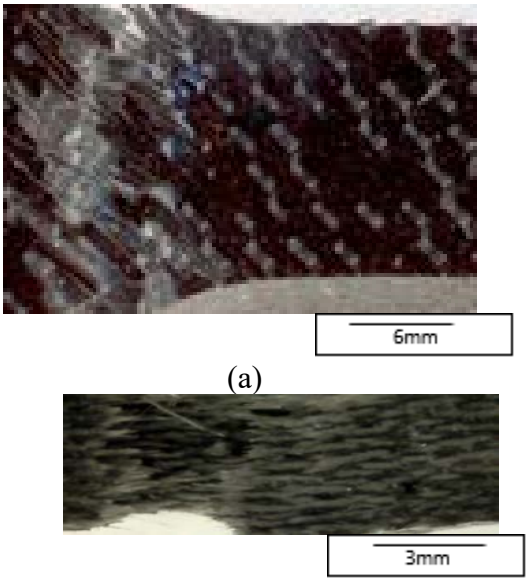

Figure 117 (a) & (b) Low magnification 8HS 7781 45° glass fiber optical micrograph of specimens under tensile loading at a rate of 1000 s^{-1} (a) front view (b) thickness view.

From the Figure 117 and types of failures suggested in the Figure 27, the failure is Angular (A), occurred in the Gage (G) and top of the gage section. Therefore, this failure can be summarized as AGT according to ASTM 3039 standards.

Table 2 shows the summarized list of peak stress and strain to failure of different test coupons with different orientations tested at dynamic rates of loading.

Composite Type	Orientation	Rate (s^{-1})	Peak Stress (MPa)	Peak Strain(%)
3K 2x2 twill woven CFE	0°	10	494	1.5
		100	419	0.83
		500	523	0.7
		1000	560	0.98
	45°	10	193	11
		100	195	7.75
		500	236	7
		1000	273	8.4
12k 2x2 twill woven CFE	0°	10	679	1.45
		100	812	1.8
		500	839	1.9
		1000	845	1.95
	45°	10	144	10.56
		100	137	9.4
		500	183	8.7
		1000	193	10.4
8HS 7781 GFE	0°	10	368	2.62
		100	436	1.84
		500	354.6	2.36
		1000	473	2.3
	45°	10	215	10.5
		100	235	8.69
		500	281	12
		1000	330	9.9

Table 2 Mechanical properties of different types of composite test coupons with different fiber orientations subjected to a tensile loading at different dynamic rates.

Figure 118 shows typical stress strain curves for 3K 2x2 twill woven carbon fiber based composites oriented at 0° subjected to different rates of loading.

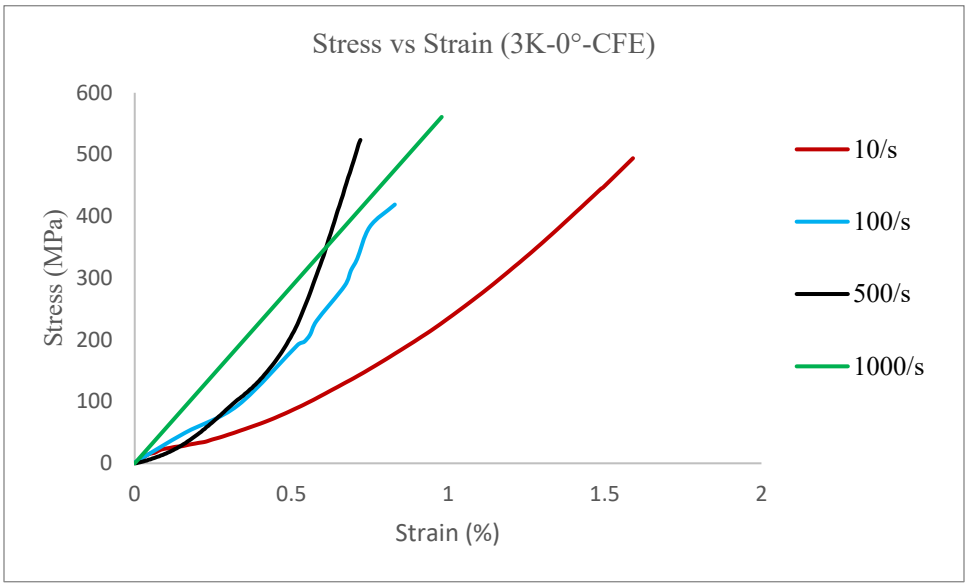

Figure 118 typical stress strain curves of 3K 2x2 twill woven carbon fiber based composites oriented at 0° subjected to different loading rates.

Figure 119 shows a typical stress strain curve of 3K 2x2 twill woven carbon fiber based composite test coupon with a fiber orientation of 45° subjected to different tensile loading rates.

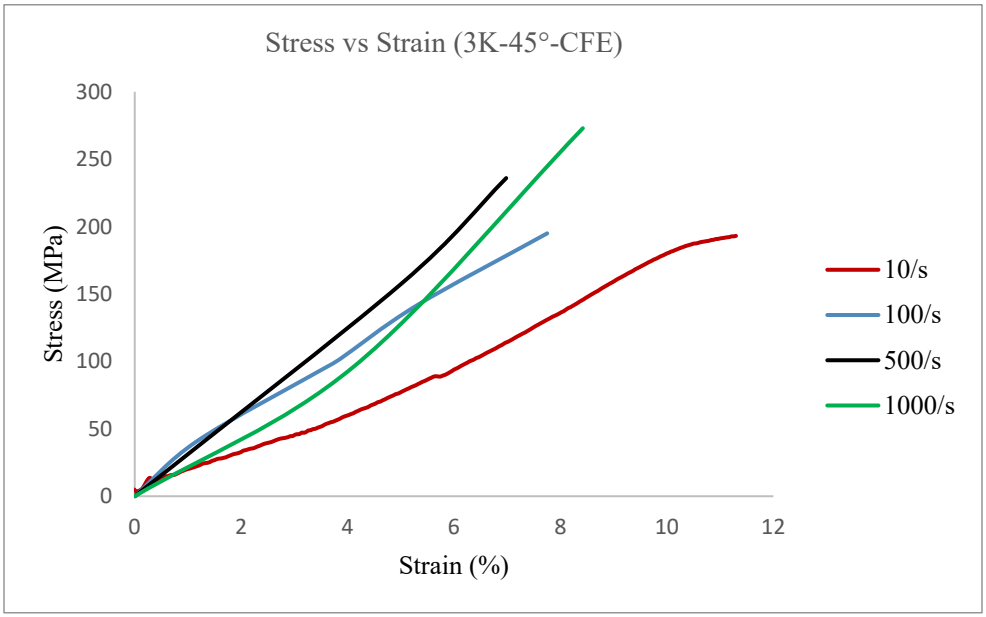

Figure 119 Typical stress-strain curves of 3K 2x2 twill woven carbon fiber based composites oriented at 45 subjected to different loading rates.

Figure 120 shows a typical stress strain curves for 12K 2x2 twill woven carbon fiber based composites oriented at 0° subjected to different rates of loading.

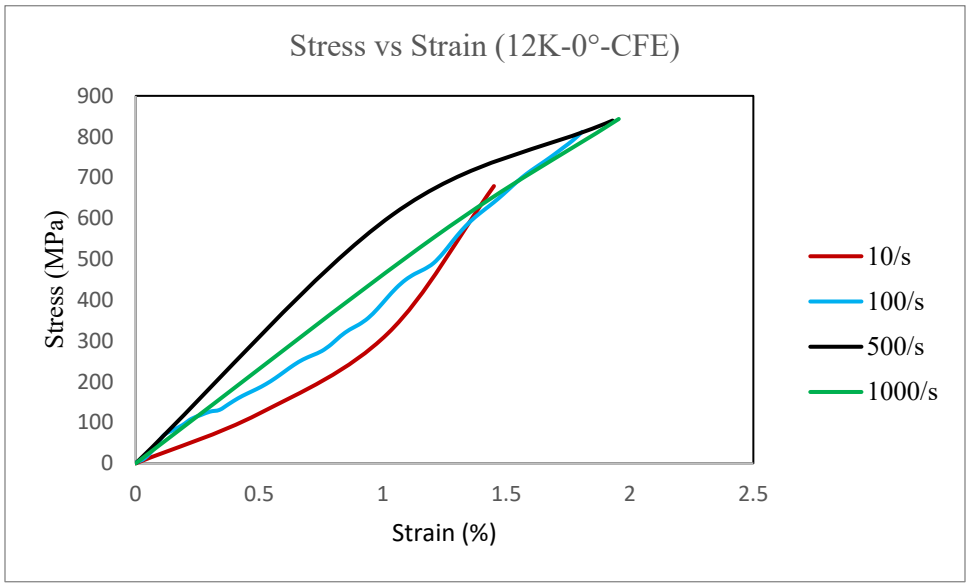

Figure 120 Typical stress strain curves of 12K 2x2 twill woven carbon fiber based composites oriented at 0° subjected to different loading rates.

Figure 121 shows a typical stress strain curve of 12K 2x2 twill woven carbon fiber based composite test coupon with a fiber orientation of 45° subjected to different tensile loading rates.

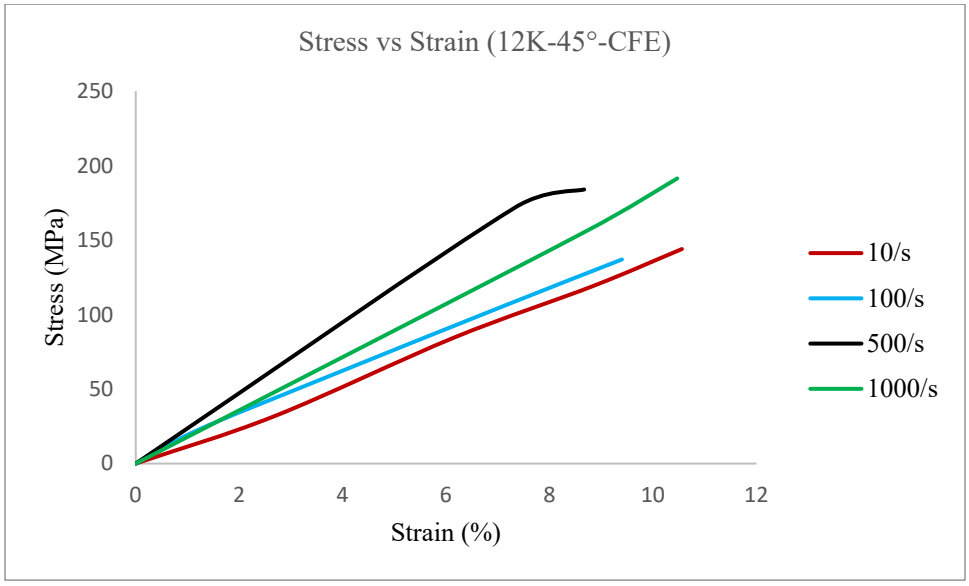

Figure 121 Typical stress strain curves of 12K 2x2 twill woven carbon fiber based composites oriented at 45° subjected to different loading rates.

Figure 122 shows a typical stress strain curve of 8HS 7781 glass fiber based composite test coupon with a fiber orientation of 0° subjected to different tensile loading rates.

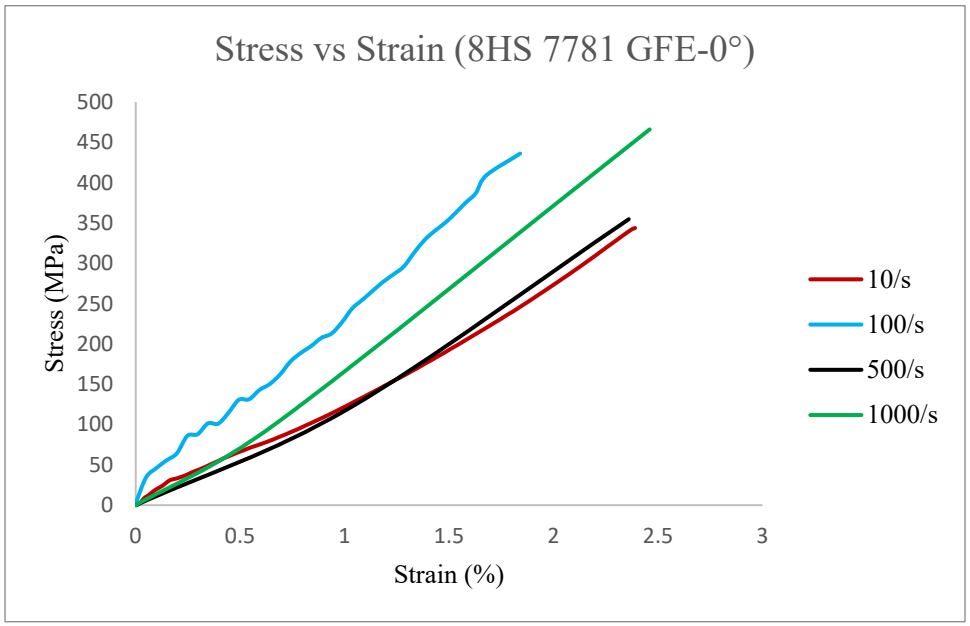

Figure 122 Typical stress strain curves of 8HS 7781 glass fiber based composites oriented at 0° subjected to different loading rates.

Figure 123 shows a typical stress strain curve of 8HS 7781 glass fiber based composite test coupon with a fiber orientation of 45° subjected to different tensile loading rates.

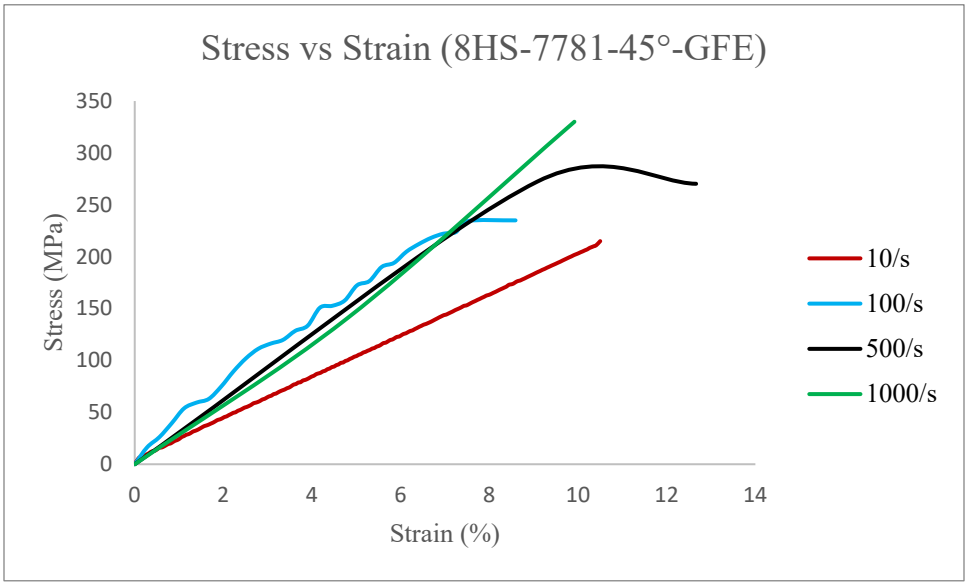

Figure 123 Typical stress strain curves of 8HS 7781 glass fiber based composites oriented at 45° subjected to different loading rates.

From the Figure 118-123, it is evident that the composite test coupons exhibited an increasing trend.

Figure 124 shows the variation of peak stress or tensile strength with respect to strain rate for a 3K 2x2 twill woven carbon fiber based composite in which fibers are oriented along 0° and 45°.

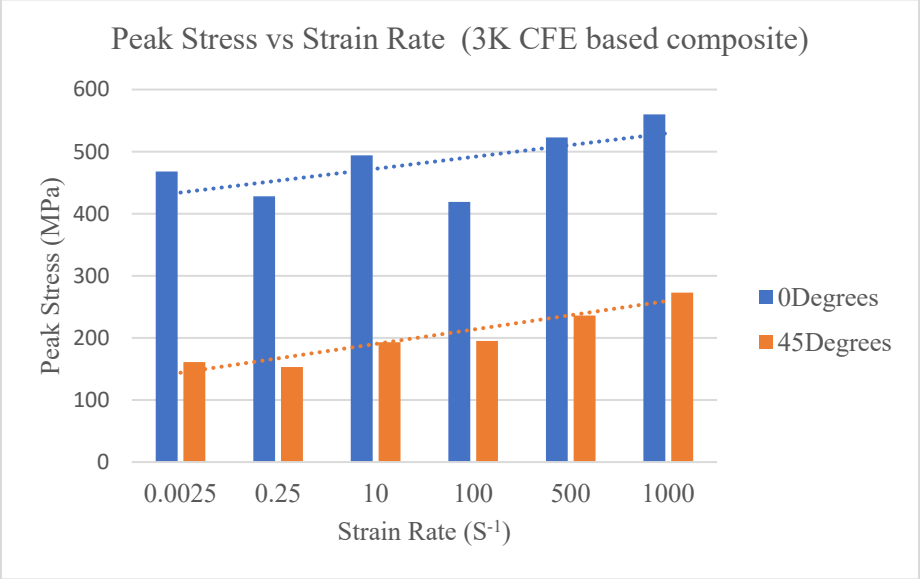

Figure 124 Variation of peak stress with strain rate for a 3K 2x2 twill woven carbon fiber based composite test coupon subjected to tensile loading at different rates.

Figure 125 shows the variation of peak stress or tensile strength with respect to strain rate for a 12K 2x2 twill woven carbon fiber based composite in which fibers are oriented along 0° and 45°.

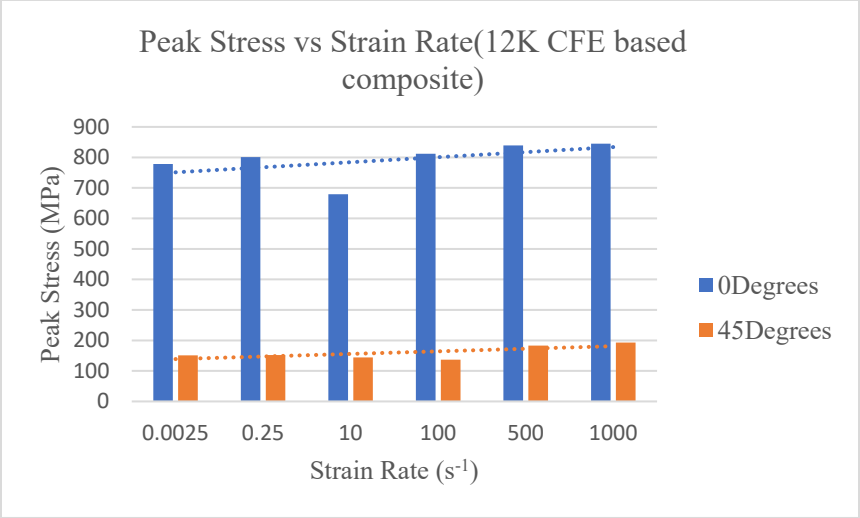

Figure 125 Variation of peak stress with strain rate for a 12K 2x2 twill woven carbon fiber based composite test coupon subjected to tensile loading at different rates.

Figure 126 shows the variation of peak stress or tensile strength with respect to strain rate for a 8HS 7781 glass fiber based composite in which fibers are oriented along 0° and 45°.

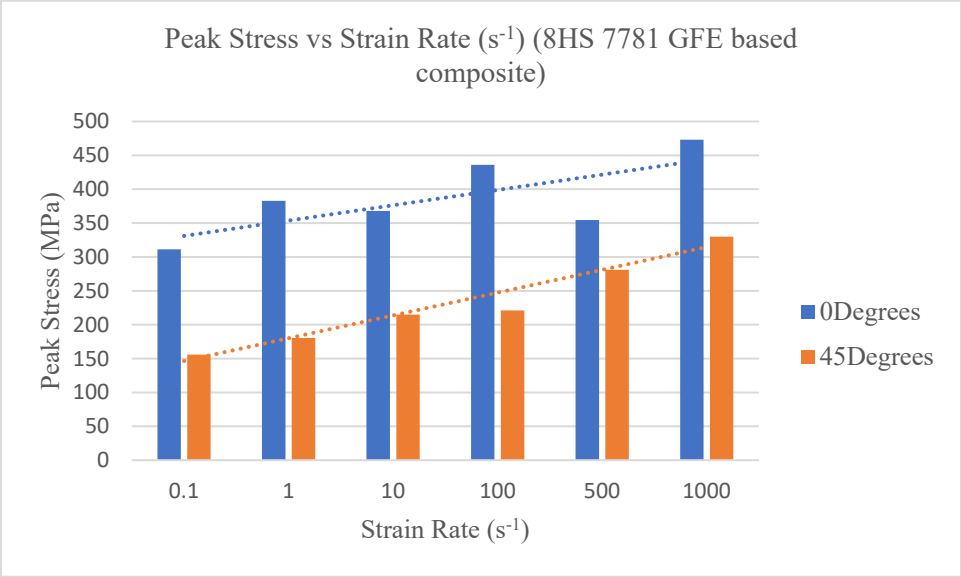

Figure 126 Variation of peak stress with strain rate for an 8HS 7781 glass fiber based composite test coupon subjected to tensile loading at different rates.

From the above Figures, it is evident that the there is a slight increase in the trend followed by peak stress in response to the strain rate for 0° and 45° orientations. However, there is a drop in the peak stress at some rates of strain for some of the composites. Generally, the mechanical properties should be enhanced with an increase in strain rate [3]. However, there are certain factors which may affect the tensile strength and other mechanical properties with increasing strain rate. In a composite laminate, matrix is responsible for distributing the load uniformly across all the fibers. During a dynamic tensile event, since the test duration decreases with increasing strain rate, there may be a slow response in the load transfer between the matrix and fiber, thus allowing the failure of composite laminate at lower tensile strengths than expected [4]. The other potential reason for this behavior maybe the molecular structure of the polymeric matrix that is used.

Figure 127 shows variation of failure strain with strain rate for a 3K 2x2 twill woven carbon fiber based test coupon in which the fibers are oriented at 0° and 45°.

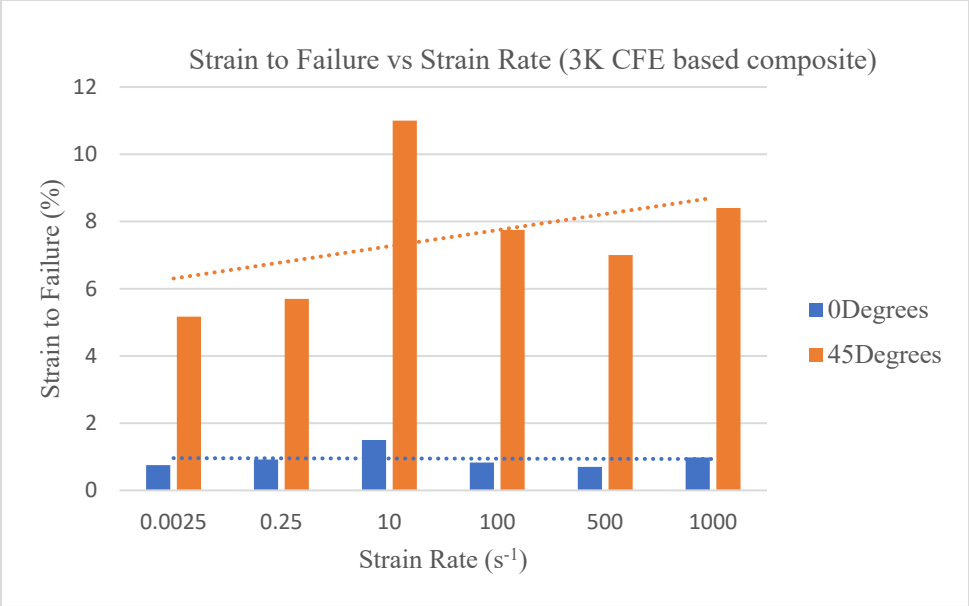

Figure 127 Variation of strain to failure with strain rate for 3K 2x2 twill woven carbon fiber based composite test coupon subjected to tensile loading at different rates.

Figure 128 shows variation of failure strain with strain rate for a 12K 2x2 twill woven carbon fiber based test coupon in which the fibers are oriented at 0° and 45°.

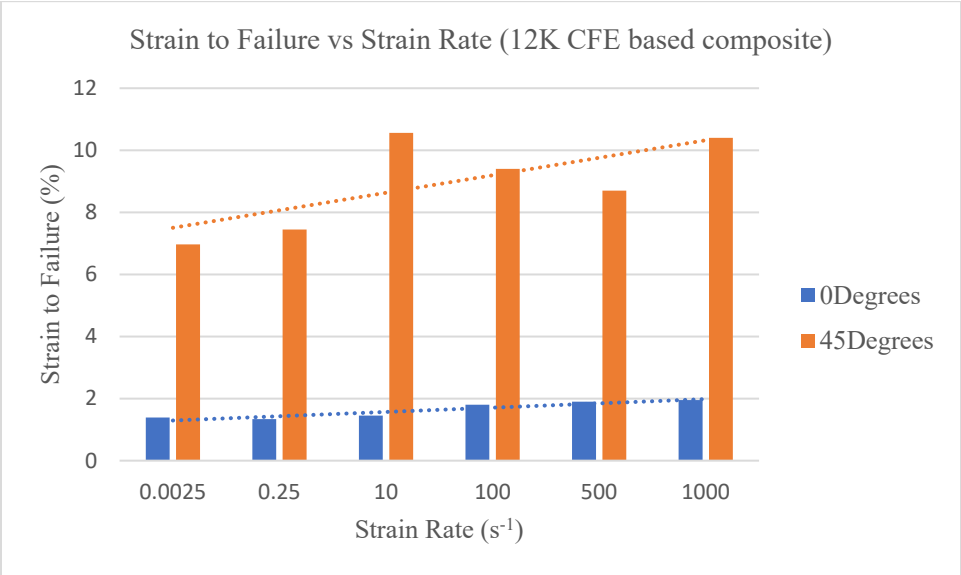

Figure 128 Variation of strain to failure with strain rate for 12K 2x2 twill woven carbon fiber based composite test coupon subjected to tensile loading at different rates.

Figure 129 shows variation of failure strain with strain rate for an 8HS 7781 glass fiber based test coupon in which the fibers are oriented at 0° and 45°.

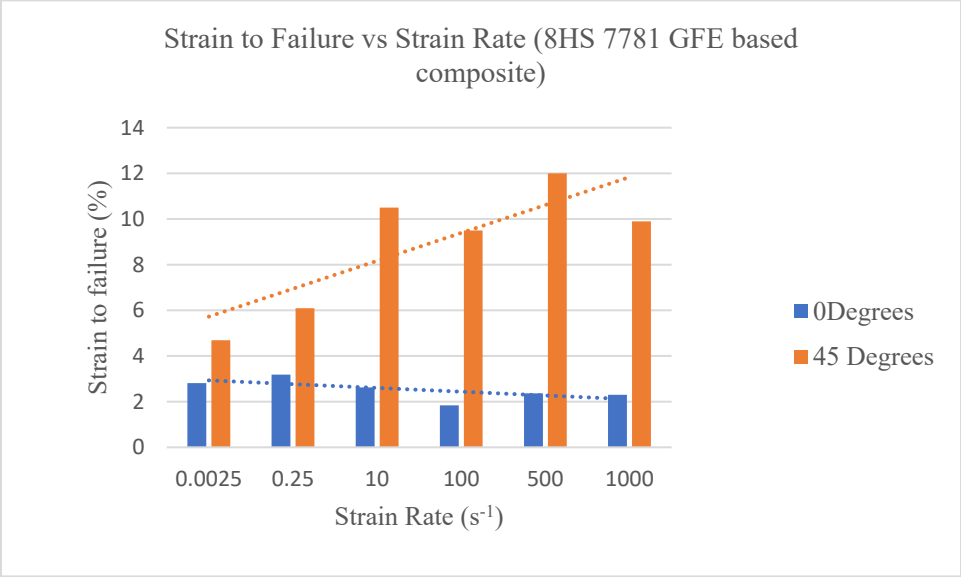

Figure 129 Variation of strain to failure with strain rate for an 8HS 7781 glass fiber based composite test coupon subjected to tensile loading at different rates.

From the above Figures, there is an increase in trend followed by 45° oriented fibers with increase in the strain rate. However, there is a very little or no effect in the trend followed by failure strain in the composites with fibers oriented along 0°.

3.3 Open Hole Tensile Testing

To evaluate the effect of a notch on the mechanical properties of composite materials, the composite test coupons are subjected to tensile loading conditions. The open hole tensile testing is used to determine the ultimate strength of notched specimens which is usually used to test structures with fastener holes. The specimens for the open hole tensile testing are prepared in accordance to the ASTM D5766 test standards which also reinforces various failure modes experienced by the composite test coupons. Figure 130 shows the failure modes of a notched specimen when subjected to a tensile loading [2].

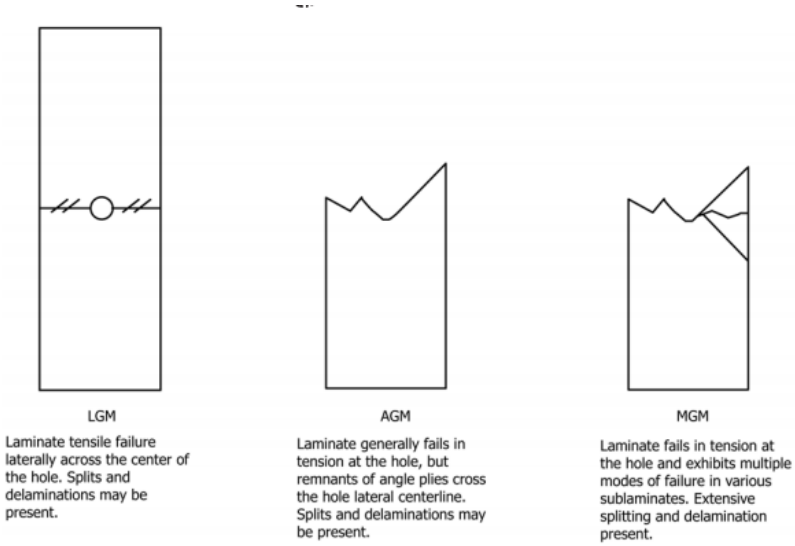

Figure 130 Acceptable failure modes of composite materials with an Open hole under tensile loading conditions [2].

3.3.1 3K 2x2 twill woven carbon fiber

Figure 131 shows a typical stress strain behavior of 3K 2x2 twill woven carbon fiber based composite subjected to a uniform tensile loading at a rate of 1mm/min (Crosshead speed) stretched along the warp direction (0°).

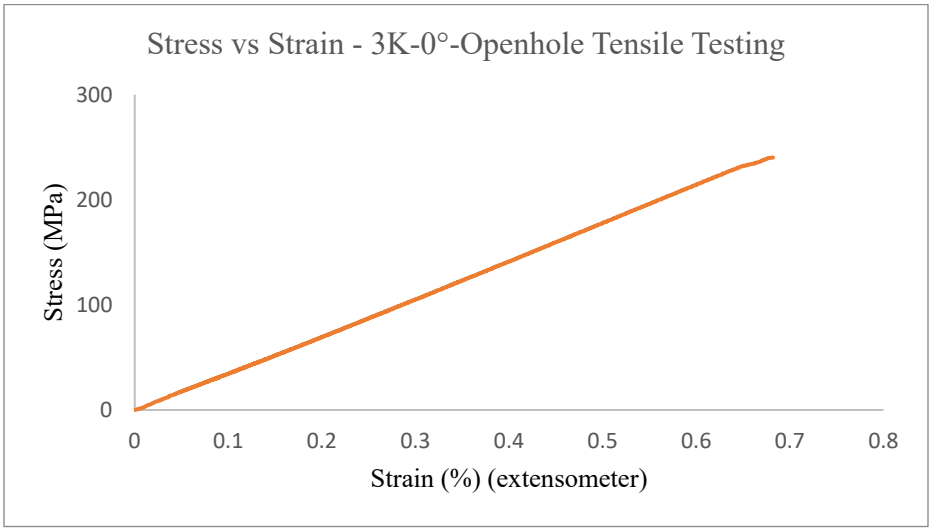

Figure 131 Tensile stress-strain behavior of 3K 2x2 twill woven carbon fiber based composite tested along the 0° orientation at a rate of 1mm/min (with extensometer).

The 3K 2x2 twill woven carbon fiber based composite exhibits a linear elastic stress-strain behavior until fracture. The failure strength in this case is much lower compared to the failure strength of a composite test coupon without any stress concentrations. The average peak stress that the open hole tensile test coupon can endure is 242 MPa and an average peak strain is

approximately around 0.7 %. Figure 132 represents a typical stress-strain plot obtained using the DIC technique.

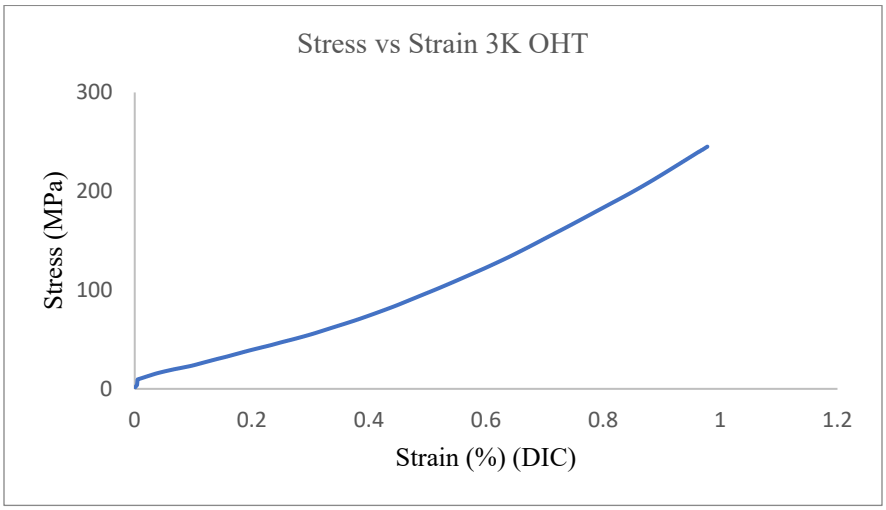

Figure 132 Tensile stress-strain behavior of 3K 2x2 twill woven carbon fiber based composite tested along the 0° orientation at a rate of 1mm/min (with DIC).

From the above graph, the peak strain at failure is approximately around 1.05 % which is approximate to the strain obtained using the extensometer. Figure 133 (a) & (b) shows the low magnification optical micrographs of 3K 0° twill woven carbon fiber based composite with a centrally located hole when tested at a rate of 1mm/min.

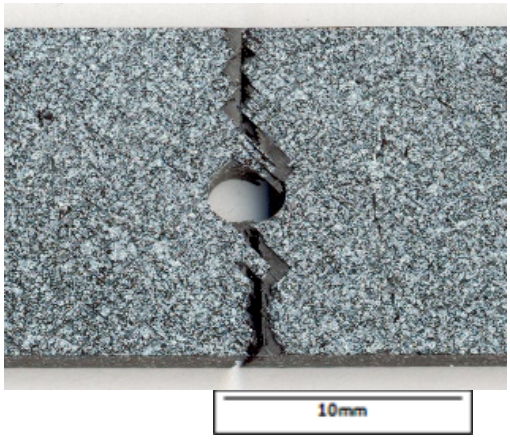

Figure 133 (a) & (b) Low magnification optical micrograph of 3K 2x2 woven carbon fiber based notched specimens tested under tensile loading at a rate of 1 mm/min (a) front view (b) thickness view.

Figure 133 (a) shows the mode of failure to be lateral (L), gage section (G) and occurred in the middle (M) of the specimen through the center of hole. Hence it can be considered as a LGM failure mode according to ASTM 5766 standard for tensile testing of composite laminates with a notch at the center. It is evident from the Figure 133 (b) that there is delamination around the region of failure and not much fiber splits. Because of the presence of the notch, the specimen failed along the notch because of higher stress concentrations. Figure 134 shows the DIC strain distribution map for 3K 0° woven composite test coupon prior to failure with maximum strain to failure of 0.7%.

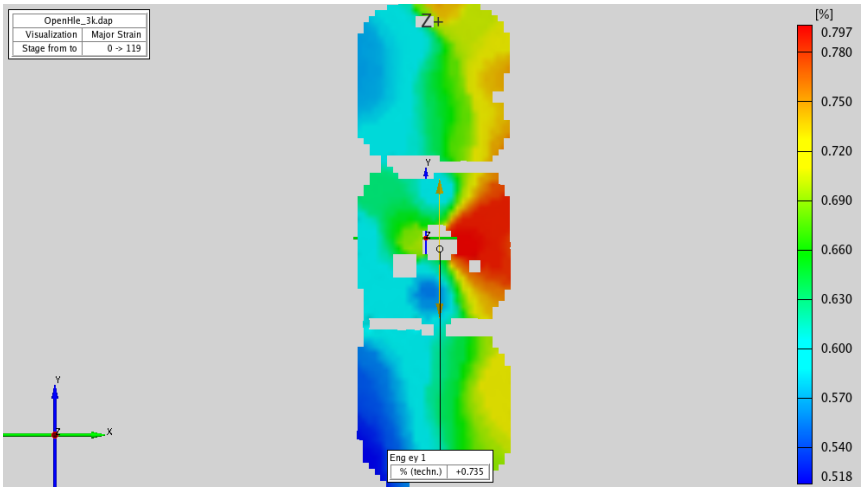

Figure 134 DIC strain distribution map of 3K 2x2 twill woven carbon fiber based notched composite subjected to tensile loading at a rate of 1mm/min.

It can be seen in the above figure that the maximum amount of strain is localized around the hole. The strain to failure obtained from the DIC correlates with the strain captured using extensometer.

3.3.2 12K 2x2 twill woven carbon fiber

Figure 135 shows a typical stress-strain behavior of 12K 2x2 twill woven carbon fiber based composite in which the fibers are along the warp direction (0°) tested at 1mm/min (Crosshead speed).

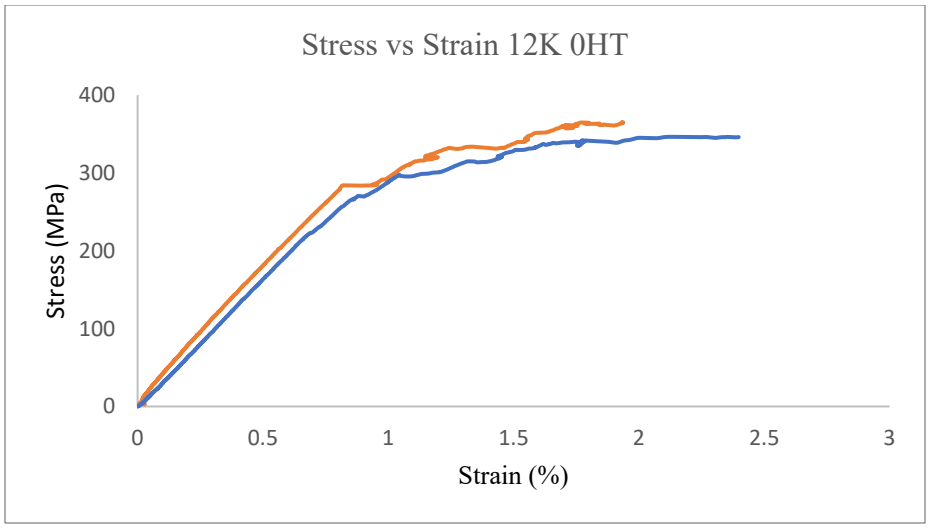

Figure 135 Tensile stress-strain behavior of 12K 2x2 twill woven carbon fiber based composite tested along the 0° orientation at a rate of 1mm/min (with extensometer).

It is clear from the above figure that the 12K test coupon exhibited a linear behavior until 280 MPa. After that the test coupon starts experiencing internal failure of fibers because of which the extensometer starts moving up and down and as a result some noise is visible in the stress strain plot. The average peak stress which the test coupon can withstand is 355 MPa and an average peak strain to failure is 2.1 %. Figure 136 shows the stress strain behavior of the 12K 2x2 twill woven composite in which the strain is calculated using DIC technique. The average peak strain calculated using the DIC technique was found to be 1.5 %.

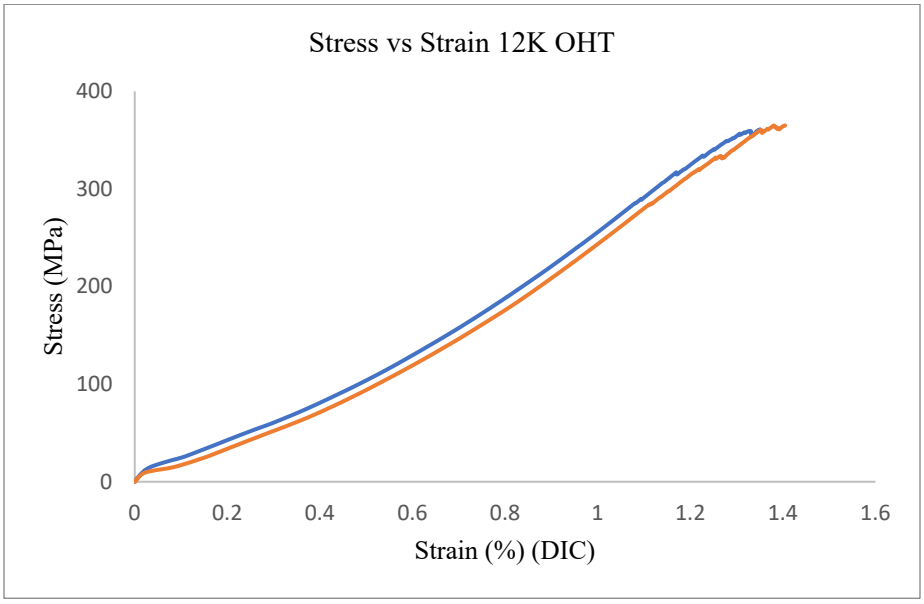

Figure 136 Tensile stress-strain behavior of 12K 2x2 twill woven carbon fiber based composite tested along the 0° orientation at a rate of 1mm/min (with DIC).

Figure 137 (a) & (b) shows low magnification optical micrographs of 12K 0° woven composite test coupon at failure when subjected to a tensile loading at a rate of 1mm/min.

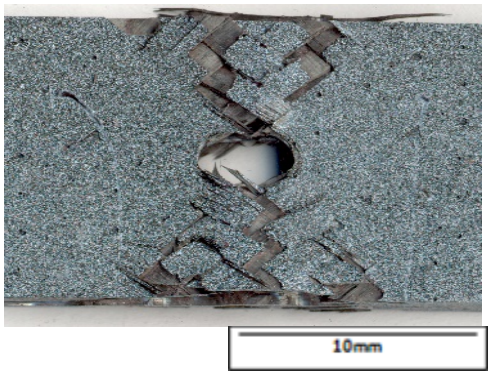

(a)

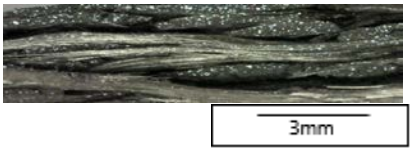

(b)

Figure 137 (a) & (b) Low magnification optical micrograph of 12K 2x2 woven carbon fiber based notched specimens tested under tensile loading at a rate of 1 mm/min (a) front view (b) thickness view.

It is visible from the Figure 137 (a) that the failure occurred across the hole and exhibits multi modes (M) of failure across the test coupon. The failure occurred at the middle of the specimen and in gage section. Hence the failure maybe termed as MGM as per the ASTM standards. From Figure 137(b) it can be deduced that the test coupon has some edge cracks and fiber pullout present on it apart from the delamination. It is also evident that there was no split across the hole unlike the other composites. This is because of superior load bearing capacity of 12K 2x2 twill woven carbon fiber based composite and also because of higher number of fibers in a tow. Figure 138 shows the DIC strain distribution map for 12K woven composite test coupon with a centrally located hole on it with strain to failure of 2.5%.

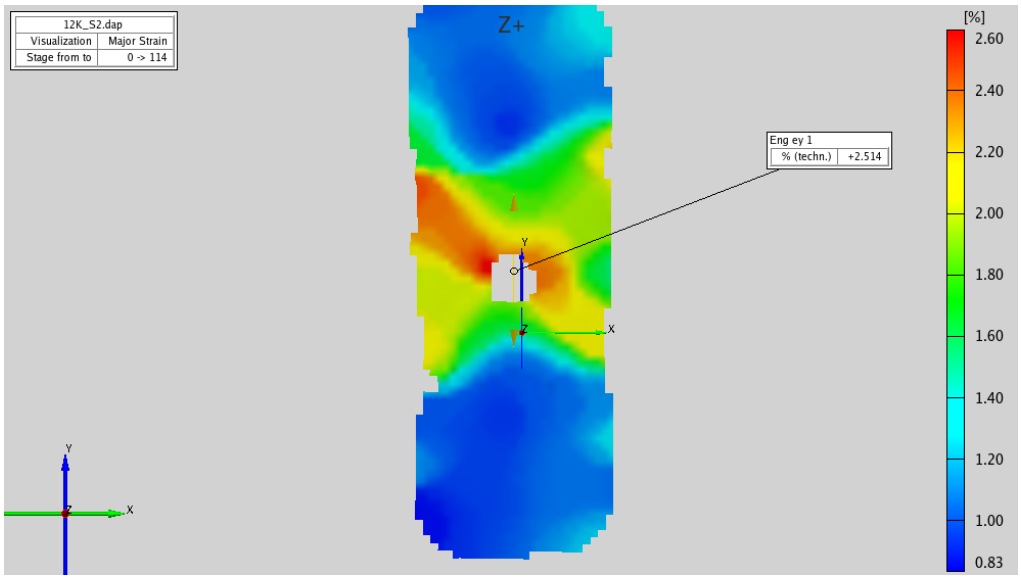

Figure 138 DIC strain distribution map of 12K 2x2 twill woven carbon fiber based notched composite subjected to tensile loading at a rate of 1mm/min.

The above figure clearly depicts that the area surrounding the hole undergoes maximum strain prior to the failure.

3.3.3 Glass Fiber 8HS-7781

Figure 139 shows a typical stress-strain behavior of glass fiber 8HS 7781 subjected to a tensile loading along the warp direction (0°) at a loading rate of 1mm/min (Crosshead speed).

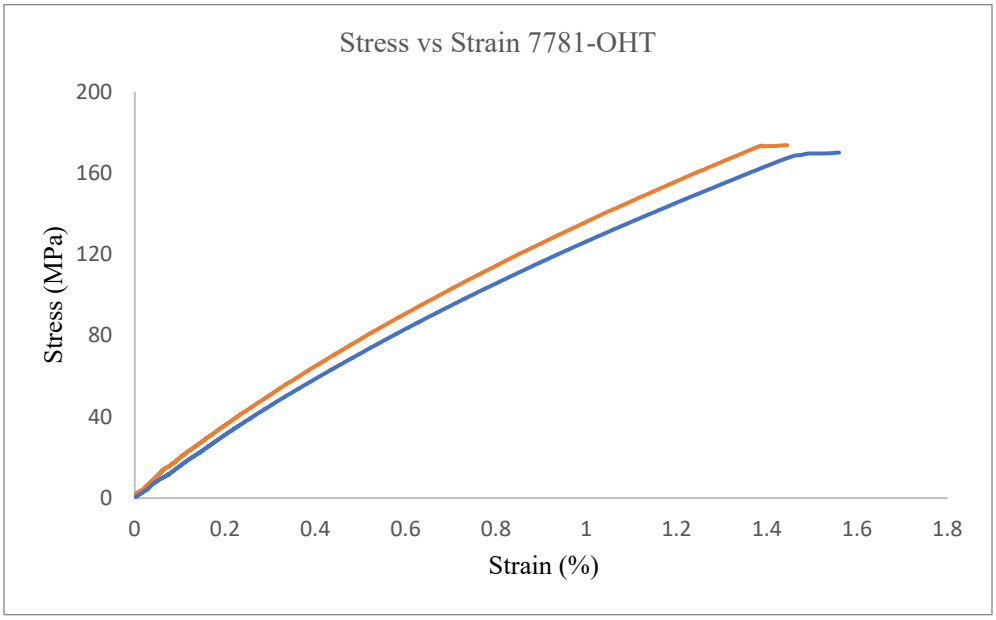

Figure 139 Tensile stress-strain behavior of 8HS 7781 glass fiber based composite tested along the 0° orientation at a rate of 1mm/min (with extensometer).

The test coupon exhibits a linear stress strain behavior until the onset of the fracture. It was experimentally investigated that an average peak stress is around 171 MPa and an average peak

strain to failure of 1.50 %. Figure 140 shows the stress strain behavior of glass fiber 8HS 7781 where the strain is calculated using the DIC technique.

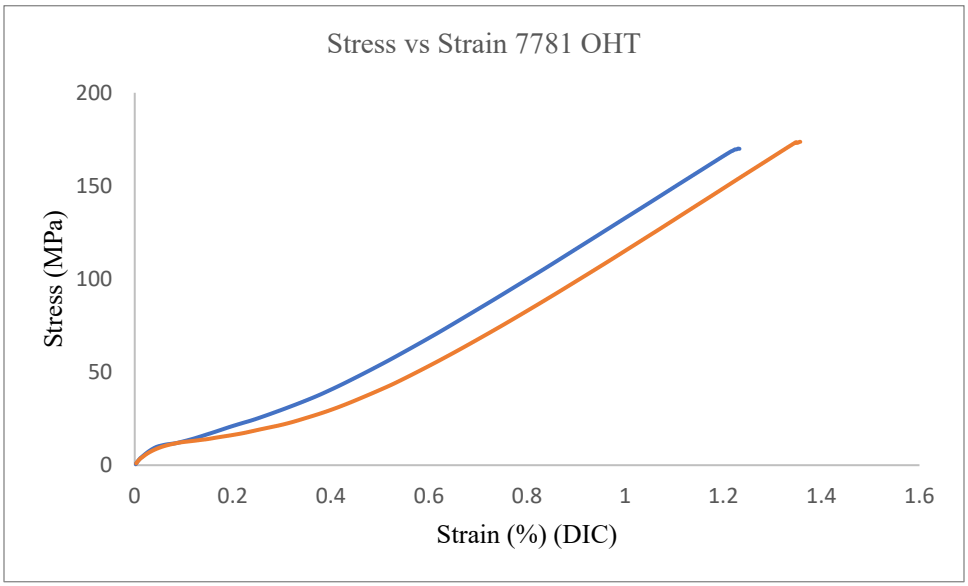

Figure 140 Tensile stress-strain behavior of 8HS 7781 glass fiber based composite tested along the 0° orientation at a rate of 1mm/min (with DIC).

The average peak strain to failure calculated using the DIC technique was found to be 1.31 %.

Figure 141 (a) & (b) shows low magnification optical micrographs of 8HS 7781 glass fiber based composite test coupon subjected to a tensile loading at a rate of 1mm/min.

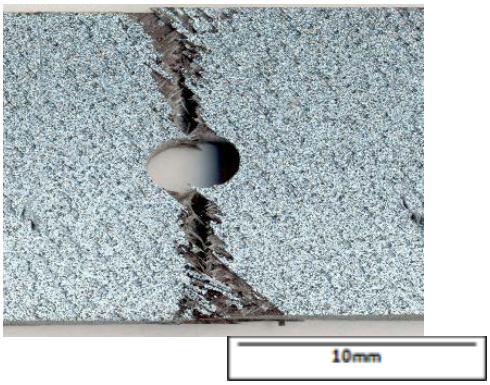

(a)

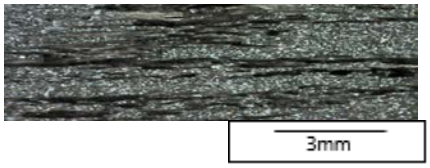

(b)

Figure 141 (a) & (b) Low magnification optical micrograph of 8HS 7781 glass fiber based notched specimens tested under tensile loading at a rate of 1 mm/min (a) front view (b) thickness view.

From the above Figure, it is evident that the mode of failure is lateral (L), with the failure in gage (G) location and in the middle (M) of the specimen. Hence the failure is considered as a LGM failure mode according to the ASTM 3039 standards. Also, delamination could be seen only in the area of fracture apart from few cracks on the edges. Figure 142 shows the strain distribution computed using DIC prior to the failure of the test coupon with a maximum strain to failure of 1.6%.

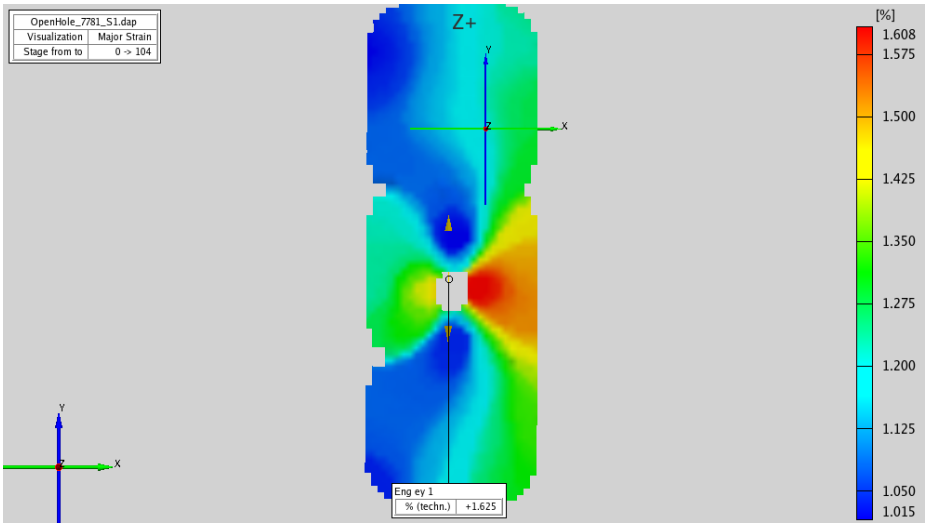

Figure 142 DIC strain distribution map of 12K 2x2 twill woven carbon fiber based notched composite subjected to tensile loading at a rate of 1mm/min.

The region surrounding the hole has undergone maximum strain because of the failure across the hole.

Table 3 shows the summarized results of the composite test coupons with a notch tested at a loading rate of 1mm/min (cross head speed).

Composite Type	Young's Modulus (GPa)	Peak Stress (MPa)	Peak Strain (%)	% Reduction in Peak Stress (compared to unnotched sample)
3K 2x2 twill woven CFE	35.71	242.5	0.96	61
12K 2x2 twill woven CFE	33.07	355.5	2.16	55
8HS 7781 GFE	11.25	171.8	1.50	57

Table 3 Mechanical properties of different types of notched composite test coupons subjected to a uniform tensile loading.

It is evident from the above table that there was considerable amount of reduction in strength of the notched composite test coupons when compared to un-notched specimens. The hole acts like

a stress concentration region and results in degradation of mechanical properties of the test coupon. Whitney-Nuismer point stress model is used to numerically evaluate the notched strength of a composite specimen when subjected to a tensile loading [5]. This model assumes that the failure in a composite test coupon occurs at a small certain fixed distance d_0 ($0.1< d_0<0.2$mm) [6]. Failure in the composite model occurs at a stress level $\sigma_{notched}$ which is given by,

$$\sigma_{notched} = \left(\frac{2}{3\lambda^4+\lambda^2+2}\right)\sigma_{unnotched} \quad (3.1)$$

$$\lambda = \frac{r}{r+d_0} \quad (3.2)$$

Where, r = radius of the drilled hole = 2.15 mm

Characteristic distance d_0 = 0.15mm

Table 4 shows the notched strength that is numerically computed using the above model.

Composite Type	Unnotched Strength (MPa)	Experimental Notched Strength (MPa)	Theoretical Notched Strength (MPa)
3K 2x2 twill woven CFE	621.8	242.5	243.8
12K 2x2 twill woven CFE	797.1	355.5	312.5
8HS 7781 GFE	404.9	171.8	158

Table 4 Experimental and Analytical notched tensile strengths of carbon and glass fiber reinforced composite test coupons.

References

[1] "Standard Test Method for Tensile Properties of Polymer Matrix Composite Materials," ASTM Standard D 3039/D 3039M – 14.

[2] "Standard Test Method for Open-Hole Tensile Strength of Polymer Matrix Composite Laminates," ASTM Standard D 5766/D 5766M – 11.

[3] Naik, N.K., Shrirao, P.,2004, "Composite structures under ballistic impact," Composite Structures, Vol.66, pp.579-590.

[4] Bilisik, Kadir, 2009, "Multidirectional Stitched Layered Aramid Woven Fabric Structures and their Experimental Characterization of Ballistic Performance," Textile Research Journal, Vol.79, pp.1331-1343.

[5] Mallick, P.K., 2007, Fiber-Reinforced Composites- Material, Manufacturing and design, CRC Press, Boca Raton FL,3rd Edition.

[6] Toubal, Lofti., Karama Moussa, 2004, "Stress Concentration in a circular hole in composite plate," Composite Structures, Vol. 68.

[7] Rolfes, R., Ernst,G., Vogler, M., Huhne,C., 2008, "Material and Failure Models for Textile Composites," Mechanical Response of Composites, Vol.10.

CHAPTER 4. CONCLUSIONS

The Mechanical behavior of woven composite materials under varying strain rate conditions was investigated in this thesis. Initially, the Carbon fiber and Glass fiber based composites were loaded quasi statically on to an Instron 5767 universal testing machine. A high resolution non-contact strain measurement system was used to examine the global and local strain deformations and strain distributions within the composite test coupon. Experimental results revealed that there was increase in the peak strength with the increase in the strain rate. It was evident from the test results that the 3K 2x2 twill woven Carbon fiber based composite and the 12K 2x2 twill woven Carbon fiber based composite have superior load bearing capacity subjected to tensile loading when fibers are oriented at 0°.

The Carbon and Glass fiber based composites were then subjected to dynamic loading conditions on a servo hydraulic and pneumatic test systems. Experimental investigation of these woven composites when subjected to dynamic loading conditions revealed that the peak strength followed an increasing trend in case of 12K 2x2 twill woven Carbon fiber, Glass fiber 8HS 7781 and 3K 2x2 twill woven Carbon fiber irrespective of the fiber orientation. However, an intermediate decrease in strength with increasing strain rate was observed in case of the 3K 2x2 twill woven Carbon fiber oriented at 0°. Failure strain was found to remain unaffected by the strain rate when the test coupons were oriented at 0° under dynamic loading. In contrast, there was a slight increase in the failure strain in the test coupons in which fibers oriented at 45°. Two high speed cameras capable of recording 200,000 frames per second were used to record the events under dynamic tensile testing. The images acquired using the high-speed cameras were integrated into the DIC software to obtain the strain maps and engineering strain in the test coupons was computed using Photron Fastcam Analysis.

Finally, the effect of a notch on the 3K 2x2 twill woven Carbon fiber, 12K 2x2 twill woven Carbon fiber and Glass fiber 7781 -8HS oriented at 0° was investigated experimentally. Results revealed that there was a considerable decrease in strength compared to unnotched specimens. Notch in the test coupon was found to act as a region of stress concentration, thus decreasing the overall strength of the test coupon. 12K 2x2 twill woven Carbon fiber based composite exhibited superior tensile strength compared to the other composite test coupons.

This project revealed that the mechanical properties of woven composites depends on factors such as woven architecture, bundle characteristics, fiber orientation and the presence of notches. Furthermore, it was found that such properties are affected by the strain rate. Such information is vital for the design of composite structures that maybe subjected to dynamic loading conditions.